orn!

OAK RIDGE NATIONAL LABORATORY

LOCKHEED MARTIN

Effective Porosity and Pore-Throat Sizes of Conasauga Group Mudrock: Application, Test and Evaluation of Petrophysical Techniques

J. Dorsch
T. J. Katsube
W. E. Sanford
B. E. Dugan
L. M. Tourkow

DISCLAIMER

Portions of this document may be illegible electronic image products. Images are produced from the best available original document.

EFFECTIVE POROSITY AND PORE-THROAT SIZES OF CONASAUGA GROUP MUDROCK: APPLICATION, TEST AND EVALUATION OF PETROPHYSICAL TECHNIQUES

J. Dorsch[1]

T. J. Katsube[2]

W. E. Sanford[1, 3]

B. E. Dugan[4]

L. M. Tourkow[5]

[1] Environmental Sciences Division, Oak Ridge National Laboratory, Oak Ridge, TN 37831-6400
[2] Geological Survey of Canada, Mineral Resources Division, Ottawa, Ontario K1A 0E8
[3] Dept. of Civil & Environmental Engineering, Univ. of Tennessee, Knoxville, TN 37996
[4] Dept. of Civil & Mineral Engineering, Univ. of Minnesota, Minneapolis, MN 55455
[5] Dept. of Earth & Atmospheric Sci., Purdue University, West Lafayette, IN 47907

Date Issued—April, 1996

Table of Contents

FIGURES

TABLES

ACKNOWLEDGMENTS

EXECUTIVE SUMMARY

Effective porosity (specifically referring to the interconnected pore space) was recently recognized as being essential in determining the effectiveness and extent of matrix diffusion as a transport mechanism within fractured low-permeability rock formations. The research presented in this report was performed to test the applicability of several petrophysical techniques for the determination of effective porosity of fine-grained siliciclastic rocks. In addition, the aim was to gather quantitative data on the effective porosity of Conasauga Group mudrock from the Oak Ridge Reservation (ORR).

The quantitative data reported here include not only effective porosities based on diverse measurement techniques, but also data on the sizes of pore throats and their distribution, and specimen bulk and grain densities. The petrophysical techniques employed include the immersion-saturation method, mercury and helium porosimetry, and the radial diffusion-cell method.

Mudrock specimens for analysis were sampled from the Conasauga Group on the ORR. Overall, 200 specimens were analyzed (132 with the immersion-saturation method, 33 with helium porosimetry, 33 with mercury porosimetry, and 2 with the radial diffusion-cell method).

Values of effective porosity for mudrock of the Conasauga Group are much higher than values previously considered characteristic (i. e., 0.1% to 3.4%). Mean values of 9.90% (immersion-saturation method), 8.1% (helium porosimetry), and 3.8% (mercury porosimetry) are reported. The majority of sampling intervals display high and corresponding effective porosity values based on the immersion-saturation method and helium porosimetry, accompanied by low values based on mercury porosimetry. This discrepancy can be explained by the fact that mercury porosimetry is not able to invade pore spaces accessed by pore throats <3 nm. Apparently, much pore space is sheltered behind access pore-throats of sizes <3 nm. Other sampling intervals display effective porosity values which are low and congruent based on the different measurement techniques. Some deviating values based on helium porosimetry apparently indicate measurement difficulties. The effective porosity data generated with the radial diffusion-cell method compare favorably with values obtained with other methods from the same/adjacent core intervals.

Effective porosity values based on the immersion-saturation method are judged as the most reliable. The data have to be considered maximum values, however, because it was not obtained under in situ conditions and because of the probable loss of

replaced meteoric cement. Both factors, nevertheless, are judged to exert only a small influence on effective porosity.

The majority of pore-throat-sizes lies between 3 nm and 100 nm (the minimum value is determined by equipment limitations). The shape of the size-distribution curves is predominantly unimodal (some bimodal) with the mode situated consistently within the 5 nm-size class. This set of data may be useful for evaluating the ability and extent of contaminant species to access the interconnected pore space of the mudrock matrix through diffusion. Data on specimen bulk-density and specimen grain-density display a mean of 2.71 $g \cdot cm^{-3}$ and 2.77 $g \cdot cm^{-3}$, respectively.

The reported pore-space characteristics reflect the importance of the diagenetic history of the Conasauga Group mudrock. Pervasive chemical diagenesis - progressive cementation and/or the development of secondary dissolution pores - most likely acted as the prime determinant for the measured values.

The successful application of the immersion-saturation method, helium porosimetry and mercury porosimetry provided a powerful combination for determining the pore-space characteristics of Conasauga Group mudrock on the Oak Ridge Reservation. Based on the research conducted for this report, the immersion-saturation method is judged to be superior to both mercury and helium porosimetry for the determination of effective porosity of Conasauga Group mudrock. The difficulty to obtain and preserve cylindrical mudrock specimens, however, necessitates the petrophysical determination of accurate specimen bulk-densities before effective porosity based on the immersion-saturation method can be calculated. The radial diffusion-cell method yielded promising results and should be tested further provided that more and better suited specimens become available.

President Llamas, in the very beginning of our symposium, talked about hydrogeology as the interaction between hydrology and the rock matrix. This symposium has been dominated by the water aspect and has had very little discussion of the geologic aspect. I think this is very prevalent through the whole hydro sciences, or whole hydrogeologic sciences, and we don't have a strong enough emphasis in understanding the geology of the system. And quite often in particular, say a low permeability system, we can use the geology as effectively as we can possibly use the hydrology of that system, in that we may not be able to do the field testing, develop the mathematical models on this sort of thing, but, if we had the rock itself and we knew the diagenetic history, we could understand far more of how that rock was functioning as an aquitard than we can with numerical models. And similarly, when we do numerical modeling and we're getting into stochastic aspects of numerical modeling, what we're doing is we're looking at the statistical variability of a parameter, such as head, or another hydrologic parameter. But, what is controlling the statistical variability of that hydrologic parameter is statistical variability of a geologic parameter. We don't do enough at looking at those geologic parameters to understand how they impact the hydrology.

Charles Kreitler

(Panel Discussion, Symposium on Hydrogeology of Rocks of low Permeability, Tucson, Arizona 1985)

PURPOSE

The purpose of this study was to apply and to test the suitability of different petrophysical techniques, identified in an earlier research project (Dorsch, 1995), to quantify the pore characteristics of mudrock[1] from the Oak Ridge Reservation (ORR). The first specific aim was to compare the performance of the different petrophysical techniques and to present recommendations on their usefulness for the investigation of the pore characteristics of mudrock. The second specific aim was to obtain quantitative data on the effective porosity of mudrock from the Conasauga Group. Accurate knowledge of this data is essential for the evaluation of contaminant transport by matrix diffusion within the low-permeability sedimentary rocks of the Conasauga Group. An additional aim was the determination of petrophysical data, such as mudrock grain- and bulk-densities, and the sizes of pore-throats and their distribution.

---

[1] the term mudrock is used throughout this report for all types of fine-grained siliciclastic rock; it follows the definition of Blatt et al. (1980); the Conasauga Group mudrock samples used in this study are predominantly mudstone and claystone, with smaller amounts of mud-shale and clay-shale; no siltstone or silt-shale samples were used; furthermore, no marlstone samples were used.

INTRODUCTION

Mudrock samples from all stratigraphic units of the Conasauga Group from both the Copper Creek and Whiteoak Mountain thrust sheets were analyzed, with the exception of the Maynardville Limestone. Petrophysical techniques employed include the immersion-saturation method, helium porosimetry, mercury porosimetry and the radial diffusion-cell method. Petrophysical data obtained with the laboratory experiments include effective porosity, pore-throat sizes and their distribution, specimen bulk-density, and specimen grain-density. The data on effective porosity and density are the first from the ORR based on modern analytical techniques, and the data on pore-throat sizes are new. It is expected that the data from this study will significantly contribute to constraining the modeling of the hydrologic behavior of the mudrock-dominated Conasauga Group, the most significant aquitard on the ORR.

Matrix Diffusion and Effective Porosity

Effective porosity is defined as the ratio of volume of interconnected pore space to total volume of a rock sample. Effective porosity is believed to be an important parameter that controls the extent and effectiveness of diffusive processes within fine-grained siliciclastic rocks (e. g., Germain and Frind, 1989; Toran et al., 1995). The importance of matrix diffusion as an agent for efficient material transport in the fractured low-permeability sedimentary rocks and saprolite at the ORR was pointed out by Wickliff et al. (1991), Solomon et al. (1992), Shevenell et al. (1994), and Sanford et al. (1994).

Figure 1 illustrates the potential importance of matrix diffusion for contaminant transport within fractured low-permeability sedimentary rocks. Contaminated water actively moves through the interconnected fracture network, but through the process of diffusion contaminants are able to access the interconnected pore space of the surrounding matrix blocks (there also may be access of contaminants to the matrix pore-space through active flow, albeit at very slow rates). Access to the pore water of the mudrock matrix is through matrix pores connected to the fracture network. The result of this mass transfer by diffusion will be an apparent retardation of the spread of the contaminant species carried by water within the interconnected fracture network (e. g., Neretnieks, 1980, Tang et al., 1981; McKay et al., 1993). This scenario will develop while the primary contaminant source is present and active. After removal of the primary contaminant source, either through remediation efforts or through simple
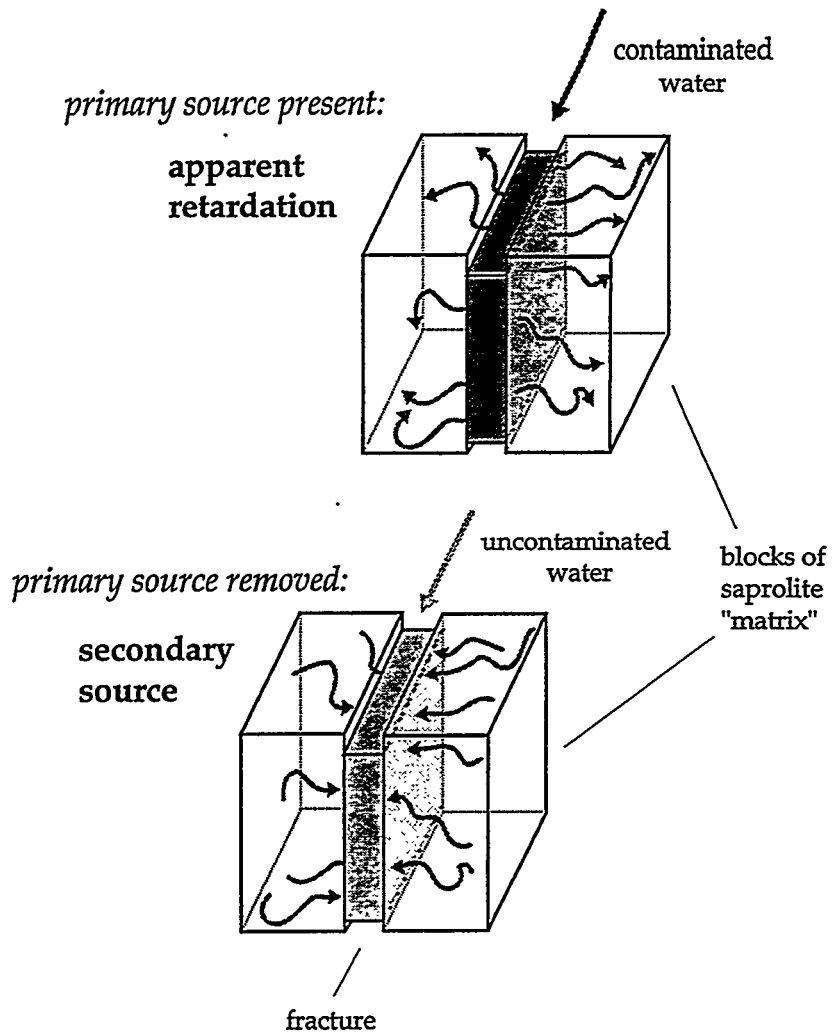
Fig. 1: Schematic block diagrams illustrating the diffusion of contaminant species from a fracture into the surrounding mudrock "matrix" (apparent retardation) and vice versa (secondary contaminant source).

depletion, the direction of diffusion will reverse. Contaminants will diffuse out of the matrix into the fracture network now occupied by uncontaminated water. This will lead to the development of a secondary contaminant source, which might be active for a long period and which will be very difficult and expensive to remediate because of the required long time spans for removing the contaminants from the matrix pore space (e. g., Germain and Frind, 1989; McKay et al., 1993). Accurate knowledge of effective porosity, therefore, is important for modeling and evaluating the possible apparent retardation of contaminant spread and the possible development of secondary contaminant sources within fractured mudrock (Toran et al., 1995).

The effective porosity of the Conasauga Group mudrock matrix consists of two components. One is the primary sedimentary porosity and the other component is microfractures. The primary sedimentary porosity developed following deposition and after experiencing compaction and chemical diagenesis (cementation, dissolution). Microfractures are considered tectonic in origin and are small enough to be part of the mudrock matrix. They do not cause the mudrock sample to fall apart into smaller blocks which might indicate that they are isolated from the interconnected fracture network. The tectonic origin of the microfractures remains speculative, however, because detailed petrographic investigations addressing this question are lacking.

The effective porosity data reported in this document are a measure of the space potentially available for diffusive processes. For all potentially available pore space to be tested, the mudrock samples were dried to an extent (see page 17 and following) to ensure that all water not part of the clay-mineral structure was driven off (see Dorsch, 1995). It is important to note, however, that some aspects have to be considered. The effective porosity will be used for diffusion in its entirety only, if it is saturated with water. Furthermore, the physical boundaries of the pores and pore throats will have a considerable effect on the water contained within the pore space and attached to the physical boundaries. Water close to solid surfaces will be strongly modified in its properties for a distance of 2 to 5 molecular layers (termed nonordinary water; Grim, 1962; Bush and Jenkins, 1970, Drost-Hansen, 1991) or up to 50 molecular layers (termed vicinal water; Drost-Hansen, 1991) influencing the diffusion characteristics of chemical species. It is, therefore, probably not correct to equate the measured effective porosity to volume of ordinary (bulk) water and its ordinary properties including diffusion characteristics. A correction might be necessary to the measured effective porosity values to estimate what part is used *efficiently* by diffusive processes. Another consideration is the extent of microfractures induced during core drilling (coring induced

fractures). Macroscopic fracturing and breaking will not be an obstacle to determining effective porosity, because it simply would cause the mudrock samples to fall apart into smaller blocks. Microfracturing, however, will lead to an increase of laboratory-measured effective porosity. To what extent this latter process was active could not be determined on the mudrock specimens of the Conasauga Group. And last, the effective porosity available in situ might be somewhat less than the values obtained in the laboratory under surface conditions because of loss of confining pressure. How large such a deviation will be is not known. The Conasauga Group mudrock, however, was buried considerably and experienced significant chemical diagenesis (see below) which led to a thorough lithification. Furthermore, the Conasauga Group mudrock was uplifted from basinal depths during and following the Alleghanian orogeny resulting in significantly reduced in situ confining pressures from present retrieval depths of less than 400 m. Therefore, elastic rebound of the mudrock matrix upon retrieval of the cores from the corehole can be considered small or nonexistent.

Geologic Framework for Conasauga Group Mudrock at the Oak Ridge Reservation

The Oak Ridge Reservation is situated within the Appalachian Valley-and-Ridge physiographic province, which corresponds to the Alleghanian foreland fold-and-thrust-belt. Stratigraphic units contained within different thrust sheets range in age from Early Cambrian to Early Pennsylvanian and are repeated and stacked (Figure 2; Hatcher et al., 1992), because the original fill of the Appalachian basin was deformed during thrusting associated with the Alleghanian orogeny. The stratigraphic units on the ORR have been grouped into regional aquifers and aquitards (Figure 3; Solomon et al., 1992).

The mudrock-dominated Conasauga Group (Middle and Late Cambrian) appears within the Copper Creek thrust sheet and the Whiteoak Mountain thrust sheet (Figure 4). The stratigraphic units underlie Melton Valley in the Copper Creek thrust sheet and Bear Creek Valley in the Whiteoak Mountain thrust sheet. Information on pore-space characteristics is especially important for the Conasauga Group, because the majority of waste sites on the ORR are constructed on these rocks.

The Conasauga Group represents the fill of a Middle to Late Cambrian intrashelf basin that developed on the Laurentian passive continental margin bordering the evolving Iapetus ocean (Markello and Read, 1981, 1982; Read, 1989; Srinivasan and Walker, 1993). The fill constitutes an alternation of mudrock- and carbonate-dominated stratigraphic units (Rodgers, 1953; Hasson and Haase, 1988; Walker et al., 1990).
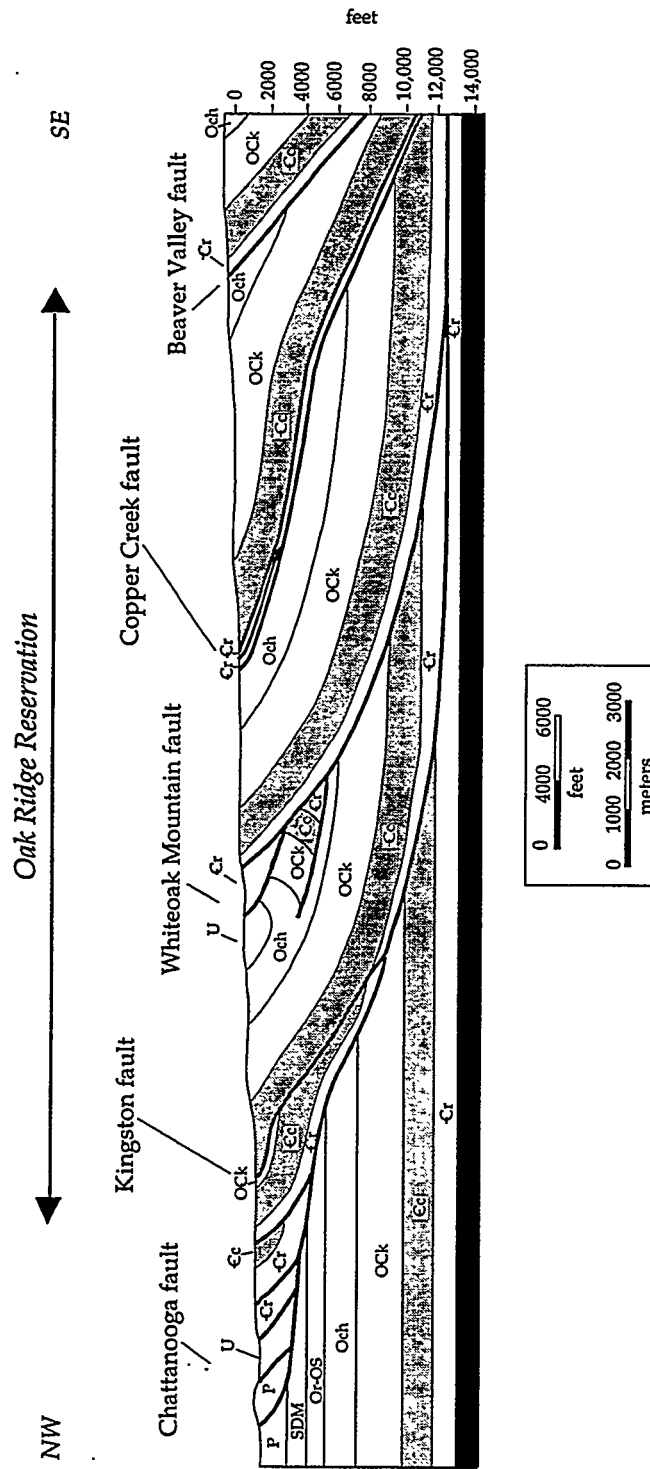
Fig. 2: Generalized geologic cross section through part of the Alleghanian fold-and-thrust belt at the longitude of the Oak Ridge Reservation (ORR). The stippled bands outline the Conasauga Group stratigraphic units (including the Maynardville Limestone), black outlines Precambrian basement (modified from Hatcher et al., 1992). Explanation of stratigraphic symbols: U = undifferentiated, P = Pennsylvanian, SDM = Silurian-Devonian-Mississippian, Or-Os = Reedsville Sh.-Sequatchie Fm., Och = Chickamauga Grp., OCk = Knox Grp., Cc = Conasauga Grp., Cr = Rome Fm.
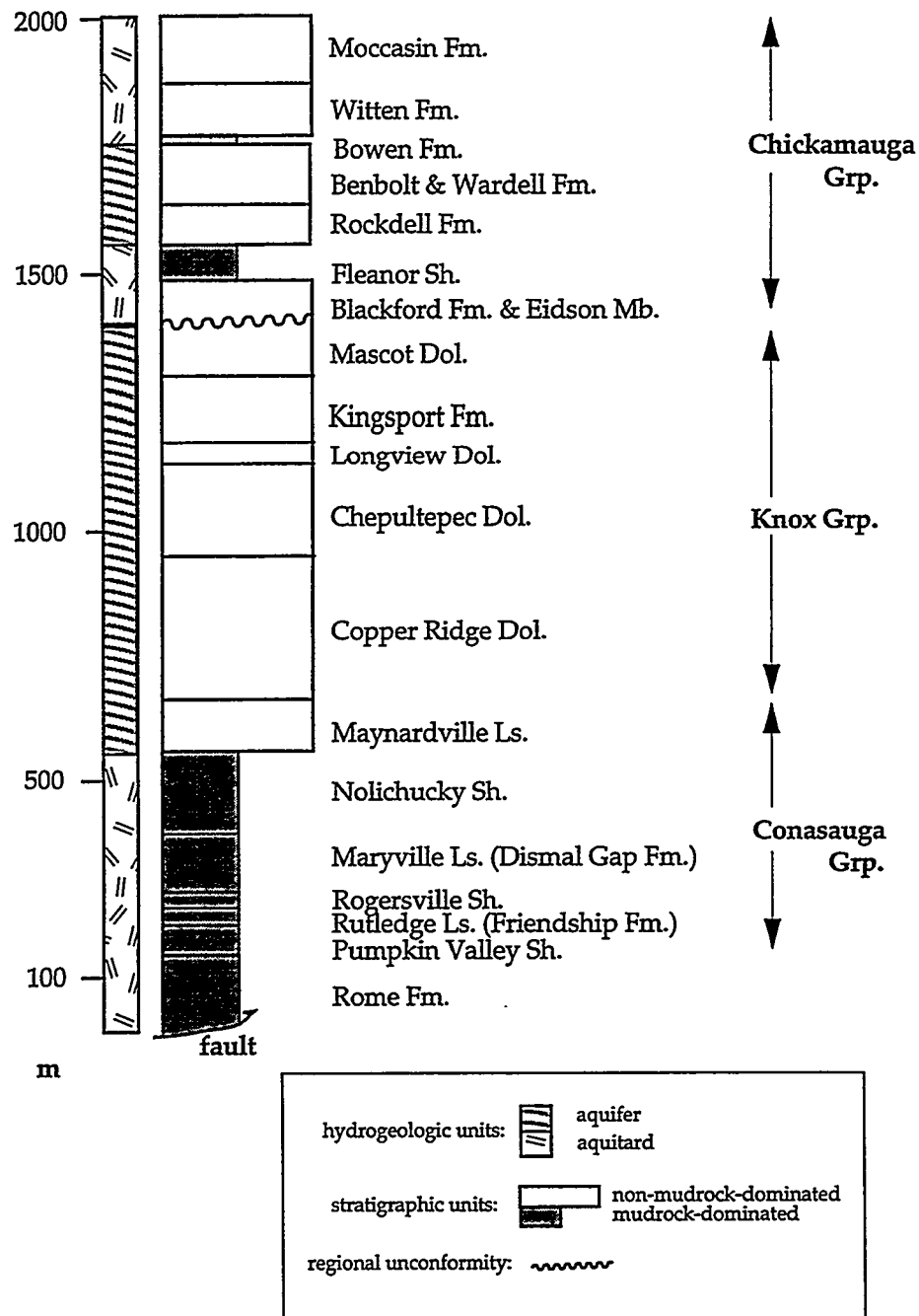
Fig. 3: Stratigraphic section for the Copper Creek and Whiteoak Mountain thrust sheets on the ORR. The vertical axis is in meters and displays the importance and stratigraphic distribution of mudrock-dominated stratigraphic units. Thickness values are averages of measured stratigraphic thicknesses. Thickness data and distribution of aquifer and aquitard hydrostratigraphic units are derived from Hatcher et al. (1992) (modified from Dorsch, 1995).

8

Fig. 4: Generalized location map. Dark stippled bands traversing the ORR outline the mudrock-dominated part of the Conasauga Group in outcrop. Barbed solid black lines indicate the location of the Whiteoak Mountain fault and of the Copper Creek fault, whereas stippled lines indicate major roads. Triangles refer to the location of coreholes from which specimens were selected: corehole Wol-1, corehole 0.5MW012A, and coreholes GW-132, -133, -134. The line connecting A and A' depicts the approximate surface trace of the cross section shown in Figure 6 (based on Hatcher et al., 1992).

9

In the area of the ORR, the Conasauga Group is dominated by mudrock (Hatcher et al., 1992; Figure 5) in contrast to well studied areas to the southeast (e. g., Srinivasan and Walker, 1993). Hatcher et al. (1992) proposed the names Dismal Gap Formation (informal) to replace Maryville Limestone, and Friendship Formation (informal) to replace Rutledge Limestone in order to reflect this characteristic. The formal stratigraphic nomenclature, however, is retained in this report.

Only limited mineralogical and petrological data are available for the Conasauga Group mudrock on the ORR. Mineralogical investigations indicate that mudrock of the Conasauga Group is illite rich with smaller amounts of chlorite and kaolinite in the clay fraction (Lee et al., 1987; 1991, Baxter, 1988; see also Weaver, 1984). Other minerals include quartz and feldspar (<22 %), glauconite and carbonate minerals. Of importance is the absence of smectites, whose swelling nature might preclude the accurate and reliable application of petrophysical techniques (Krushin, 1993).

Of special significance for the pore characteristics is the diagenetic history of the mudrock. Compaction of freshly deposited mud and mudrock is the primary determinant in reduction of original sedimentary porosity. Data on the maximum burial of Conasauga Group mudrock of the Whiteoak Mountain thrust sheet was provided by Foreman (1991). According to basin-subsidence modeling the Conasauga Group mudrock experienced burial of up to 4 km. Structural evidence, however, indicates that the Copper Creek thrust sheet was on top of the Whiteoak Mountain thrust sheet following the Alleghanian orogeny (P. Lemiszki, pers. comm.), thus making a larger burial depth more likely. Conasauga Group strata in Virginia are believed to have been buried to between 6 and 8.5 km (Mussman et al., 1988; Montanez, 1994).

Chemical diagenesis (later-stage precipitation and dissolution of cements) can have a marked effect on the pore characteristics of mudrock (e. g., Katsube and Williamson, 1994). Based on TEM and SEM analysis Lee et al. (1987, 1991) report a general paucity of cement in mudrock samples of the Nolichucky and Pumpkin Valley shales, and the occurrence of micropores. Nevertheless, pore filling organic matter (?), calcite, authigenic quartz, and framboidal pyrite was found. Sample coverage from the Nolichucky and Pumpkin Valley shales, however, was very limited. Only two 1 m-intervals from the core of the Joy-2 well in the Copper Creek thrust sheet were sampled. Baxter (1988) conducted a more detailed investigation of the diagenetic history of the Pumpkin Valley Shale from the Copper Creek thrust sheet. She noted the following (chemical) diagenetic events: 1) crystallization of framboidal and authigenic pyrite, 2) glauconite formation and alteration, 3) formation of pseudohexagonal kaolinite booklets,
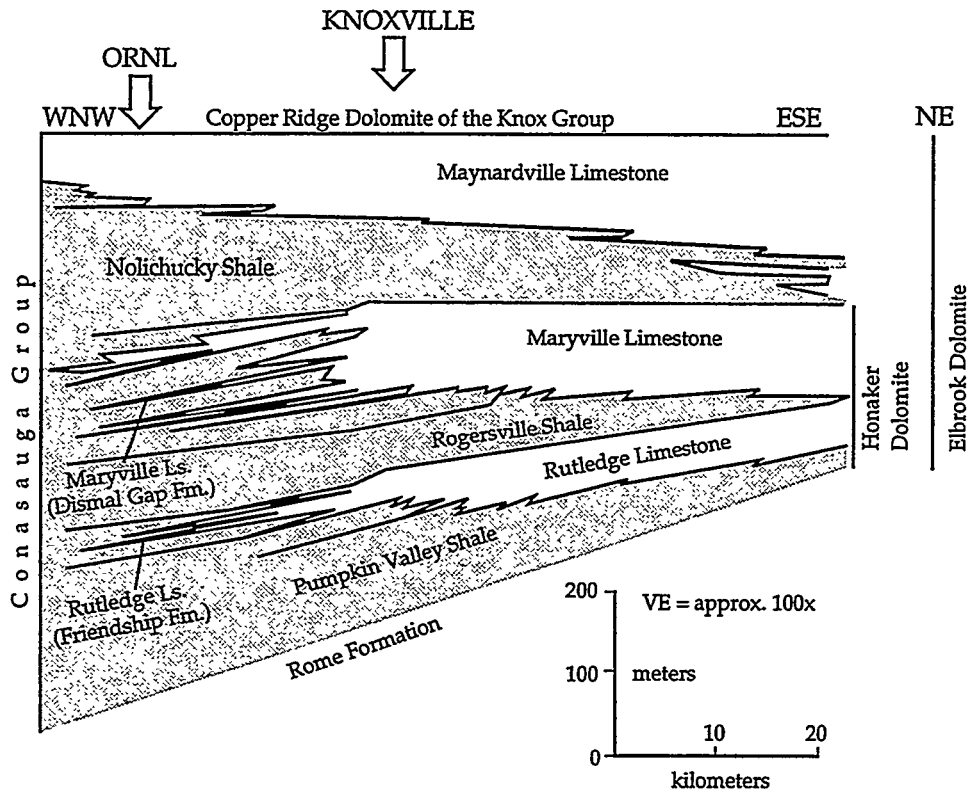
Fig. 5: Stratigraphic cross section of the Conasauga Group along an
ESE to WNW transect. Stipple pattern denotes the predominance of mudrock,
whereas the unpatterned part of the cross section denotes the predominance
of carbonate rock. Note the increase in mudrock away from the eastern carbonate-
dominated area, and the proposed change in stratigraphic nomenclature within the
area of the ORR (informal stratigraphic designations provided in parentheses);
(modified from Walker et al., 1990, Hatcher et al., 1992; based on Rodgers, 1953).

4) formation of authigenic quartz-overgrowths, 5) feldspar dissolution, 6) illitization and chloritization of kaolinite and chloritization of biotite, 7) crystallization of fine-grained kaolinite, 8) precipitation of carbonate cement, and 9) crystallization of barite associated with carbonates. Precipitation of mineral phases will lead to a reduction in primary porosity, whereas dissolution of feldspar will lead to the development of secondary porosity. Pseudohexagonal kaolinite is only a minor diagenetic phase (Baxter, 1988) but, together with the quartz-overgrowths, will lead to a reduction in porosity. The secondary porosity developed through feldspar dissolution is thought to be counterbalanced by the ubiquitous pore-filling fine-grained kaolinite (Baxter, 1988). The carbonate cement is important for its presence and especially for the patchiness of its occurrence.

Data on the porosity of Conasauga Group mudrock available until now is very scarce. Porosity values provided by deLaguna et al. (1968), Diment and Robertson (1963), and Goldstrand and Menefee (in preparation) range between 0.1 and 3.4% (Table 1). No discussion of the measurement technique was furnished by deLaguna et al. (1968) and Diment and Robertson (1963), but some form of water-immersion/drying technique apparently was used. Goldstrand and Menefee (in preparation) used a bulk specific gravity method. Based on the methodologies employed the reliability of the currently available porosity values for Conasauga Group mudrock have to be questioned.

Table 1: Summary of effective porosity data of mudrock from the ORR reported in earlier studies. Sources are Diment and Robertson (1963), deLaguna et al. (1968), and Goldstrand and Menefee (unpublished data). Methods employed were versions of the immersion-saturation method for the first two sources and a bulk specific gravity method for Goldstrand and Menefee.

source	corehole	strat. unit	drill depth [m]	eff. porosity [%]
Diment and Robertson	Joy-1	?	?	2.2
deLaguna et al.	Joy-1	?	47.2	1.3
"	"	?	154.8	1.1
"	"	Pumpkin Valley Sh.	201.2	0.46
"	"	Pumpkin Valley Sh.	219.2	1.1
"	"	Pumpkin Valley Sh.	244.2	1.9
Goldstrand and Menefee	05MW013A	Maryville Ls.	52.1	0.4
"	"	Maryville Ls.	52.7	0.1
"	"	Maryville Ls.	57.9	1.1
"	"	Maryville Ls.	58.5	0.4
"	"	Maryville Ls.	65.1	0.3
"	"	Maryville Ls.	66.1	1.5
"	"	Maryville Ls.	71.8	0.7
"	"	Maryville Ls.	73.0	0.1
"	"	Maryville Ls.	77.0	2.0
"	"	Maryville Ls.	80.2	0.8
"	"	Maryville Ls.	81.7	1.9
"	"	Maryville Ls.	83.5	2.7
"	"	Maryville Ls.	93.9	1.5
"	"	Maryville Ls.	94.6	1.9
"	"	Rogersville Sh.	105.8	3.4
"	"	Rogersville Sh.	107.3	1.8
"	"	Rogersville Sh.	115.9	1.3
"	"	Rogersville Sh.	116.3	0.9
"	"	Rogersville Sh.	122.7	1.0
"	"	Rogersville Sh.	130.8	2.3
"	"	Rogersville Sh.	132.6	1.3
"	"	Rogersville Sh.	135.3	1.4
"	"	Rogersville Sh.	138.1	2.1
"	"	Rogersville Sh.	141.4	1.7
"	"	Rogersville Sh.	141.7	1.6
"	"	Rogersville Sh.	147.2	0.8
"	"	Rogersville Sh.	151.5	0.6

SAMPLING[2]

Cores

Mudrock specimens for the petrophysical measurements were obtained from coreholes drilled into the Whiteoak Mountain and Copper Creek thrust sheets. From the Whiteoak Mountain thrust sheet, cores GW-132, GW-133, and GW-134 (Figure 6) were used, and from the Copper Creek thrust sheet, cores Wol-1 and 0.5MW012A were used (Figure 4). For both thrust sheets, specimens were selected from each of the mudrock-dominated stratigraphic units of the Conasauga Group (i. e., Nolichucky Shale, Maryville Limestone, Rogersville Shale, Rutledge Limestone, and Pumpkin Valley Shale; Figure 5).

Sampling Intervals

The cores were inspected visually and sampling intervals were selected. Selection criteria were: a) macroscopic homogeneity of the sampling interval, b) absence of excessive deformation, c) mudrock lithology, d) stratigraphic coverage. A sampling interval is generally ≤ 30 cm in length and was used for obtaining specimens for the different petrophysical measurement techniques. Appendix II gives an overview of the selected sampling intervals (core, drill depth, stratigraphic unit). Overall, 42 sampling intervals were selected from the different cores.

Specimens for Helium Porosimetry, Mercury Porosimetry, and the Immersion-Saturation Method

Specimens from each sampling interval fall into two types: irregularly shaped specimens and cylindrically shaped specimens. The specimens, regardless of shape, were generally <10 g. Both types of specimens were obtained as close to the center of core segments as possible. This was planned to avoid marginal areas of the cores which might have been affected by invading drilling fluids and clay detritus, or coring-induced microfracturing. In addition, macroscopically visible mineralized fractures were also avoided.

---

[2]note: see Appendix I for a detailed explanation of the notation system for cores, sampling intervals, and specimens.

S3 POND-AREA CROSS SECTION

* OFFSET FROM SECTION LINE
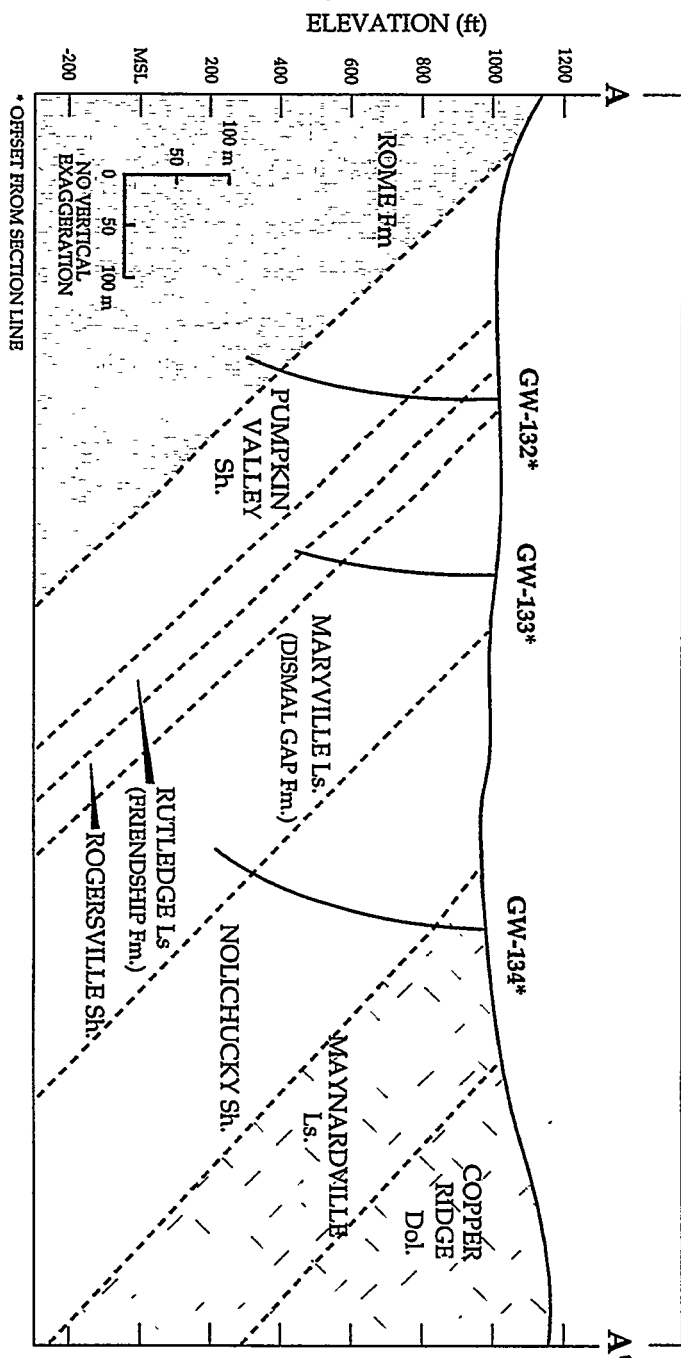
Fig. 6: Schematic cross section along section line A to A' (see Fig. 4). The stippled pattern highlights the clastic redbed succession of the Rome Formation, the cross-hatched pattern indicates the carbonate rocks of the (lower) Knox aquifer (Copper Ridge Dolomite, Maynardville Limestone), whereas the unpatterned part of the cross section refers to the mudrock-dominated units of the Conasauga Group (Nolichucky Shale, Maryville Limestone, Rogersville Shale, Rutledge Limestone, Pumpkin Valley Shale); stratigraphic names in parantheses (Dismal Gap Formation, Friendship Formation) are informal stratigraphic designations introduced by Hatcher et al. (1992). Location of wells GW-132, -133, and -134 are shown together with the stratigraphic units penetrated by each well (modified from Dreier and Koerber, 1990).

Irregularly shaped specimens were pieces of mudrock broken off of core segments. Pocket knife, small hammer, kimwipe® tissues to soften light blows with the hammer, small flat-head chisel for splitting rocks along bedding planes, nail clippers, and pliers were used to obtain the specimens. Overall, 186 irregularly shaped specimens were analyzed with the different petrophysical techniques (120 with the immersion-saturation method, 33 with helium porosimetry, 33 with mercury porosimetry).

The cylindrically shaped specimens were obtained by drilling core plugs of various lengths from coherent core segments at the University of Tennessee Engineering Machine Shop. These core plugs were drilled using a drill press with a 1 in inner diameter diamond coring bit and tap water as coolant. A coring bit with an outer diameter of 3/8 in was also used in a few instances. Thirty-four core segments were taken for drilling, from which 26 usable core plugs and parts of core plugs were obtained. Some core segments yielded several potentially useful specimens, because core plugs could be split easily along bedding providing several cylinders. The core plugs were then lightly abraded at the ends with 220 - 400 grit sandpaper and measured with a caliper and straight-edged rulers to ensure that the surfaces were parallel and flat. Twelve usable cylinders with a length of generally ≤0.75 cm were finally available for testing with the immersion-saturation method.

Specimens for the Radial Diffusion-Cell Method

Sealed mudrock intervals from core 0.5MW012A were used for the radial diffusion-cell method. Coring was accomplished in February and March of 1994. Mudrock intervals were wrapped into cellophane paper and then immediately sealed (airtight) into thick aluminum foil upon retrieval from the corehole. Sealed intervals of mudrock are necessary for the radial diffusion-cell method to ensure continued saturation of the specimens for the experiment (see below). Overall, 11 sealed intervals with a length between 4.6 and 15.2 cm were available. Of these intervals 8 were of sufficient length and apparent structural integrity. After opening the original seals most mudrock intervals proved to be unsuitable because they broke along bedding into smaller segments. Only 3 core segments were of sufficient integrity and length to be potentially useful. The ends of these 3 core segments were trimmed flat and parallel with a diamond trim saw using tap water as a coolant. Following this, two core segments were coated at the sides with a rubber heat-shrink mantle using a heat gun; the third core segment was too short for this procedure. Breaking of the original seal, inspection, trimming, and rubber mantling were accomplished within 30 minutes to minimize loss of

fluid from the core segments; the core segments were then covered with cellophane and immersed in water within plastic sample containers. Inner reservoirs were drilled at the University of Tennessee Engineering Machine Shop (equipment described above, core bit of 3/8-in outer diameter) providing two core segments for laboratory experiments.

PETROPHYSICAL MEASUREMENT TECHNIQUES

Effective porosity values for Conasauga Group mudrock from the ORR were obtained by using a suite of laboratory-based petrophysical techniques. These techniques include helium porosimetry, mercury porosimetry, the immersion-saturation method, and the radial diffusion-cell method. The first three techniques are well established and are commonly used for determining the effective porosity of hydrocarbon reservoir rocks. These techniques, however, have also been applied to fine-grained, low-permeability deposits, such as mudrock (Issler and Katsube, 1994; Loman et al., 1993; Katsube et al., 1992a; Katsube and Scromeda, 1991; Katsube and Best, 1992; Soeder, 1988). All of these techniques generate porosity data using a sample size commonly less than 10 g.

The radial diffusion-cell method is a new technique (van der Kamp et al., in press; Novakowski and van der Kamp, in press). In contrast to the first three techniques, it determines the effective porosity over a larger volume of rock material. For the experiments reported here, the chosen core segments were about 50 times the volume of the specimens used for the other porosimetry techniques.

The specimens used for helium porosimetry, mercury porosimetry, and the immersion-saturation method were dried at temperatures above 100°C. This was done to ensure the measurement of all interconnected pore space available for water storage. Drying of specimens above 100°C will drive off all pore water in the specimen and all water adsorbed to clay minerals (Scromeda and Katsube, 1993). It will not affect the crystal-lattice water, which is part of the clay minerals (Dorsch, 1995).

Immersion-Saturation Method

Principle. The immersion-saturation method is based on determining the difference in specimen weight between the fully saturated state and the dry state of the sample. Re-saturation of the specimen with a liquid (deionized water) is assumed to penetrate all of the interconnected pore space (Katsube et al., 1992a; Katsube, 1992).

Effective Porosity. Effective porosity can be calculated by:

$$\phi_I = \delta_r \left[(W_w - W_d) / W_d \cdot \delta_w) \right] \tag{1}$$

> ϕ_I = effective porosity (determined with the Immers.-Sat. Method)
> δ_r = bulk density of the rock specimen
> W_w = sample weight wet
> W_d = sample weight dry
> δ_w = bulk density of water.

Effective porosity can also be calculated from:

$$\phi_I = V_p / V_b \tag{2}$$

$$\phi_I = \left[(W_w - W_d) / \delta_w \right] / V_b \tag{3}$$

> V_p = pore volume of specimen
> V_b = bulk volume of specimen
> (this can easily be determined by caliper on a regularly shaped specimen [e.g., cylinder]).

$$V_b = A \cdot h \tag{4}$$

$$V_b = \pi \cdot r^2 \cdot h \tag{5}$$

$$V_b = \pi \cdot (d / 2)^2 \cdot h \tag{6}$$

> V = volume of cylinder
> h = length of cylinder
> A = area of base/top surface of cylinder
> π = constant
> r = radius of cylinder
> d = diameter of cylinder.

Procedure. The following analytical procedural steps for the immersion-saturation method were followed during the experiments (Figure 7). The procedure corresponds to the one employed at the Geological Survey of Canada (Katsube and Scromeda, 1991; Katsube et al., 1992b; Scromeda and Katsube, 1993, 1994; N. Scromeda-Perez, pers. comm. 1995).

On *day one* of the procedure, the specimens, contained in dry glass beakers, were subjected to 15 minutes of vacuum degassing using a vacuum chamber and an applied

Immersion-Saturation Method

```
Day I ──┤   ┌─────────────────────────────────────────────┐
        │   │  Vacuum Degassing at 27"-28.5" Hg            │
        │   │  15 min                                       │
        │   └─────────────────────────────────────────────┘
        │                      │
        │   ┌─────────────────────────────────────────────┐
        │   │  Saturation of Sample with Deionized (DI) H₂0 │
        │   └─────────────────────────────────────────────┘
        │                      │
        │   ┌─────────────────────────────────────────────┐
        │   │  Vacuum Degassing at 27"-28.5" Hg            │
        │   │  15 min                                       │
        │   └─────────────────────────────────────────────┘
        │                      │
        │   ┌─────────────────────────────────────────────┐
        │   │  Sample left in DI H₂0 at Atmospheric Pressure │
        │   │  24 h                                          │
        │   └─────────────────────────────────────────────┘
```

Vacuum Degassing at 27"-28.5" Hg
15 min

Saturation of Sample with Deionized (DI) H_2O

Vacuum Degassing at 27"-28.5" Hg
15 min

Sample left in DI H_2O at Atmospheric Pressure
24 h

Weigh and Inspect Saturated Sample (W_{SAT})

Oven Drying of Sample at 112°-116°C
24 h

Cool Samples in Desiccator
20 min

Weigh and Inspect Dry Sample (W_{DRY})

Day I

Day II

Day III

Fig. 7: Flow chart outlining the procedural steps for the immersion-saturation method as used for the data reported in this study. Flow chart is based on the procedure employed at the Geological Survey of Canada (Katsube and Scromeda, 1991; Katsube et al., 1992a; N. Scromeda-Perez, pers. comm., 1995).

vacuum ranging from 27 to 28.5 in Hg (68.6 to 72.4 cm). Following vacuum degassing, the hood of the vacuum chamber was removed and the specimens were submerged by filling the beakers with deionized water. Thereafter, the vacuum chamber was closed again and another period of vacuum degassing (for 15 min, at an applied vacuum between 27 to 28.5 in Hg) was administered. Day one concluded with removal of the water-filled specimen beakers from the vacuum chamber. The specimen beakers remained under atmospheric pressure for 24 h ensuring complete saturation of the specimens.

On *day two* of the procedure, one specimen at a time was carefully removed from the water-filled beaker and the water was discarded from the beaker. The specimen and the beaker were touched only with tweezers or a kimwipe® tissue. The surface of the specimen was carefully patted with a kimwipe® tissue to ensure that all surface water was removed from the specimen (no reflection sheen left), but avoiding to completely dry the surface. It is important to keep this drying process consistent for each specimen and to accomplish this task quickly. During this phase, the specimen was studied carefully for any irregularities, such as breakage. Thereafter, the specimen was weighed to determine the saturated weight (W_{SAT}). Specimen weights were recorded in g to the fourth decimal using a balance with a sensitivity of ±0.1 mg. Following weighing, the specimen was put back into an empty glass beaker and placed into an oven preheated to 112 to 116°C. The specimens remained in the oven at this temperature for 24 h to ensure complete drying of the specimens.

Day three of the procedure started with removing the specimens from the oven. The specimen beakers were quickly put into a desiccator and remained there shielded from the laboratory air for 20 min to cool. Then, one specimen beaker at a time was removed from the desiccator using tongs and weighed (see above). This step was accomplished quickly to avoid the specimen drawing moisture from the laboratory air. Following this, the specimen was removed from the glass beaker and the empty beaker was weighed. At this point the specimen was again carefully inspected for irregularities. The dry specimen weight (W_{DRY}) was determined by subtracting the weight of the beaker from the combined specimen and beaker weight.

Specimens and Decisions. Specimens for the immersion-saturation method were either of irregular shape or cylinders. Both types of specimen were handled the same way during the procedure.

The cylindrical specimens were used to determine the effective porosity only if they remained intact during the procedure. The bulk volume was determined by

measuring the dimensions of the cylinders with a caliper. Formula (6) and (3) were used to calculate the effective porosity (Appendix III).

The determination of effective porosity of the irregularly shaped specimens required data on the bulk density and the use of formula (1). Bulk densities were either determined from the mercury-porosimetry tests or were assumed in a few cases. Assumed values were constrained, however, by bulk-density values from adjacent sampling intervals. The value of effective porosity was considered reliable, if the specimen survived the experimental procedures completely intact. The value was *judged* to be reliable, if cracking occurred only after final drying (i. e., no material was lost and the specimen was intact after water saturation). A specimen exhibiting cracks following water immersion was discarded because of the artificial increase in pore space infilled with water. A specimen exhibiting disintegration following water immersion was lost for measurement. In a few cases, cracks appeared following water immersion just on the outer fringes of a specimen. If these fringe areas could be removed and the rest of the specimen remained intact, the specimen was used in the experiment. The effective porosity value of the specimen was then judged reliable (Appendix IV).

Five specimens were analyzed using a 1N NaCl solution as the saturation fluid. This was undertaken to prevent the specimen from disintegrating during water immersion. The performance of these specimens during the experiments, however, was not better than that of other specimens from the same sampling interval. Furthermore, the procedure was not repeated because of the uncertainty whether halite crystals would form within the pore-space, thus adding additional weight to the specimens following oven drying. Two observations have to be noted: 1) no halite crystals were visible on the outside of the specimens following experiments, 2) effective porosity values compare well with reliable values of other specimens from the same sampling intervals (A6, A12) when data based on both types of saturation fluids are available. The effective porosity results from these five specimens are not considered in the final evaluation.

Mercury Porosimetry

Principle. Mercury porosimetry involves the forceful injection of a non-wetting liquid (mercury) into a specimen in discrete pressure steps using a mercury porosimeter. The pressures required to force mercury into the specimen correspond to the size of the pore throats and pores (Washburn, 1921; Rootare, 1970; Wardlaw, 1976; Kopaska-Merkel, 1988; Wardlaw et al., 1988; Kopaska-Merkel, 1991). With each increasing pressure step, successively smaller pore throats are accessed by mercury. Mercury

porosimetry results are displayed as capillary-pressure curves that plot the amount of intruded mercury versus injection pressure (Figure 8). The amount of intruded mercury can be converted to volume of mercury, and the injection pressure can be converted to pore-throat diameters with the Washburn Equation (see below). Mercury porosimetry, therefore, provides quantitative information on the distribution of pore-throat sizes. The sizes of pore throats are important because they control access to pores. Pores of the same size might be accessed through throats of different sizes, but mercury enters the pore space only after a certain injection pressure is reached (Figure 9). The pore space with the larger sized pore throat will be accessed earlier than the pore space of equal size but with a smaller pore throat.

Washburn Equation. The Washburn Equation relates the amount of pressure required to force mercury into pores to the pore-throat diameter greater or equal to d (e.g., Katsube and Issler, 1993). Cylindrical pore shapes are assumed to characterize the pore system in mudrock (Katsube and Issler, 1993), and therefore

$$d = (-4\gamma \cos\theta) / p \qquad\qquad (7)$$

> d = throat size
> γ = interfacial (surface) tension (for Hg/vacuum = 0.48 N · m^{-1})
> θ = contact angle (for Hg/vacuum = 30°)
> p = intrusion pressure (MPa).

With the help of the Washburn Equation a corresponding pore-throat size can always be *calculated* from a *measured* injection pressure.

Procedure. Prior to the petrophysical measurements the specimens were dried in a vacuum oven at a temperature of 105°C for 24 h. All specimens were of irregular shape and less than 10 g (generally between 2 to 6 g). Following oven drying the specimens were cooled in a desiccator.

A Micromeritics Autopore 9200 porosimeter was employed for the petrophysical measurements. This mercury porosimeter can generate pressures from 0.14 to 420 MPa, which corresponds to an equivalent pore-throat size ranging from 10 to 0.003 μm (10000 to 3 nm). A measurement accuracy for volume of intruded mercury of ±0.0015 cm^3 or smaller, but certainly not larger, can be expected (Kopaska-Merkel, 1991).

During the petrophysical experiments the mercury-injection pressure was increased successively in discrete steps (56 steps from 0.14 to 420 MPa), more or less equally dividing the available pressure range provided by the apparatus on a logarithmic scale. Following each step, time is allotted for equilibration of the system so that no change in volume of mercury taken up by the specimen with time occurs. Equilibrium
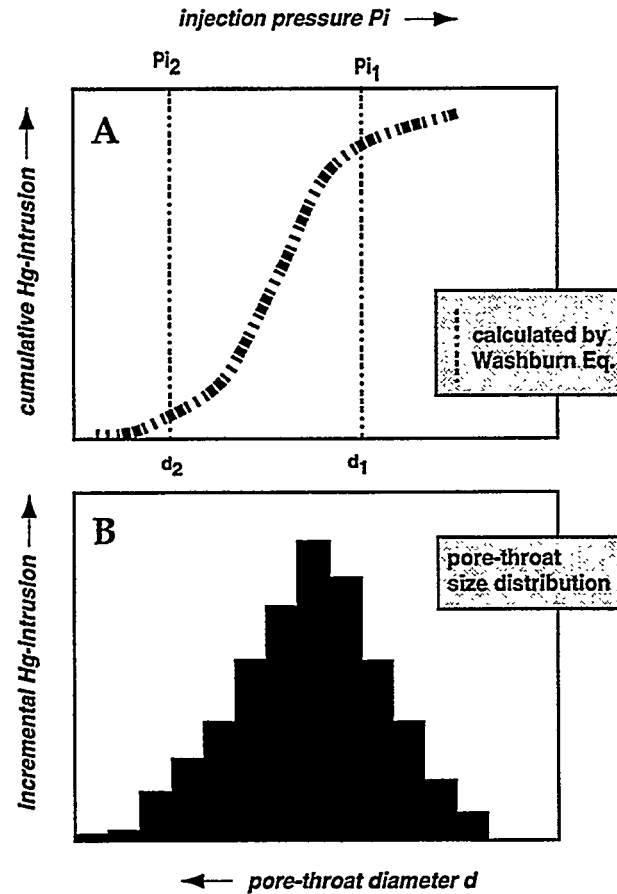
Fig. 8: Capillary-pressure curves, plotting the measured injection pressure and/or the calculated pore-throat diameter versus the amount of intruded mercury (arrows point toward higher values).
A) cumulative intrusion curve, where the total amount of intruded mercury can be read at the right-side end of the curve; d_1 and d_2 are pore-throat diameters calculated from intrusion pressures Pi_1 and Pi_2 using the Washburn Equation.
B) incremental intrusion curve showing the amount of mercury intruded at the chosen consecutive pressure steps. Note the pore-throat size distribution obtained in this way. The larger pore throats are invaded earlier at lower injection pressures (from Dorsch, 1995).
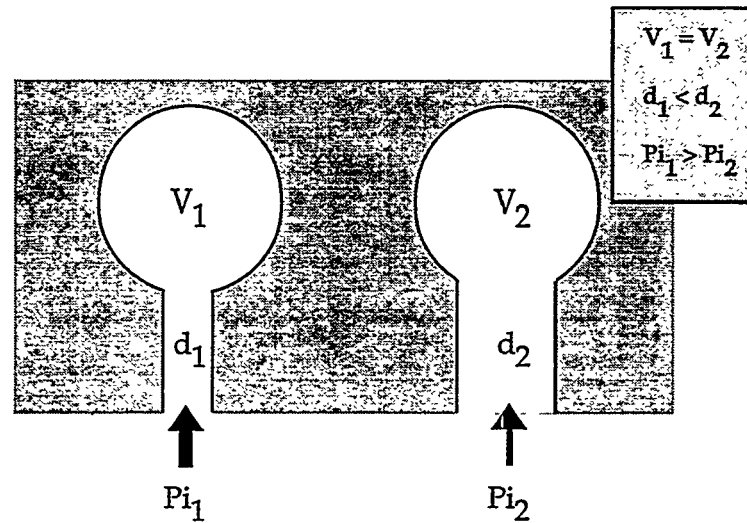
Fig. 9: Illustration of the importance of pore throats for controlling access to pores. Pores of the same size (V = volume) are accessed by pore throats of different sizes (d = diameter); mercury enters the pore throat only after an injection pressure (= Pi) is reached to force mercury through the pore throat. The pore accessed by the larger pore throat will be invaded earlier at a lower injection pressure than the pore of equal size but with a smaller entry pore-throat (from Dorsch, 1995).

times were about 40 s for high pressure steps (> 0.7 MPa) and 10 s for low pressure steps (< 0.7 MPa) (Katsube and Issler, 1993). For each pressure step the volume of mercury intruding the sample is recorded. Based on the Washburn Equation each discrete pressure step corresponds to a certain pore-throat size. The volume of mercury intruding the specimen at each discrete pressure step can be converted into the porosity for that pore-throat size and for pores accessed through pore throats of that size (Katsube and Best, 1992; Katsube and Issler, 1993).

Effective Porosity. The effective porosity of the specimen (ϕ_{Hg}) can be determined by summing up all partial porosity values. Partial porosity ϕ_a refers to the porosity contributed by each chosen range of pore-throat sizes (Katsube and Best, 1992). Partial porosity ϕ_a is calculated for each pore-throat-size range by using the volume of the intruded mercury at this size range and the bulk volume of the sample. The bulk-sample volume was determined with calculations involving the penetrometer volume and its weight (with mercury, with sample and mercury). Katsube and Issler (1993) split ϕ_{Hg} into a ϕ_{Hg1} (sum of all ϕ_a from pore-throat sizes ≤10 μm) and a ϕ_{Hg2} (sum of all ϕ_a from pore-throat sizes ≤250 μm). The reason for this split is that ϕ_{Hg2}

might contain measurement errors induced by the space left between sample and penetrometer wall. ϕ_{Hg1} is more likely to reflect a true effective porosity of the sample for pore sizes of 3 to 10000 nm.

Tabulation of partial porosities provides the distribution of pore-throat sizes for the analyzed specimen. Pore-throat-size data are grouped into size classes, with each decade of the logarithmic pore-throat-size scale being subdivided into 5 size ranges of equal physical spacing (Katsube and Issler, 1993; Katsube and Williamson, 1994).

Helium Porosimetry

Principle. Helium porosimetry is based on the Boyle-Mariotte Law. A change in gas volume or gas pressure causes a commensurate change in gas pressure or volume, given that the temperature remains constant. Important for helium porosimetry is that an increase in available space causes the gas to expand resulting in the decrease in gas pressure (American Petroleum Institute, 1960; Luffel and Howard, 1988).

Procedure. Prior to the petrophysical measurements, the specimens were dried in a vacuum oven at a temperature of 105°C for 24 h. All specimens were irregularly shaped and less than 10 g (generally between 2 to 6 g). Following oven drying the specimens were cooled in a desiccator.

For helium porosimetry the specimen is placed into a steel chamber of known volume. Helium isothermally expands into the chamber from a reservoir of known volume and pressure until equilibrium pressure is reached ≤30 min to 1 h). From the new gas pressure the grain volume can be calculated. The bulk volume of the sample is then determined by immersion of the specimen in mercury (measuring volume of mercury displaced from a pycnometer, or measuring the buoyant force, based on the Archimedes principle).

Effective Porosity. Effective porosity is calculated by subtracting the grain volume from the bulk volume, and dividing the result by the bulk volume of the specimen.

$$\phi_{He} = (V_{bimm} - V_g) / V_{bimm} \tag{8}$$

ϕ_{He} = effective porosity (determined with helium porosimetry)
V_g = grain volume
V_{bimm} = bulk specimen-volume measured with mercury immersion.

Radial Diffusion-Cell Method

Principle. The radial diffusion-cell method is based on the diffusion of a dissolved tracer from a cylindrical reservoir into the porous matrix of the surrounding rock. Due to the existing concentration gradient between the water in the reservoir and the water in the matrix, tracer will diffuse into the matrix pore-space until the gradient no longer exists. The effective pore volume of the rock is determined from the final steady-state concentration of the tracer in the reservoir.

Procedure. A cylindrical (axial) reservoir was drilled into a segment of core (Figure 10). The sides of the rock specimen were sealed with heat-shrink tubing to prevent water loss. The internal reservoir was completely filled with a NaBr solution containing 1000 ppm Br⁻ and the ionic strength adjuster required for analysis. Rubber gaskets were placed on the top and bottom of the specimen between two aluminum plates, which were tightened using connecting screws to form a water-tight seal.
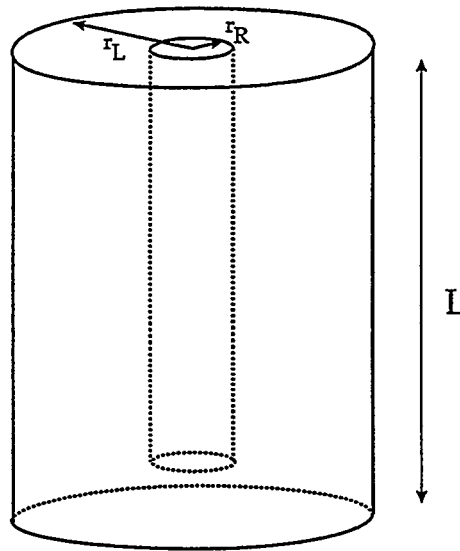
Fig. 10: Diffusion cell used for the effective porosity measurement with the radial diffusion-cell method. Abbreviations: L = length of the full core section used, r_L = full core radius, r_R = radius of the central reservoir

(from Novakowski and van der Kamp, in press).

Samples of the reservoir solution were collected periodically with a syringe by puncturing the top gasket with a needle through a small access hole in the top plate. The 2-ml sample was analyzed for Br⁻ concentration using an Orion® solid state ion-selective electrode with an Orion® single-junction reference electrode. After measurement, the sample was injected back into the reservoir.

Two specimens (C6-d, C8-d) were used for the experiments. The dimensions of the specimens are provided in Table 2. Because of some irregularities in the dimensions of the specimens and the drilled internal reservoirs, minor corrections were necessary in order to arrive at more accurate specimen and internal reservoir volumes (Table 2).

Table 2: Data on the specimens used for the radial diffusion-cell method and mass-balance calculations.

		specimen	
		C6-d	C8-d
specimen diameter [cm]	d_s	4.62	4.71
specimen length [cm]	l_s	5.60	5.45
reservoir diameter [cm]	d_r	1.22	1.23
reservoir length [cm]	l_r	4.65	4.35
specimen volume [cm³] (corrected)	V_s	95.55	94.96
reservoir volume [cm³] (corrected)	V_r	5.27	5.17
rock volume [cm³]	$V_x = V_s - V_r$	90.28	89.79
initial Br⁻ concentration	C_o		
[mg·l⁻¹]		1060 ·	1020
[mg·cm⁻³]		1.06	1.02
final Br⁻ concentration	C_f		
[mg·l⁻¹]		692	764
[mg·cm⁻³]		0.692	0.764
final reservoir-liquid volume [cm³]	V_{fl}	1.5	1.5
initial mass of Br⁻ [mg]	$M_i = C_o · V_r$	5.59	5.27

Irregularities include a small chip-off at the top of one specimen and a small piece of protruding rock remaining at the bottom of one drilled internal reservoir.

Effective Porosity. A mass-balance method was used for determining the effective porosity of the two specimens used in the radial diffusion cells. This method is a modification of a procedure used by van der Kamp et al. (in press). The concentration histories of the tracer in the reservoirs are given in Appendix V and shown graphically in Figures 11 a and b. During the tests, two problems were encountered: 1) the volume of liquid in the reservoirs of both specimens slowly decreased with time necessitating the addition of distilled water at 14:35 on 06/05/95 ; and 2) liquid was spilled during the analysis of the sample taken from specimen C8-d, requiring further addition of distilled water (at 8:23 on 06/02/95). Because of these problems, not all the data was used in the determination of effective porosity. For specimen C6-d, the data used covered 12.94 d to just prior to the addition of distilled water and for specimen C8-d, the data from the first 9.94 d was used (to just before the spill). It was assumed that both systems reached equilibrium conditions within these time intervals. Additional assumptions were: 1) the core segment was initially completely saturated with water and contained no bromide; 2) there was no bromide lost during the experiment; and 3) the core segment was completely saturated at the end of the experiment.

The effective porosity of the specimens was determined using the following equation (compare to data and abbreviations in Table 2):

$$C_f [V_{fl} + V_x \cdot \phi_{wm}] = M_i \tag{9}$$

C_f = final concentration of Br$^-$ in reservoir [mg $\cdot$ cm^{-3}]
V_{fl} = final volume of liquid in reservoir [cm^3]
V_x = rock volume [cm^3]
ϕ_{wm} = effective porosity based on radial diffusion-cell m. [cm$^3 \cdot$ cm^{-3}]
M_i = initial mass of bromide added to reservoir [mg].

Both specimens remained intact throughout the preparation process and the experiments. This was verified at the end of the experiments when the rubber sealing was removed.
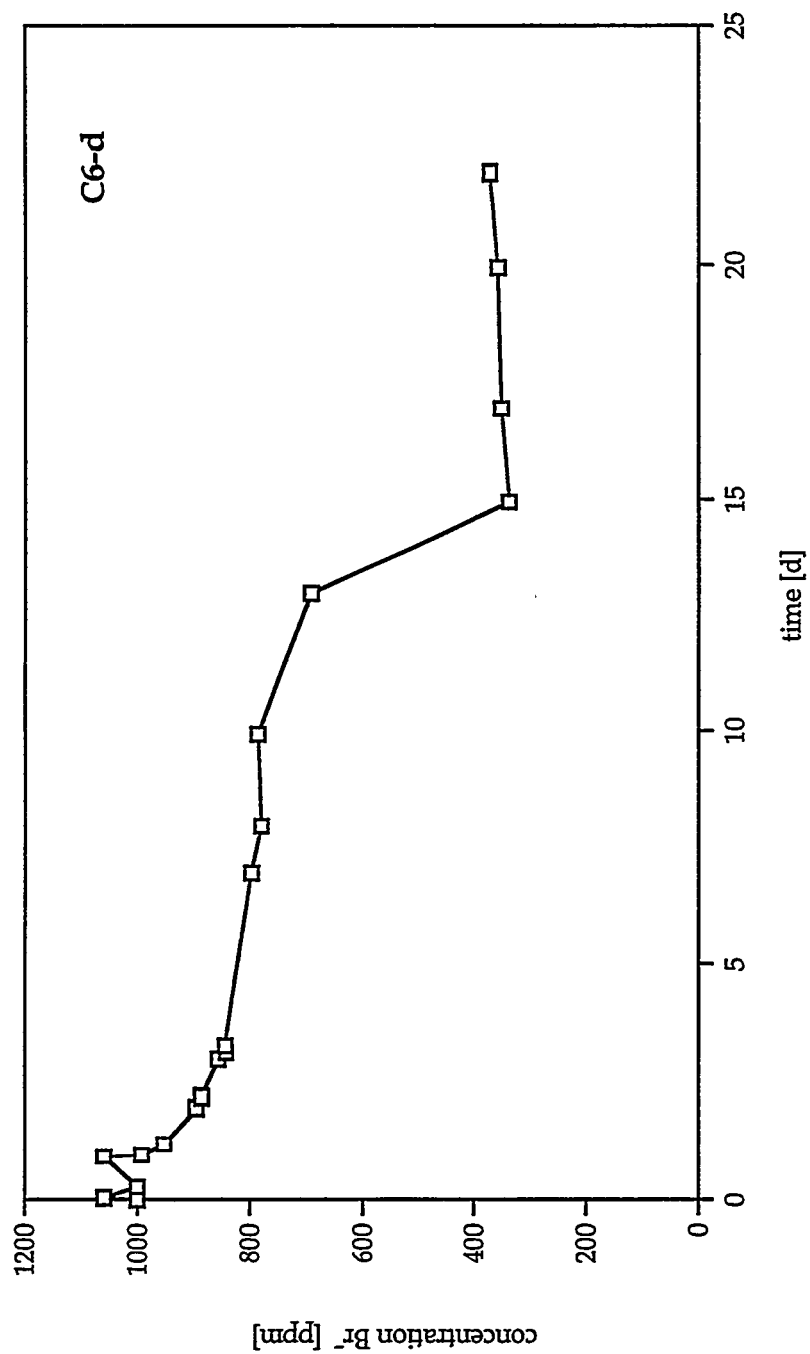
Fig. 11 a: Concentration of bromide versus time in specimen C6-d (corresponds to sample #2 in Bechtel core 0.5MW012A).
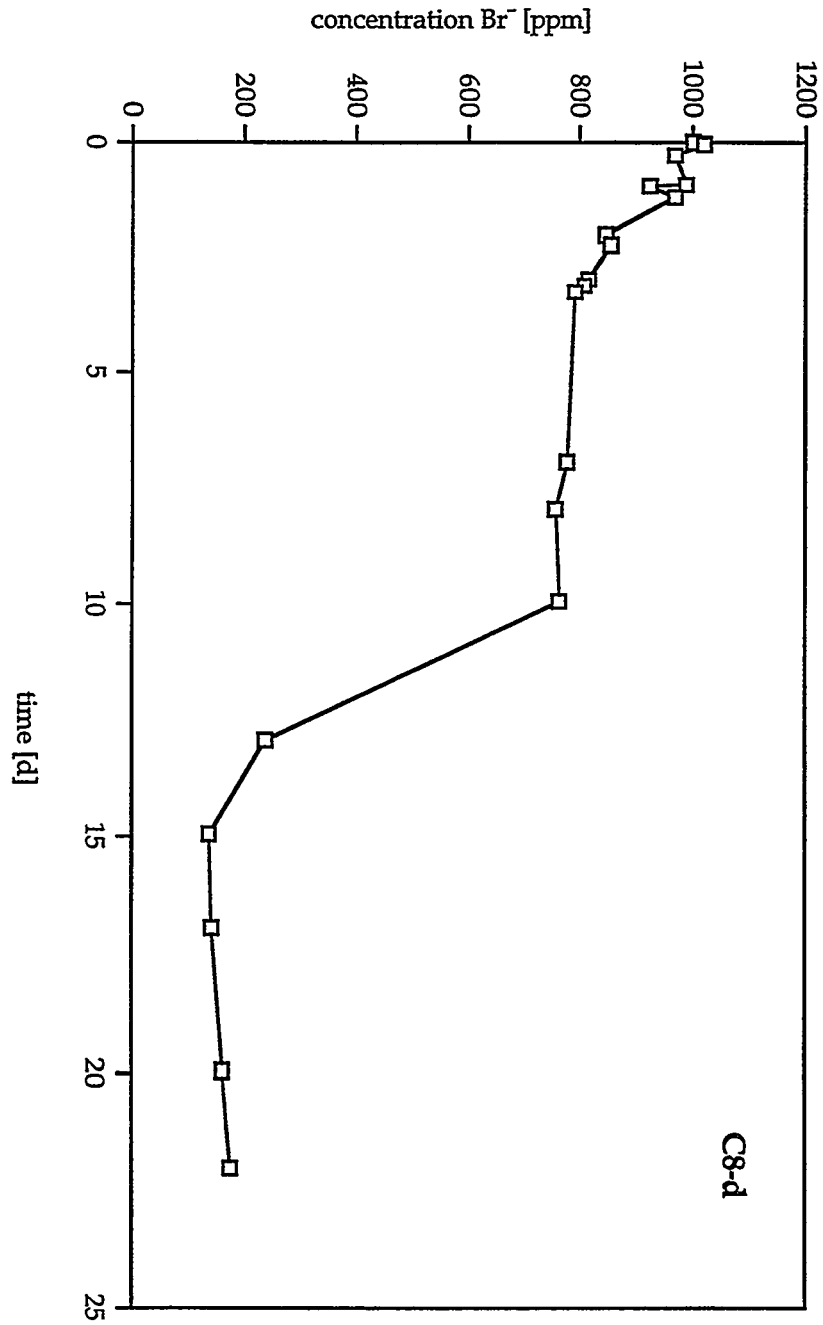
Fig. 11 b: Concentration of bromide versus time in specimen C8-d (corresponds to sample #24 in Bechtel core 0.5MW012A).

GRAIN-DENSITY AND BULK-DENSITY DATA

Specimen Bulk-Density

Thirty-three bulk density measurements were obtained from specimens during mercury porosimetry (Appendix VI). The values range from 2.67 to 2.74 $g \cdot cm^{-3}$ with a minimum value of 2.64 $g \cdot cm^{-3}$ and a maximum value of 2.77 $g \cdot cm^{-3}$ (Figure 12). The arithmetic mean for all data is 2.71 (± 0.03) $g \cdot cm^{-3}$. For the Whiteoak Mountain and Copper Creek data the means and standard deviations are 2.71 (± 0.03) $g \cdot cm^{-3}$ and 2.72 (± 0.03) $g \cdot cm^{-3}$, respectively. In general, bulk-density values are higher from the Copper Creek thrust sheet than from the Whiteoak Mountain thrust sheet on the formation level.

Table 3 gives an overview of the calculated mean values and standard deviations of bulk density for different formations. There is a considerable spread in values for particular formations, so it is important to consult the original data as provided in Appendix VI. Note also that some of the statistical measures are based on a small number of samples.
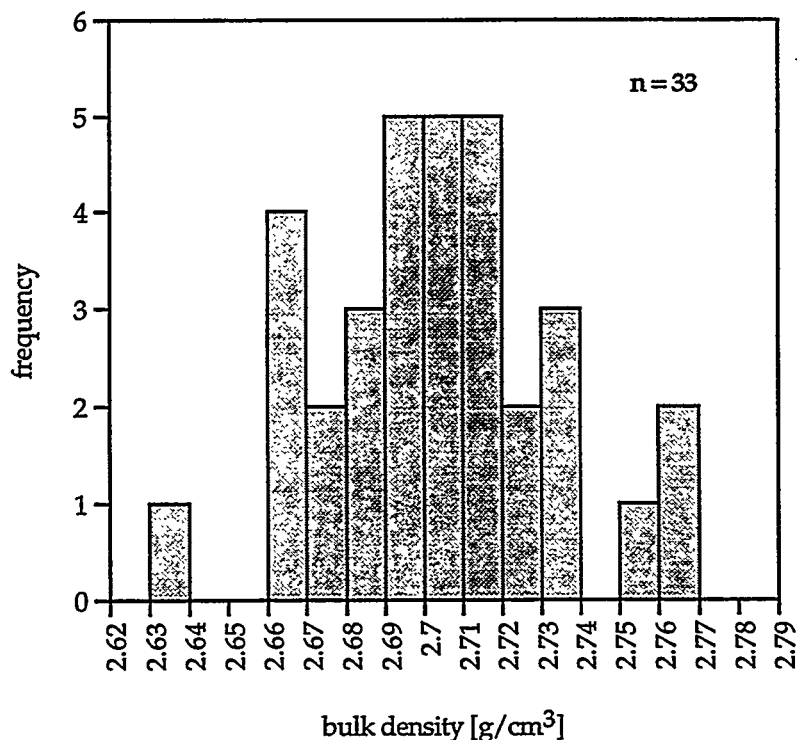
Fig. 12: Frequency distribution of bulk-density data for mudrock of the Conasauga Group based on mercury immersion.

Table 3: Some statistical measures of specimen-density data. Abbreviations: WOM = Whiteoak Mountain thrust sheet; CC = Copper Creek thrust sheet; x = arithmetic mean; sx = standard deviation; n = number of specimen analyses. Note: statistical measures were calculated for all stratigraphic units, for the sake of completeness, even if the data base was too small (rendering some statistical measures statistically unreliable).

		Bulk-Density			Grain-Density	
		x	sx	n	x	sx
All Units	WOM+CC	2.71	0.03	33	2.77	0.03
	WOM	2.71	0.03	22	2.77	0.03
	CC	2.72	0.03	11	2.79	0.02
Nolichucky Sh	WOM+CC	2.70	0.03	14	2.78	0.03
	WOM	2.70	0.03	10	2.77	0.03
	CC	2.72	0.01	4	2.80	0.03
Maryville Ls	WOM+CC	2.70	0.03	6	2.76	0.02
	WOM	2.70	0.04	4	2.75	0.02
	CC	2.72	0.04	2	2.78	0.01
Rogersville Sh	WOM+CC	2.71	0.03	5	2.77	0.04
	WOM	2.71	0.04	3	2.76	0.05
	CC	2.70	0.02	2	2.78	0.02
Rutledge Ls	WOM+CC	2.71	0.03	3	2.77	0.03
	WOM	2.72		1	2.73	
	CC	2.71	0.04	2	2.79	0.01
Pumpkin Valley Sh	WOM+CC	2.73	0.03	5	2.78	0.02
	WOM	2.73	0.03	4	2.78	0.03
	CC	2.76		1	2.79	

The values of bulk density of Conasauga Group mudrock are higher than values commonly reported for "shale" (Oelhoeft and Johnson, 1989; Katsube and Issler, 1993) and are closer to values reported for slate (Oelhoeft and Johnson, 1989). Bulk-density values ranging from 2.64 to 2.77 $g \cdot cm^{-3}$, to as high as 2.80 $g \cdot cm^{-3}$, however, are reported for tight shales from the Ventura gas field offshore Nova Scotia (Katsube et al., 1991).

Specimen Grain-Density

Thirty-three measurements are available for specimen grain-density (Appendix VII). These measurements were obtained from the same sampling intervals as the measurements for bulk density. The values of grain density for Conasauga Group mudrock range from a minimum of 2.70 $g \cdot cm^{-3}$ to a maximum of 2.83 $g \cdot cm^{-3}$ (Figure 13). The modal value is 2. 79 $g \cdot cm^{-3}$ with a mean of 2.77 (± 0.03) $g \cdot cm^{-3}$ based on all measurements. Values from the Whiteoak Mountain thrust sheet have a mean of 2.77 (± 0.03) $g \cdot cm^{-3}$, whereas values for the Copper Creek thrust sheet have a mean of 2.79
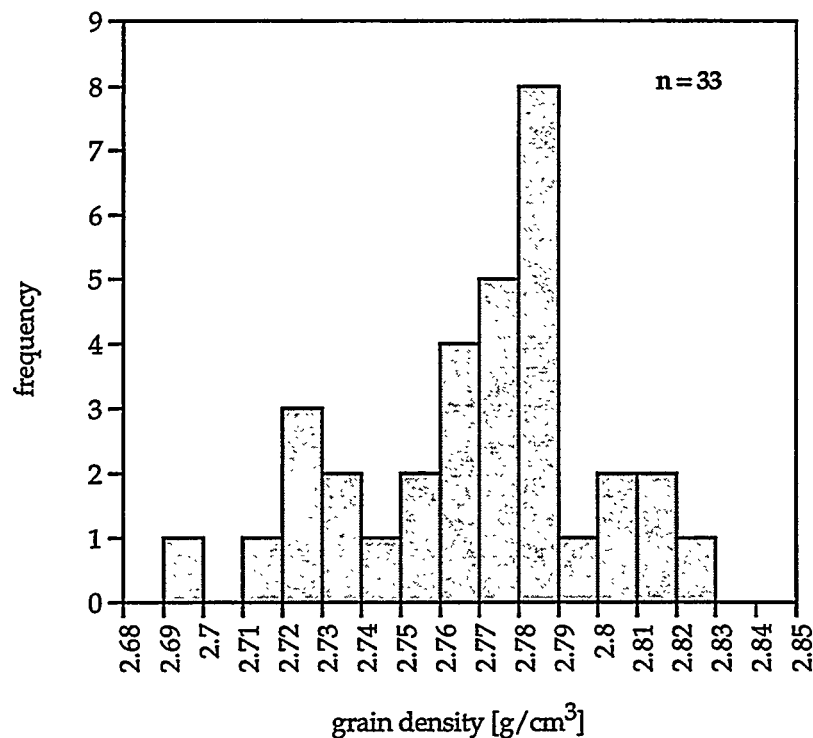
Fig. 13: Frequency distribution of grain-density data for mudrock of the Conasauga Group based on helium porosimetry.

(± 0.02) $g \cdot cm^{-3}$. Comparison of formations across the two thrust sheets reveals that grain-density values from the Copper Creek thrust sheet are consistently slightly higher than values from the same formation within the Whiteoak Mountain thrust sheet.

Table 3 gives an overview of the mean values and standard deviations of grain density for different formations. There is a considerable spread in values for particular formations, so it is important to consult the original data as provided in Appendix VII. Note also that some statistical measures are based on a small number of samples. Overall, the measured grain-density values compare well with values reported from other basinal shale sequences (Katsube and Issler, 1993).

PORE-THROAT SIZE DATA

Quantitative data on the sizes of pore throats, their distribution, and geometric means for the different sampling intervals were obtained with mercury porosimetry. Overall, 33 measurements were made from specimens in the Whiteoak Mountain and Copper Creek thrust sheets. The measurement results are provided in Appendix VIII and the pore-throat-size distribution curves for each specimen are presented in Appendix IX.

All pore-throat-size distribution curves have several aspects in common (Figure 14). First, the lowermost reported pore-throat-size value is 3.2 nm (geometric mean for the lowermost size class). This can be explained by the fact that the highest intrusion pressures generated by state-of-the-art mercury porosimeters can force mercury only through pore throats ≥ 3 nm. Pores and their attendant partial effective porosity accessed by pore throats <3 nm will, therefore, not be characterized. Second, the mode on each curve resides in the size class with a geometric mean of 5.0 nm (Appendix IX). Third, the curves are skewed toward lower values, with a rather sharp drop toward smaller sizes and a long tail toward higher values. The equipment limitations on available intrusion pressures and the resulting limit on pore-throat sizes which can be characterized (see below) will probably influence the modal values and the shape of the pore-throat-size distribution curves.

The shape of most pore-throat-size distribution curves is unimodal (some with a weak secondary mode) with a smaller percentage being bimodal. The secondary mode always resides within a larger size class. There are also three specimens displaying polymodal pore-throat-size distribution curves. The pore-throat sizes range from about 3 nm to about 5000 nm. The vast majority of pore-throat sizes are, however, between 3 nm and 100 nm. Some size curves display rare outliers in larger size classes.

The shapes of the pore-throat-size distribution curves suggest that the mudrock specimens of the Conasauga Group are well compacted and have experienced burial depths in excess of 2.5 km, based on comparison with other basinal mudrock sequences (Katsube and Williamson, 1994; 1995; Katsube et al., 1995). Furthermore, the distribution curves imply that the main fluid-transport pores (Katsube at al., 1992b) are likely accessed and connected by pore throats in the size range of 4 to 60 nm. This interpretation is based on comparison of porosity studies of basinal mudrock samples with permeability measurements and formation-factor determinations on the same samples (Katsube et al., 1991, 1992b).
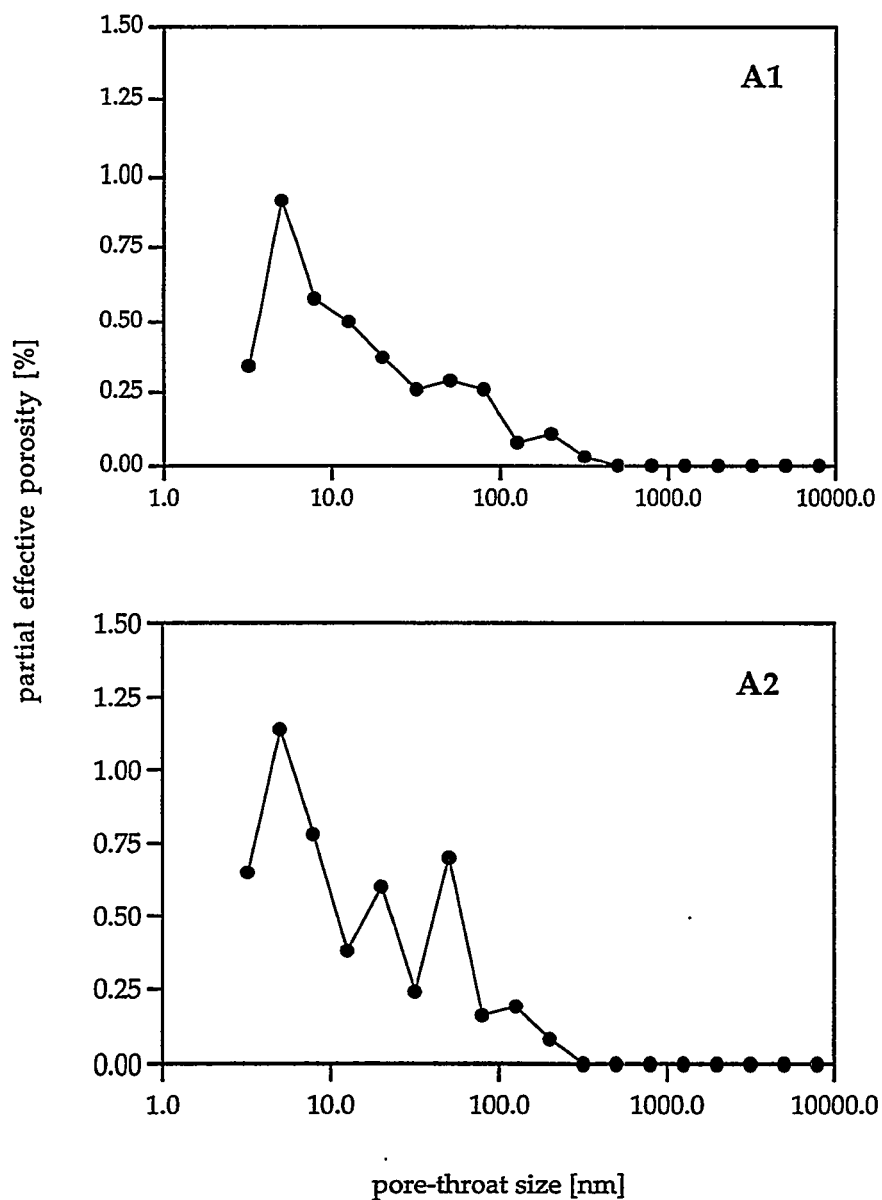
Fig. 14: Examples of pore-throat-size distribution curves
displaying typical characteristics of Conasauga Group mudrock
from the ORR. See text for discussion.

Following Katsube and Issler (1993), the geometric mean of the *entire* pore-throat-size distribution of a specimen was calculated using the equation

$$\log\,(d_{Hg}) = \frac{(1/n)\,\sum_{i=1}^{n}\,[\phi_{ai} \cdot \log\,(d_{ai})]}{\sum_{i=1}^{n}\,\phi_{ai}} \qquad (10)$$

ϕ_a = partial effective porosity
d_{Hg} = geometric mean of the entire
             pore-throat-size distribution
d_a = geometric mean of distinct pore-size range
n = number of distinct pore-size ranges.

The geometric means for specimens from the different sampling intervals are listed in Table 4. The maximum geometric mean value is 96.8 nm (sampling interval B3) and the minimum value is 18.1 nm (sampling interval C2). There is no trend with depth discernible from the data (Table 4). An exception is the Nolichucky Shale from the Copper Creek thrust sheet (core Wol-1) which displays a decrease of geometric mean value with depth. This trend is based, however, on only four measurements.

The reported data on measured pore-throat sizes and their distribution may be useful for evaluating whether pore throats are able to exclude or retard certain contaminant species from accessing the interconnected pore space of the mudrock matrix through diffusion. Contaminant species larger or of nearly the same size as the dominant entry pore-throats/connecting pore throats might be forced to continue their journey by advective transport within the interconnected fracture network of Conasauga Group mudrock. Even contaminant species smaller than the reported dominant pore-throat sizes might be slowed considerably in invading the interconnected pore space, because the narrow physical confines of these pore throats (and their effect on the adsorbed molecular layers of water) will influence the diffusion characteristics of the respective contaminant species. For comparison, hydrated radii of common ions are smaller than 0.5 nm (Nightingale, 1959), much smaller than the most common pore-throat sizes obtained from Conasauga Group mudrock. Ion pairs, chelated organic compounds and colloids, however, will be larger (J. F. McCarthy and P. M. Jardine, pers. comm.), and their behavior within the matrix pore-space should be evaluated.

Table 4: Summary of geometric means (d_{Hg}) calculated from pore-throat-size distribution data obtained through mercury porosimetry.

Specimen	d_{Hg} [nm]	Strat. Unit	Specimen	d_{Hg} [nm]	Strat. Unit
A1-a	30.5	Maryville Ls.	B1-a		
A2-a	24.5	Maryville Ls.	B2-a		
A3-a	51.3	Maryville Ls.	B3-a	96.8	Nolichucky Sh.
A4-a			B4-a	41.5	Nolichucky Sh.
A5-a	33.9	Maryville Ls.	B5-a	49.1	Nolichucky Sh.
A6-a	40.7	Rogersville Sh.	B6-a		
A7-a	19.2	Rogersville Sh.	B7-a	30.9	Nolichucky Sh.
A8-a	49.3	Rogersville Sh.	B8-a	54.0	Maryville Ls.
A9-a			B9-a	51.1	Rutledge Ls.
A10-a	35.9	Rutledge Ls.	B10-a	50.4	Pumpkin V. Sh.
A11-a	41.1	Pumpkin V. Sh.			
A12-a	38.7	Pumpkin V. Sh.	C2-a	18.1	Maryville Ls.
A13-a			C3-a	27.2	Rutledge Ls.
A14-a	26.2	Pumpkin V. Sh.	C4-a	23.3	Rogersville Sh.
A15-a	66.5	Pumpkin V. Sh.	C5-a		
A16-a	31.9	Nolichucky Sh.	C6-a		
A17-a	51.2	Nolichucky Sh.	C7-a	33.3	Rogersville Sh.
A18-a	25.4	Nolichucky Sh.	C8-a		
A19-a	42.7	Nolichucky Sh.			
A20-a	56.6	Nolichucky Sh.			
A21-a	51.9	Nolichucky Sh.			
A22-a	58.2	Nolichucky Sh.			
A23-a	38.0	Nolichucky Sh.			
A24-a	23.1	Nolichucky Sh.			
A25-a	49.8	Nolichucky Sh.			

EFFECTIVE POROSITY DATA

Immersion-Saturation Method

Fifty-six reliable effective porosity values were determined with the immersion-saturation method. These measurements cover all mudrock-dominated stratigraphic units of the Conasauga Group from both the Whiteoak Mountain and Copper Creek thrust sheets. Five reliable measurements were obtained from cylindrical specimens (Appendix III), whereas the other 51 reliable measurements were obtained from irregularly shaped specimens (Appendix IV). The accuracy of the immersion-saturation measurements is estimated to be within 10% of the reported value.

A good to excellent match between results based on cylindrically shaped and irregularly shaped specimens is apparent from sampling intervals where both types of specimen were tested (Figure 15; Appendices III, IV; sampling intervals A1, B10, C7). Multiple reliable data from irregularly shaped specimens are available for 11 sampling intervals (Appendix IV). In general, there is an excellent correspondence between the different measurements within the same sampling interval (Appendix IV, Figure 15), with the difference between the maximum and minimum measured effective porosity value[3] ranging from 0.13 to 1.87%. The exceptions are sampling interval A1, with a considerable difference of 6.18%, and interval A17, with a difference of 4.15% (Appendix IV, Figure 15).

The effective porosity values cluster between 9% to 12% (Figure 16), with a mode at 11 to 12%. Values tail off sharply to both sides from this cluster. A smaller secondary mode is developed at 5 to 6% (Figure 16). Maximum and minimum measured values are 15.87% and 3.67% respectively (Appendices III, IV).

The mean value of effective porosity is 9.90 ($\pm$2.62)% (Table 5). The mean for the data (n = 39) from the Whiteoak Mountain thrust sheet is slightly higher (10.61%) with a smaller standard deviation of 1.95% (Table 5). This indicates a smaller scatter of the data (Figure 15), especially when the wider range of values for sampling interval A1 is disregarded. The mean effective porosity value for specimens from the Copper Creek thrust sheet is lower with 8.3% (n = 17). The standard deviation, however, is higher (3.33%) (Table 5), emphasizing the wider scatter of effective porosity data within the Copper Creek thrust sheet (Figure 15).

[3] note: difference Δ % = $\phi_{eff-max}$ % - $\phi_{eff-min}$ %
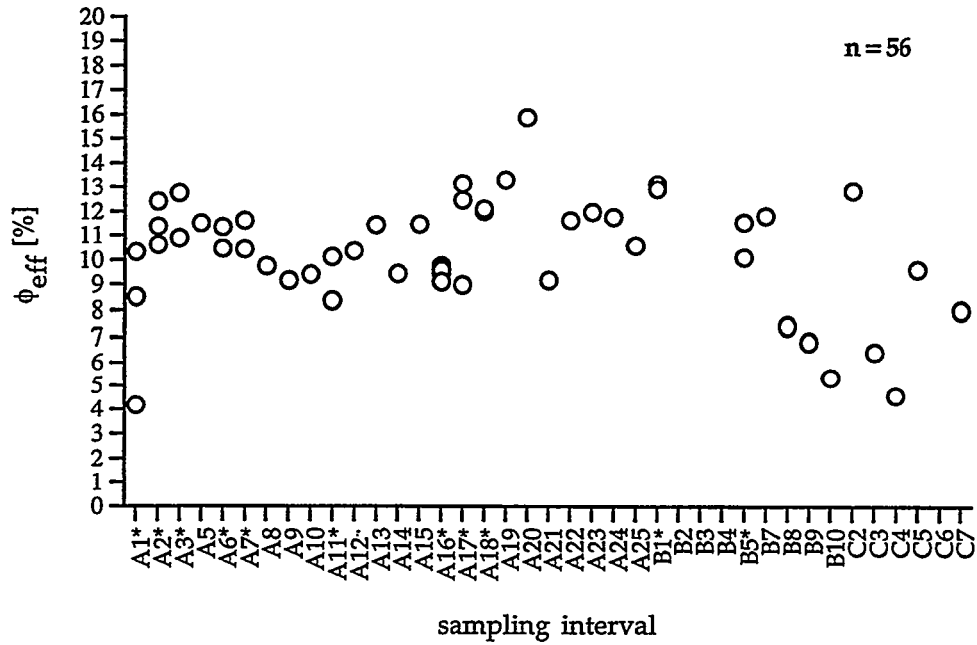
Fig. 15: Scatter plot of effective porosity data obtained with the immersion-saturation method. The asterisk denotes sampling intervals from which several specimens were analyzed yielding a multiple of reliable effective porosity values.
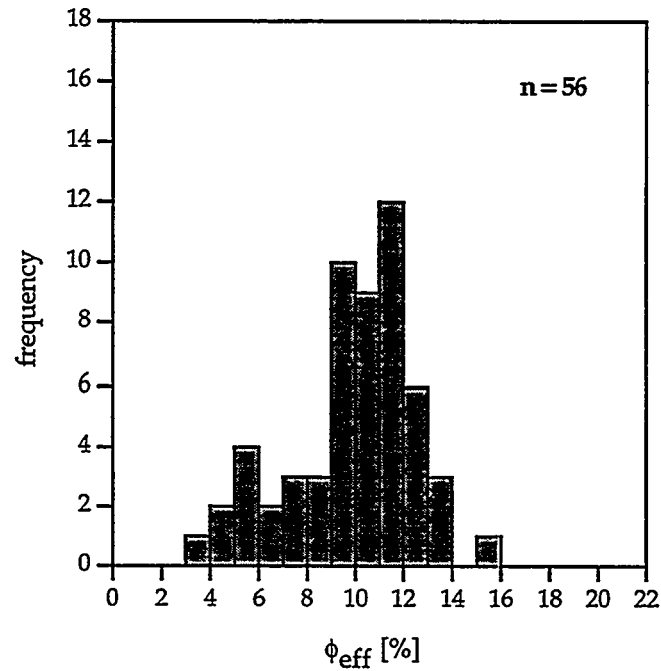
Fig. 16: Frequency distribution of effective porosity values based on the immersion-saturation method.

Table 5: Some statistical measures of effective porosity obtained with the immersion-saturation method. Abbreviations: WOM = Whiteoak Mountain thrust sheet; CC = Copper Creek thrust sheet; x = arithmetic mean; sx = standard deviation; n = number of specimen analyses. Note: statistical measures were calculated for all stratigraphic units, for the sake of completeness, even if the data base was too small (rendering some statistical measures statistically unreliable).

		x	sx	n
All Units	WOM + CC	9.90	2.61	56
	WOM	10.60	1.95	39
	CC	8.27	3.33	17
Nolichucky Sh	WOM + CC	11.08	2.39	22
	WOM	11.29	1.93	16
	CC	10.52	3.53	6
Maryville Ls	WOM + CC	9.64	2.86	13
	WOM	9.97	2.66	10
	CC	8.56	3.84	3
Rogersville Sh	WOM + CC	9.08	2.43	9
	WOM	10.72	0.76	5
	CC	7.02	2.21	4
Rutledge Ls	WOM + CC	7.96	1.53	4
	WOM	9.28	0.16	2
	CC	6.64	0.28	2
Pumpkin Valley Sh	WOM + CC	8.95	2.49	8
	WOM	10.18	1.19	6
	CC	5.25	0.14	2

Mean effective porosity data are highest within the Nolichucky Shale in both thrust sheets. A steady decline in mean effective porosity is discernible with increasing stratigraphic age within the Copper Creek thrust sheet. Notice, however, the often small sample number on which this trend is based. The trend cannot be observed within the Whiteoak Mountain thrust sheet (Table 5). A further discussion of these observations will be presented in the chapter 'Effective Porosity and Depth.'

Mercury Porosimetry

Thirty-three measurements of effective porosity with mercury porosimetry are available, covering all mudrock-dominated stratigraphic units of the Conasauga Group within the Whiteoak Mountain and Copper Creek thrust sheets (Table 6). The results are tabulated in Appendix VI. The data used for evaluation are the ϕ_{Hg1}-values, which correspond to pore space accessed through pore throats $\leq$10 μm. This is based on the inference that the ϕ_{Hg2}-values (pore space accessed through pore throats $\leq$250 μm) are more likely to contain measurement errors (Katsube and Issler, 1993). As expected, the ϕ_{Hg2}-values are consistently slightly higher than the ϕ_{Hg1}-values, the deviation ranging from 0.3% to 1.9%. The accuracy of the measurements is estimated to be within 10 to 20% of the measured value.

The effective porosity data display a strongly unimodal distribution with a modal value at 3 to 4% (Figure 17). Significant are the consistent relatively low values with a mean for all specimens of 3.8% with a small standard deviation of 0.7%, indicating a very small scatter of the data. The narrow range of measured effective porosity values, with a minimum of 3.0% and a maximum of 5.2%, for all stratigraphic units from both thrust sheets is shown in the scatter plot (Figure 18).

Helium Porosimetry

Effective porosity data based on helium porosimetry are derived from exactly the same sampling intervals as the data based on mercury porosimetry, providing for a total of 33 measurements. The results of effective porosity measurements based on helium porosimetry are tabulated in Appendix VII. As for mercury porosimetry, the accuracy of the measurements is estimated to be within 10 to 20% of the measured value.

Table 6: Some statistical measures of effective porosity obtained with **mercury porosimetry**. Abbreviations: WOM = Whiteoak Mountain thrust sheet; CC = Copper Creek thrust sheet; x = arithmetic mean; sx = standard deviation; n = number of specimen analyses. Note: statistical measures were calculated for all stratigraphic units, for the sake of completeness, even if the data base was too small (rendering some satistical measures statistically unreliable).

		x	sx	n
All Units	WOM + CC	3.8	0.7	33
	WOM	3.7	0.7	22
	CC	3.9	0.7	11
Nolichucky Sh	WOM + CC	4.0	0.7	14
	WOM	3.9	0.7	10
	CC	4.2	0.8	4
Maryville Ls	WOM + CC	3.6	0.7	6
	WOM	3.8	0.8	4
	CC	3.3	0.2	2
Rogersville Sh	WOM + CC	3.9	0.6	5
	WOM	3.6	0.7	3
	CC	4.4	0.2	2
Rutledge Ls	WOM + CC	3.6	0.8	3
	WOM	2.9		1
	CC	4.0	0.7	2
Pumpkin Valley Sh	WOM + CC	3.5	0.6	5
	WOM	3.6	0.7	4
	CC	3.2		1
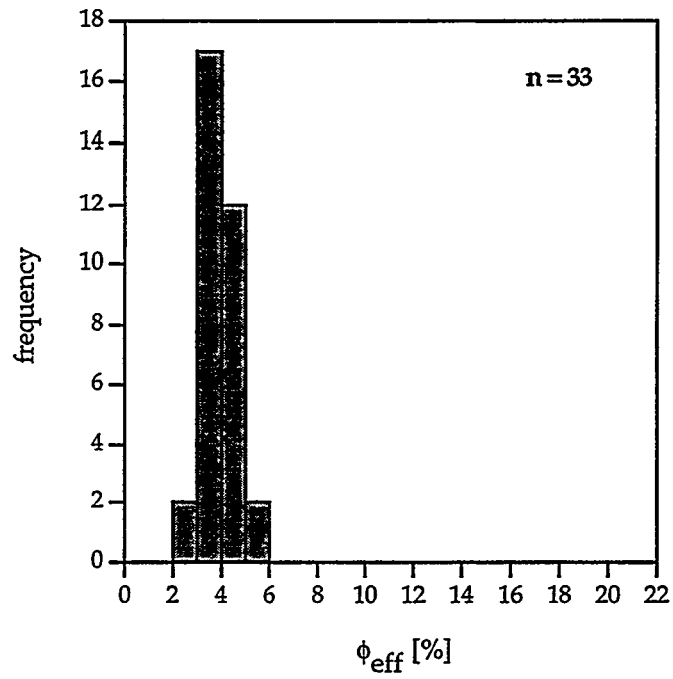
Fig. 17: Frequency distribution of effective porosity values based on mercury porosimetry.
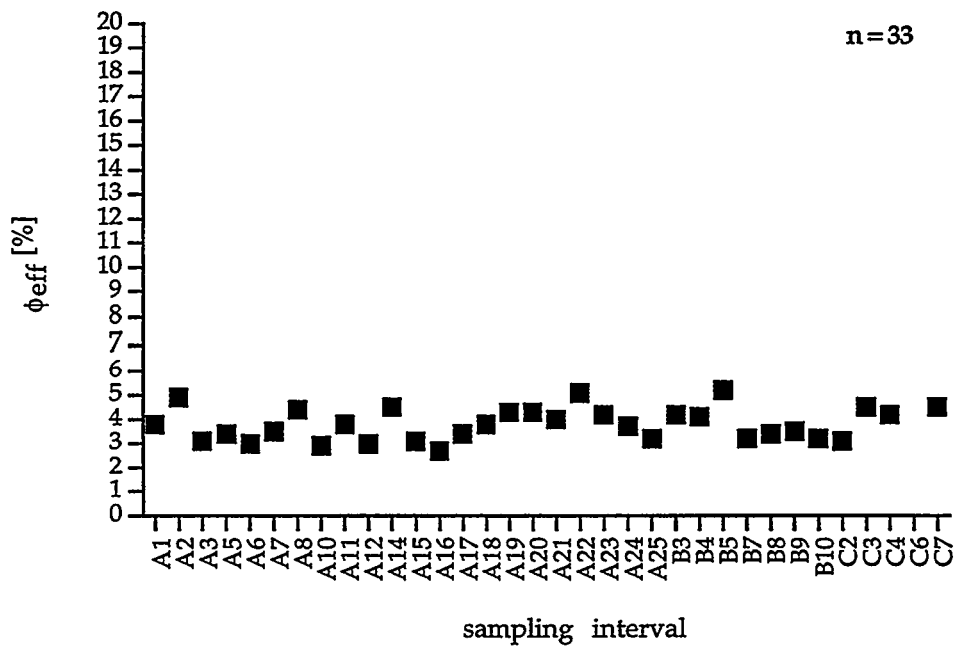
Fig. 18: Scatter plot of effective porosity data obtained with mercury porosimetry.

Significant is the bimodal distribution of the values, with one mode centered at 3 to 4% and the second mode centered at 10 to 11% (Figure 19). Overall, there is a considerable spread in the data ranging from a minimum value of 2.9% to a maximum value of 19.2%, although the vast majority of data clusters from 3% to 13% (Figures 19, 20). The mean based on all data is 8.1 (±4.3)%. The standard deviations for the data from the Whiteoak Mountain (n = 22) and Copper Creek (n = 11) thrust sheets are similarly large (4.4% vs. 4.1%), with respective means of 8.7% and 6.9% (Table 7). The large spread in the data within stratigraphic units makes it imperative to look at the raw data (Appendix VII). For example, within the Whiteoak Mountain thrust sheet, data from the Maryville Limestone show a good accordance (n = 4) whereas data from the Nolichucky Shale display a bimodality of values <5% and ≥10%.
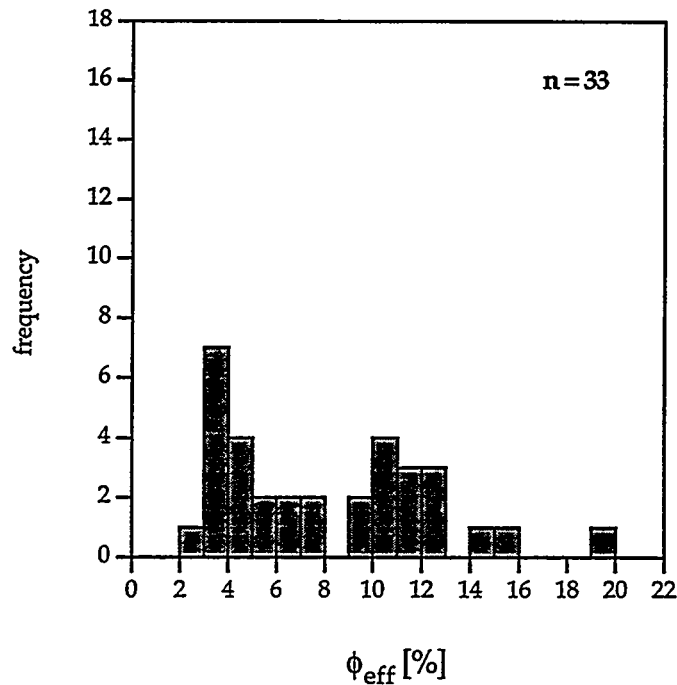
Fig. 19: Frequency distribution of effective porosity values based on helium porosimetry.
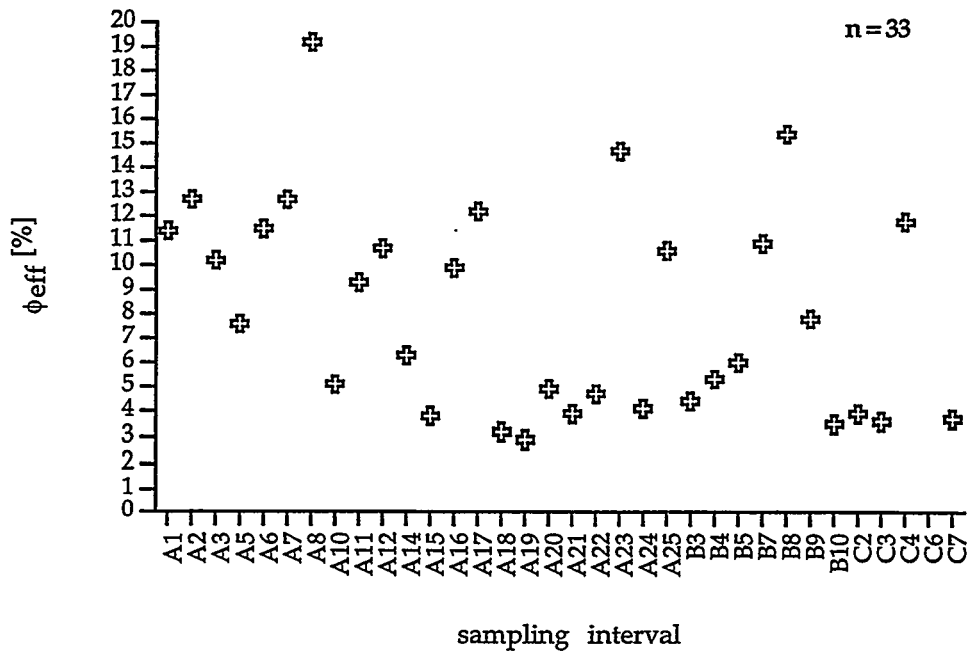
Fig. 20: Scatter plot of effective porosity data obtained with helium porosimetry.

Radial Diffusion-Cell Method

Only two effective porosity results are available using the radial diffusion-cell method due to problems preparing adequate core segments. Both were obtained from corehole 0.5MW012A from the Copper Creek thrust sheet. Effective porosities are 6.0% for specimen C8-d from the Rogersville Shale, and 7.3% for specimen C6-d from the Maryville Limestone.

Table 7: Some statistical measures of effective porosity obtained with **helium porosimetry.** Abbreviations: WOM = Whiteoak Mountain thrust sheet; CC = Copper Creek thrust sheet; x = arithmetic mean; sx = standard deviation; n = number of specimen analyses. Note: statistical measures were calculated for all stratigraphic units, for the sake of completeness, even if the data base was too small (rendering some statistical measures statistically unreliable).

		x	sx	n
All Units	WOM + CC	8.1	4.3	33
	WOM	8.7	4.4	22
	CC	6.9	4.1	11
Nolichucky Sh	WOM + CC	7.0	3.8	14
	WOM	7.1	4.3	10
	CC	6.1	3.4	4
Maryville Ls	WOM + CC	10.2	4.0	6
	WOM	10.5	2.2	4
	CC	9.7	8.1	2
Rogersville Sh	WOM + CC	11.8	5.5	5
	WOM	14.5	4.1	3
	CC	7.8	5.7	2
Rutledge Ls	WOM + CC	5.5	2.1	3
	WOM	5.1		1
	CC	5.7	3.0	2
Pumpkin Valley Sh	WOM + CC	6.7	3.2	5
	WOM	7.5	3.1	4
	CC	3.5		1

48

Comparison of Effective Porosity Data

Effective Porosity. In general, effective porosity values obtained with the immersion-saturation method are consistently high, whereas data generated with mercury porosimetry are consistently low. Effective porosity values obtained with helium porosimetry show a distinct dichotomy of low and high values (Table 8). Several characteristic data triads can be identified (Figures 21, 22). Data triads refer to effective porosity values obtained for the same sampling interval with helium porosimetry, mercury porosimetry and the immersion-saturation method.

The *type I data triad* appears to be the most common form. It is characterized by high (some medium high) and corresponding effective porosity values based on the immersion-saturation method and helium porosimetry, accompanied by low effective porosity values based on mercury porosimetry (Table 8; Figures 21, 22). The type I data triad is exemplified by values from sampling intervals A3, A11, A17, and B7.

This pattern can be explained by the fact that the mercury porosimeter is limited to mercury intrusion-pressures which correspond to a minimum accessible pore-throat size of 3 nm Apparently, much pore space is sheltered behind access pore-throats of sizes <3 nm. In contrast, water (immersion-saturation method) and helium (helium porosimetry) are believed to be able to access all pores and pore throats (Katsube, 1992; Issler and Katsube, 1994). A large number of pore throats are <3 nm either through compaction or, more likely, because of diagenetic overprint with cement coating the surfaces of pore throats and thereby narrowing the connecting and access paths to pores. Furthermore, the fact that the analyzed mudrock specimens appear to be well compacted (based on the pore-throat-size distribution curves) but yield high effective porosity values (helium porosimetry, immersion-saturation method) might also point toward the possibility that the specimens contain secondary dissolution pores, connected by pore throats <3 nm. The values based on the immersion-saturation method and helium porosimetry most likely approach the true effective porosity of the analyzed sampling interval.

The *type II data triad* displays a low and congruent effective porosity value based on helium porosimetry, the immersion-saturation method, *and* mercury porosimetry (e. g., sampling intervals B3, B10; Table 8; Figures 21, 22). This observation can be explained by an absence of interconnected pore space accessed by pore throats <3 nm. Type II data triads can be interpreted as a final stage in the development from type I data triads with continuing cementation, whereby much of the connecting pore throats are occluded. Should this interpretation be correct, the possibility of significant isolated

Table 8: Summary overview of effective porosity values for Conasauga Group mudrock from the ORR. Effective porosity ϕ is given in %; subscripts He, Hg, I1, I2, and wm refer to helium porosimetry, mercury porosimetry, the water-immersion method (1: irregularly shaped specimens, 2: cylindrically shaped specimens), and the radial diffusion-cell method, respectively. The asterisk denotes averaged effective porosity values (water-immersion method) for sampling intervals where several reliable specimens were available.

Spl. Inter.	Depth [m]	ϕ_{He} [%]	ϕ_{Hg} [%]	ϕ_{I1} [%]	ϕ_{I2} [%]	ϕ_{wm} [%]
A1	41.07	11.4	3.8	7.67*	7.08	
A2	67.18	12.7	4.9	11.47*		
A3	80.52	10.2	3.1	11.83*		
A4	95.86					
A5	114.53	7.6	3.4	11.51		
A6	138.73	11.5	3.0	10.90*		
A7	163.12	12.7	3.5	11.03*		
A8	165.56	19.2	4.4	9.75		
A9	45.95			9.16		
A10	65.33	5.1	2.9	9.39		
A11	90.73	9.3	3.8	9.24*		
A12	102.97	10.7	3.0	10.35		
A13	130.71			11.41		
A14	130.76	6.3	4.5	9.43		
A15	187.83	3.8	3.1	11.44		
A16	44.45	9.9	2.7	9.46*		
A17	58.27	12.2	3.4	11.52*		
A18	80.29	3.2	3.8	12.04*		
A19	99.8	2.9	4.3	13.29		
A20	109.53	4.9	4.3	15.87		
A21	151.59	3.9	4.0	9.16		
A22	158.27	4.7	5.1	11.60		
A23	171.86	14.7	4.2	11.95		
A24	181.14	4.1	3.7	11.74		
A25	201.19	10.4	3.2	10.57		
B1	12.04			13.00*		
B2	12.95					
B3	26.67	4.4	4.2		3.67	
B4	38.41	5.3	4.1			
B5	57.38	6.0	5.2	10.81*		
B6	81.43					
B7	99.9	10.9	3.2	11.80		
B8	243.84	15.4	3.4	7.43		
B9	320.09	7.8	3.5	6.84		
B10	352.6	3.5	3.2	5.35	5.15	
C2	51.44	3.9	3.1	12.84		
C3	148.1	3.6	4.5	6.44		
C4	83.1	11.8	4.2	4.58		
C5	118.1			9.59		
C6	38.34				5.41	7.3
C7	135.13	3.7	4.5	7.97	5.94	
C8	138.83					6.0
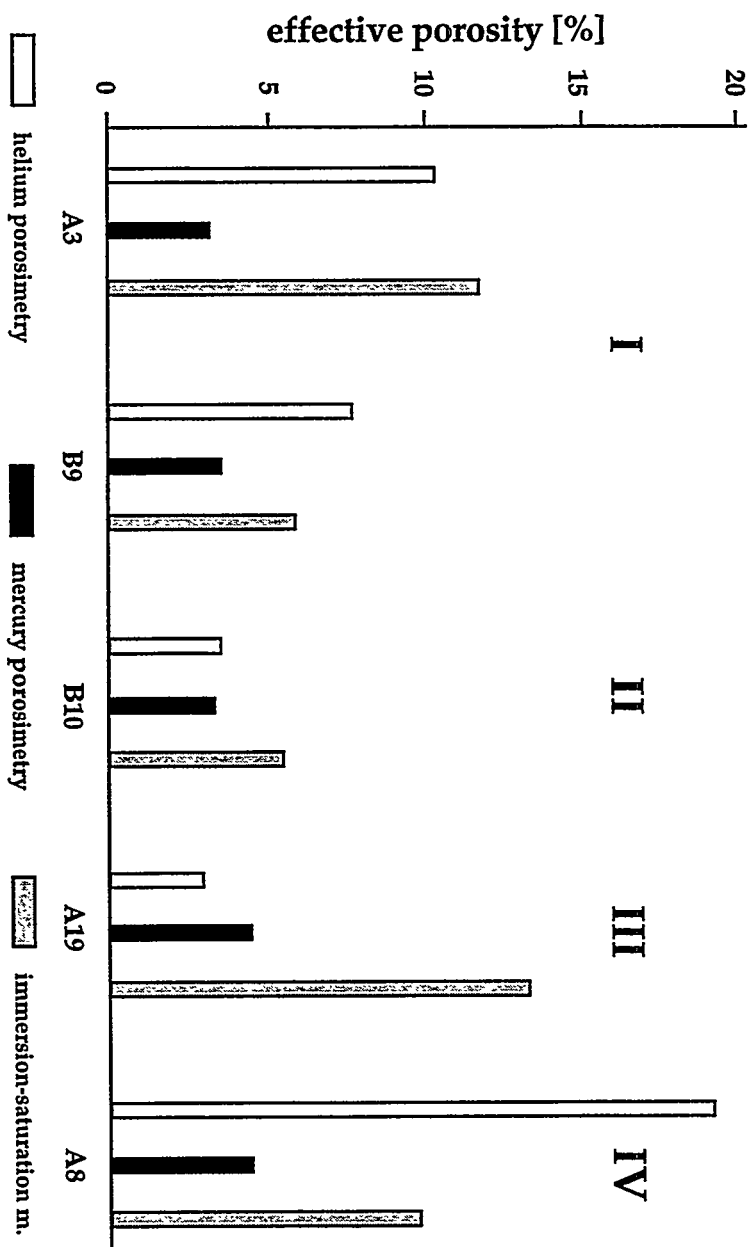
Fig. 21: Plot of effective porosity based on different petrophysical techniques to show the characteristics of the different data triads (I = type-I data triad, II = type-II data triad, III = type-III data triad, IV = type-IV data triad). The type-I data triad is represented by two examples - one with high effective porosity and one with lower effective porosity values (based on helium porosimetry and the immersion-saturation method). Sampling intervals are indicated on horizontal axis.
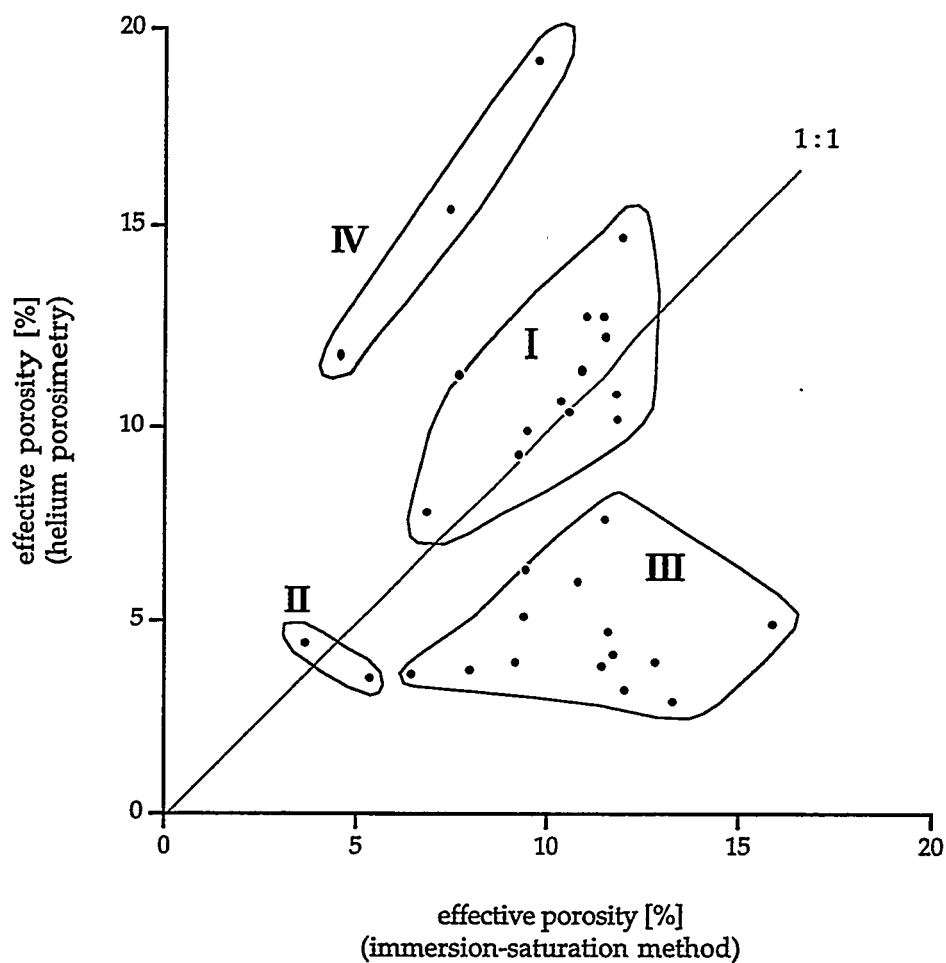
Fig. 22: Discrimination diagram to differentiate data triads.
Effective porosity based on helium porosimetry is plotted against
effective porosity based on the immersion-saturation method. Data
points group into fields representing type-I (I), type-II (II), type-III (III),
and type-IV (IV) data triads. Mercury-porosimetry values are neglected
because they consistently fall between 2.7 and 5.2%.

pore space diagenetically decoupled from the interconnected pore space exists. Alternatively, the type II data triad can be seen as the 'initial situation' after cementation, with secondary dissolution increasing the effective porosity to the level of the type I data triad, but retaining a predominance of pore throats <3 nm. Type I data triads with medium high effective porosity values generated with helium porosimetry and the immersion-saturation method, which are closer to the low mercury porosimetry values (e. g., sampling interval B9), might constitute an 'intermediate stage' between the end members of type I and type II data triads.

The typical *type III data triad* displays a high (or some medium high) value of effective porosity based on the immersion-saturation method and a low value based on mercury porosimetry (same as for the type I data triad), but with a low value based on helium porosimetry which is as low as (or lower than) the mercury-porosimetry value (Table 8; Figures 21, 22). This pattern might indicate a problem with helium porosimetry. This interpretation is supported by the fact that some helium-porosimetry values are smaller than mercury-porosimetry values for the same sampling interval (e. g., sampling intervals A18, A19). Furthermore, type III data triads alternate with type I data triads with both types of data triads displaying similar effective porosity values based on the immersion-saturation method throughout the corehole, indicating the deviating nature of the helium-porosimetry data of the type III data triads (e. g., Nolichucky Shale of the Whiteoak Mountain thrust sheet).

Another problematic set of helium-porosimetry data are encountered in sampling intervals where helium-porosimetry data are much higher than accompanying immersion-saturation data (e. g., A8, B8, C4). These *type IV data triads* can be interpreted as type I data triads with helium-porosimetry data deviating at the higher end (Figures 21, 22). There might be the possibility that small cracks developed within some of the analyzed specimens, as was observed during experiments with the immersion-saturation method, and that this induced porosity was measured and added to the specimen effective porosity. Differential cementation within the same sampling interval could also serve as an explanation for the apparently anomalous helium-porosimetry data. Specimens within sampling intervals were chosen, however, from homogeneous mudrock intervals based on macroscopic criteria. The immersion-saturation values most likely approach the true effective porosities for sampling intervals exhibiting type III or type IV data triads.

Overall, the diverse effective porosity data combined with the quantitative information on pore-throat sizes emphasize the apparent importance of the chemical diagenetic history of the Conasauga Group for mudrock pore-characteristics.

Cementation appears to be important, and may be even pervasive, together with dissolution. The pore connectivity most likely will not be very good. This interpretation is based on unpublished data (T. J. Katsube) which show that cementation has a very negative effect on pore connectivity. Mudrock exhibiting the same degree of compaction and the same values of porosity can display marked differences in pore connectivity/permeability, with cemented mudrock showing much lower pore connectivity/permeability than uncemented mudrock. However, a more solid interpretation of the influence of chemical diagenesis on the pore characteristics of the Conasauga Group mudrock requires further study, especially the use of optical analysis techniques (SEM, TEM, and quantitative image analysis). This is especially true for deciding whether type I data triads developed from type II data triads through secondary dissolution or whether type II data triads developed from type I data triads through progressive cementation.

Effective porosity values generated with the radial diffusion-cell method should be considered separately because of the large difference in analyzed mudrock volume. Nevertheless, the values of 6.0% for specimen C8-d and 7.3% for specimen C6-d match well with immersion-saturation effective porosities from the same core. Both specimens appear to be well cemented and solid, with specimen C8-d displaying abundant bioturbation.

There are, however, several aspects which might shed some negative light on the results. The rubber sealing may not be good enough to completely insulate the specimens (K. Novakowski, pers. comm., 1995). Furthermore, it is not certain that all of the specimen material was saturated at the start of the experiments. Fluid might have been lost during storage time (despite plastic wrap and aluminum sealing) between core retrieval and experiments and/or from the rims of the core segments during the heat shrinking process to put on the rubber seal. The results might also be biased toward the core segments which were best cemented and were the only ones solid enough to withstand the preparation process.

Effective Porosity and Depth. A typical characteristic of basinal mudrock is the exponential decrease in porosity with depth, mainly through compaction (e. g., Rieke and Chilingarian, 1974; Katsube and Williamson, 1995). At burial depths in excess of 2 km the decrease in porosity is small. Recent studies (e. g., Katsube and Williamson, 1994; 1995) suggest that maximum compaction of mudrock is approached at the critical depth of burial (CDB) at about 2.5 to 3.0 km. According to these studies, while porosity will rapidly decrease with depth until the CDB, porosity will show little

decrease or may even show a slight increase with depth at burial depths greater than the CDB (Katsube and Williamson, 1994; 1995). The burial depth of the Conasauga Group mudrock on the ORR is estimated as (at least) 4 km (Foreman, 1991; P. Lemiszki, pers. comm.) suggesting that the mudrock should have reached the CDB for the Conasauga basin.

Figure 23 shows the effective porosity values obtained by mercury porosimetry, helium porosimetry and the immersion-saturation method with depth in coreholes from the Whiteoak Mountain thrust sheet. Rather than a continuous corehole through all formations of the Conasauga Group, several coreholes had to be used to cover the targeted stratigraphic interval (Figure 6). For each of the coreholes the depth interval characterized in terms of effective porosity is small reaching a maximum of 150 m. The depths shown on the figure represent present depth below ground surface following structural and erosional uplift since the Permian and not the original burial depth. The uniformly low mercury-porosimetry values again highlight the notion that much pore space is shielded by pore throats <3 nm, which cannot be accessed with the currently available mercury porosimeters. Helium-porosimetry values in general either match immersion-saturation data reasonably well or are much lower. Immersion-saturation data do not show a trend of decreasing porosity with depth conforming to expectations for mudrock buried to a depth of 4 km or more. The data from corehole GW-132 might even suggest an increase in effective porosity with depth, but the analyzed depth range spans only 142 m rendering this interpretation questionable.

Figures 24 and 25 show effective porosity-versus-depth plots for coreholes Wol-1 and 0.5MW012A from the Copper Creek thrust sheet. The depth intervals from which specimens were available span 340 m for corehole Wol-1 (Figure 24) and only 100 m for corehole 0.5MW012A (Figure 25). In contrast to the data from the Whiteoak Mountain thrust sheet, the two plots from the Copper Creek thrust sheet display an apparent decrease in effective porosity with depth based on immersion-saturation data. This raises the question why these mudrock specimens, which have experienced burial of 4 km or more, show this steady decrease in effective porosity based on the immersion-saturation method, but not on helium and mercury porosimetry.

A possible explanation to this question is that meteoric water has caused replacement of some cement in the mudrock, and at least part of that replaced cement has dissolved during the immersion-saturation experiments to determine effective porosity in the laboratory. If the degree of replacement increases toward the present day surface, the effective porosity determined by this method is likely to show a steady decrease with depth, as displayed in Figures 24 and 25, until the amount of replacement
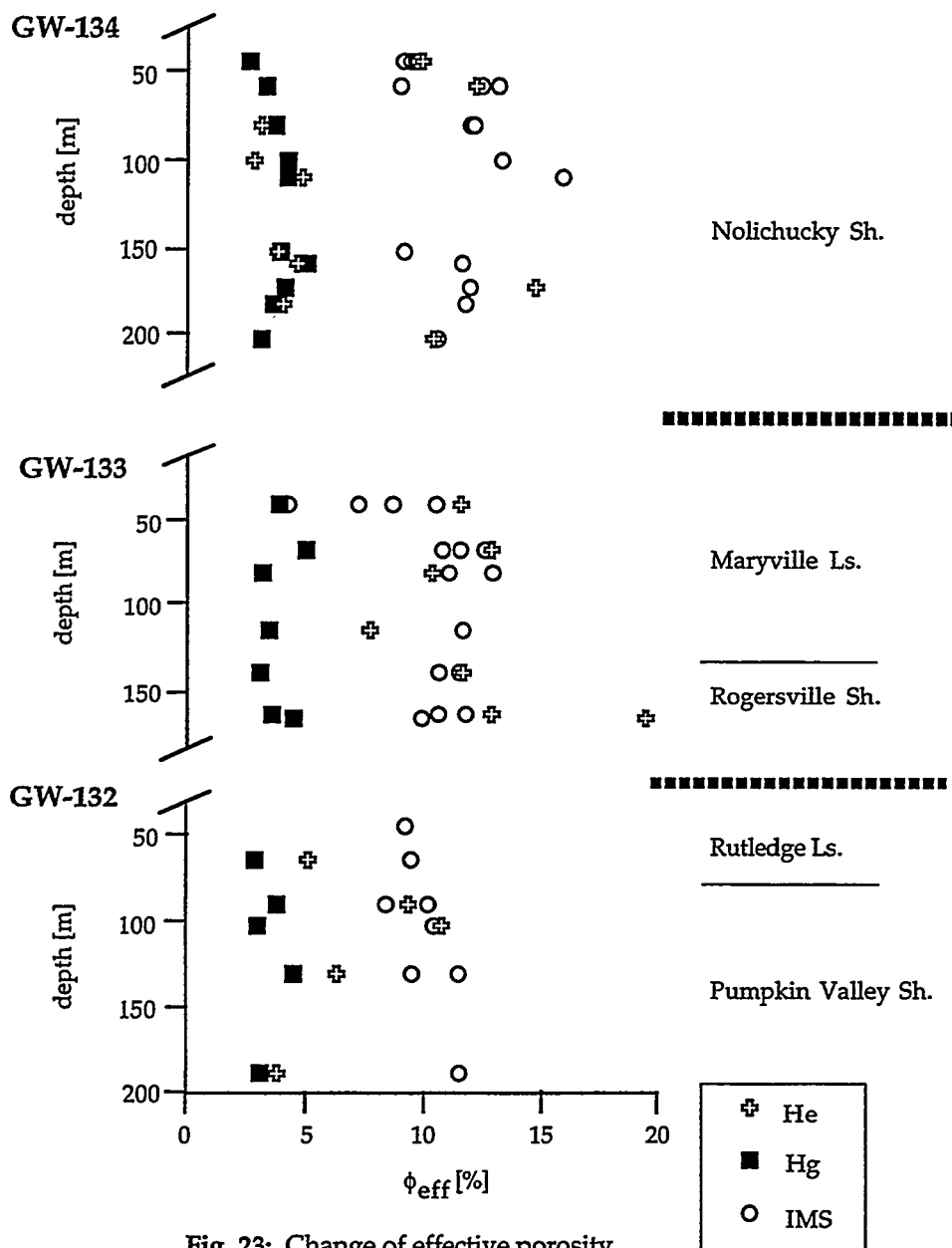
Fig. 23: Change of effective porosity with depth below ground surface within coreholes GW-132, GW-133, and GW-134 (Whiteoak Mountain thrust sheet). He, Hg, and IMS refer to effective porosity values obtained, respectively, through helium porosimetry, mercury porosimetry, and the immersion-saturation method.
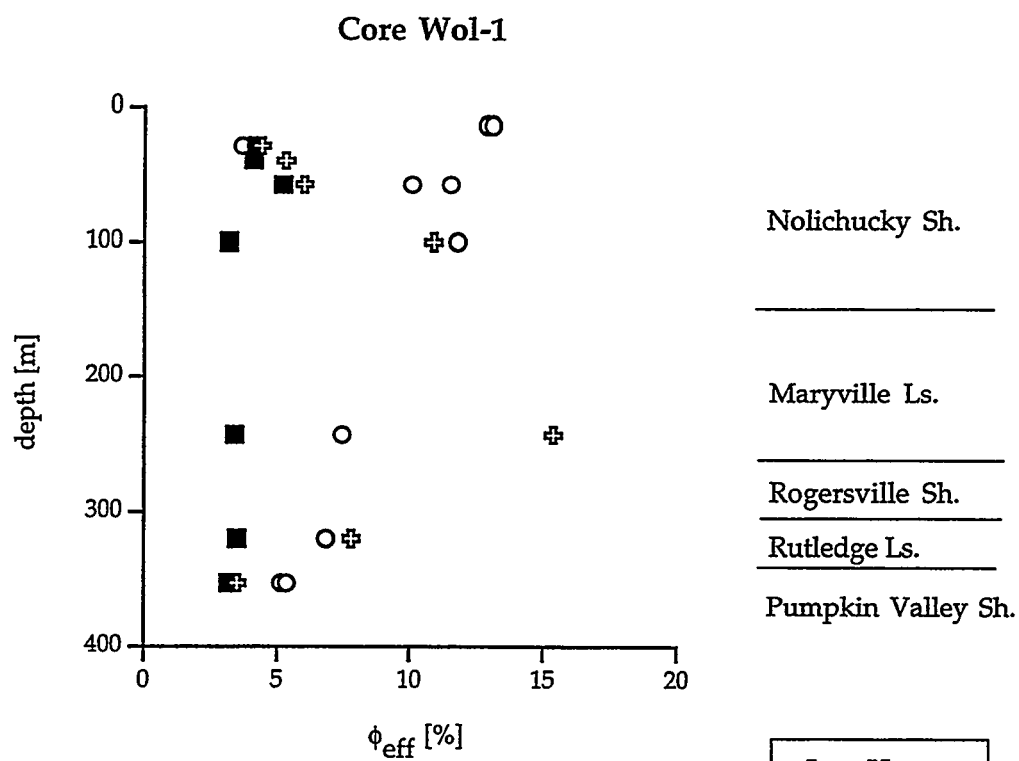
Core Wol-1

Fig. 24: Change of effective porosity with depth below ground surface within corehole WOL-1 (Copper Creek thrust sheet). He, Hg and IMS refer to effective porosity values obtained, respectively, through helium porosimetry, mercury porosimetry, and the immersion-saturation method.
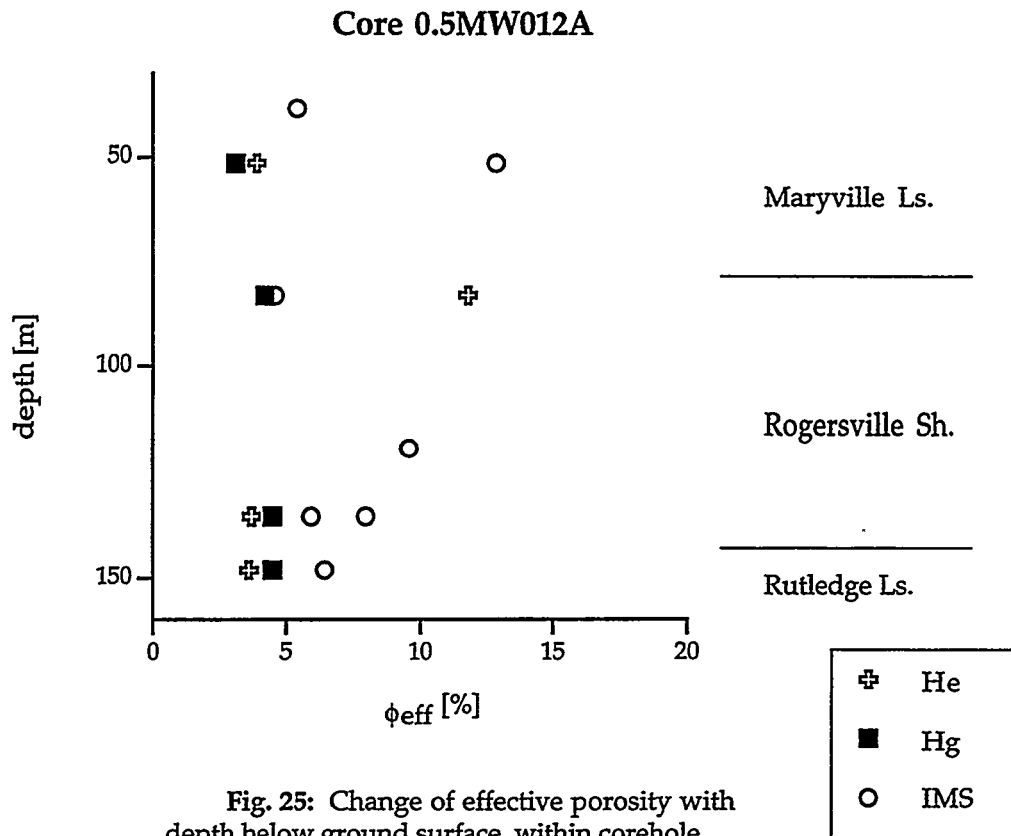
Fig. 25: Change of effective porosity with depth below ground surface within corehole 0.5MW012A (Copper Creek thrust sheet). He, Hg and IMS refer to effective porosity values obtained, respectively, through helium porosimetry, mercury porosimetry, and the immersion-saturation method.

cement is zero. Analysis of mudrock texture, using for example SEM, light microscopy, and X-ray diffraction, is necessary to test this hypothesis. Low effective porosity values based on the immersion-saturation method from sampling intervals close to the present day surface might reflect pervasive cementation indicative of type II data triads (e.g., Figure 24, sampling interval at 27 m). Meteoric diagenetic effects might have preferentially affected type I data triads with the higher effective porosity values.

Loss of replaced meteoric cement during immersion-saturation experiments might also explain the effective porosity values of 13 to 16% (Figures 15, 23, 24, 25; Appendix IV) that seem rather high for mudrock specimens that have experienced such burial depths (Katsube et al., 1991, 1992a; Katsube and Williamson, 1994). High effective porosity values (>10 %) based on the immersion-saturation method have to be considered close to accurate, however, if they are corroborated by matching values based on helium porosimetry (Figures 23, 24).

Summary of Effective Porosity of Conasauga Group Mudrock. Effective porosity values determined from mudrock specimens of the Conasauga Group are higher than previously measured (Diment and Robertson, 1963; deLaguna et al., 1968; Goldstrand and Menefee, in preparation; Tables 1 and 8) or assumed (Toran et al., 1995) values.

In situ effective porosity will be somewhat less than the values reported in this study because of the existing confining pressure at depth. The deviation from the reported values must be considered small, however, because Conasauga Group mudrock experienced a thorough lithification. Furthermore, the retrieval depth of the analyzed specimens was less than 400 m thus minimizing the potential effect of porosity increase due to loss of confining pressure (Katsube and Williamson, 1994; Katsube et al., 1996).

In general, reported values of effective porosity based on the immersion-saturation method are considered to most accurately approach the true values of effective porosity of the analyzed specimens. However, the possible loss of replaced meteoric cement during immersion-saturation porosimetry, presented to explain the anomalous porosity-versus-depth trends in coreholes from the Copper Creek thrust sheet, implies that these effective porosity values must be considered as maximum values. The mean effective porosity of 9.90% for Conasauga Group mudrock on the ORR based on the immersion-saturation method should be corrected to a slightly lower value reflecting the possibility of cement loss during the laboratory measurements. This is especially true for individual immersion-saturation data from sampling intervals close to the present day surface and for specimens whose effective porosity is not independently corroborated by helium-porosimetry data.

While the concept of replaced cement must remain speculative in the absence of data on mudrock texture, it could have important implications if it were true. For example, will the chemical characteristics of the contaminated water migrating through the waste-disposal facilities have an effect on the cementation of the mudrock? If it does, will it have a dissolving or enhancing effect on the cementation? If it has such effects would it increase or decrease effective porosity and thereby influence the retardation capacity of the mudrock? The potential impact of the chemical characteristics of contaminated water on the porosity of the surrounding rock is unknown at this time.

COMPARISON OF PETROPHYSICAL TECHNIQUES

The immersion-saturation method is judged to be appropriate for determining the effective porosity of Conasauga Group mudrock, although there was much loss of rock material during experiments and during preparation of some specimens. It is the most inexpensive of the methods used during the research project. Furthermore, the method is simple, not too time consuming, and was easily installed in one of the laboratories at the Environmental Sciences Division. It has the further advantage that the specimens can be observed and studied following the different procedural steps, thus increasing the likelihood that only intact (or judged to be intact) specimens are used. The method requires some experience for inspecting the specimens following each procedural step and for judging the reliability of the results. Repeat measurements on specimens from the same sampling interval are recommended and very often are necessary because many of the specimens do not survive the procedural steps intact. Reliable data from specimens of cylinder shape require much effort to obtain in contrast to reliable data from specimens of irregular shape. Cylindrically shaped specimens are difficult to acquire from the mudrock-dominated stratigraphic units of the Conasauga Group and often do not preserve their exact volume during the experiments. For calculation of reliable effective porosities based on specimens of irregular shape accurate data on specimen bulk-densities are indispensable. These data should be gathered with state-of-the-art petrophysical measurement techniques, such as mercury immersion.

Mercury porosimetry is by far the most expensive petrophysical measurement technique used in this research project. Because of the nature of the Conasauga Group mudrock specimens and the mechanical limitations of the currently available mercury porosimeters, mercury porosimetry tended to underestimate effective porosity for the majority of the sampling intervals. The method provided, however, important data on pore-throat sizes and their distribution, and required data on specimen bulk-density.

Helium porosimetry is a less expensive method than mercury porosimetry. It proved valuable in conjunction with the immersion-saturation method to characterize the effective porosity of mudrock from the Conasauga Group. There were, however, deviating values (generally too low, in a few cases too high) which might indicate possible analytical problems.

In general, all three analysis techniques constituted a highly useful combination in characterizing the pore characteristics of Conasauga Group mudrock from the ORR. These methods provide a powerful set of complementary techniques to investigate and clarify the pore-space characteristics of fine-grained siliciclastic rocks. Overall,

however, with the emphasis on determination of effective porosity for this research project, the immersion-saturation method should be given preference based on the reliability of the results and the analysis costs. For a detailed characterization of the pore-space characteristics of fractured mudrock and for predictive purposes, all three petrophysical techniques should be combined and augmented by petrographical methods (SEM, TEM, polarizing microscope).

The usefulness of the radial diffusion-cell method is currently limited by the type and nature of the specimens available from the Conasauga Group. Furthermore, some aspects of the experimental set up may have to be reconsidered. The method, however, should be tested further provided that more and better suited specimens become available through future drilling campaigns. The use of solutes with this method has the potential to better mimic the behavior of contaminants within the interconnected pore space of mudrock specimens.

CONCLUSIONS

1. In order to quantify effective porosity for mudrock of the Conasauga Group several petrophysical techniques were employed, including the immersion-saturation method, helium porosimetry, mercury porosimetry, and the radial diffusion-cell method. The latter technique is novel and is currently in its experimental stages, whereas the first three methods are commonly used for reservoir core-analysis in the petroleum industry. Apart from effective porosity, the experiments yielded quantitative data on specimen grain-densities, specimen bulk-densities, and the size of pore throats and their distribution.

2. Effective porosity values for mudrock-dominated stratigraphic units of the Conasauga Group on the ORR (Table 9) are significantly higher than previously measured (reported to range between 0.1% and 3.4%) and assumed values. The mean value of effective porosity measured with the immersion-saturation method is 9.90 (±2.61)% based on a total of 56 measurements. Helium porosimetry yielded a mean effective porosity value of 8.1 (±4.3)% based on 33 measurements. However, there is a considerable spread in the data. Data generated with mercury porosimetry display a mean of 3.8% with a standard deviation of 0.7% (n = 33). The effective porosity data generated with the radial diffusion-cell method (7.3%, 6.0%) compare favorably with values obtained with other methods from the same/adjacent core intervals.

3. Overall, effective porosity values based on the immersion-saturation method are considered to provide the most reliable measures of effective porosity of Conasauga Group mudrock. The results have to be considered as maximum effective porosity values, because in situ conditions were not simulated and because of a possible loss of

Table 9: Summary of petrophysical data of mudrock from the Conasauga Group on the ORR. Abbreviations: Sampl. I. = sampling interval from which specimens were removed; Depth = drill depth below ground surface; ϕ_{He} = effective porosity measured with helium porosimetry, ϕ_{Hg} = effective porosity measured with mercury porosimetry, ϕ_I = effective porosity measured with the immersion-saturation method (1 - irregularly shaped specimens, 2 - cylindrically shaped specimens), ϕ_{WM} = effective porosity measured with the radial diffusion-cell method, d_{Hg} = geometric mean of pore-throat-size distribution, δ_{He} = specimen grain-density, δ_{Hg} = specimen bulk-density, Strat. Unit = stratigraphic unit. Asterisk indicates that the value is an average of several values for this sampling interval.

Core	Sampl. I.	Depth [m]	ϕ_{He} [%]	ϕ_{Hg} [%]	ϕ_{I1} [%]	ϕ_{I2} [%]	ϕ_{WM} [%]	d_{Hg} [nm]	δ_{He} [g·cm⁻³]	δ_{Hg} [g·cm⁻³]	Strat. Unit
GW-133	A1	41.07	11.4	3.8	7.67*	7.08		30.5	2.73	2.64	Maryville Ls.
GW-133	A2	67.18	12.7	4.9	11.47*			24.5	2.78	2.71	Maryville Ls.
GW-133	A3	80.52	10.2	3.1	11.83*			51.3	2.74	2.73	Maryville Ls.
GW-133	A4	95.86									Maryville Ls.
GW-133	A5	114.53	7.6	3.4	11.51			33.9	2.74	2.70	Maryville Ls.
GW-133	A6	138.73	11.5	3.0	10.90*			40.7	2.72	2.67	Rogersville Sh.
GW-133	A7	163.12	12.7	3.5	11.03*			19.2	2.75	2.71	Rogersville Sh.
GW-133	A8	165.56	19.2	4.4	9.75			49.3	2.81	2.74	Rogersville Sh.
GW-132	A9	45.95			9.16						Rutledge Ls.
GW-132	A10	65.33	5.1	2.9	9.39			35.9	2.73	2.72	Rutledge Ls.
GW-132	A11	90.73	9.3	3.8	9.24*			41.1	2.77	2.70	Pumpkin V. Sh.
GW-132	A12	102.97	10.7	3.0	10.35			38.7	2.76	2.72	Pumpkin V. Sh.
GW-132	A13	130.71			11.41						Pumpkin V. Sh.
GW-132	A14	130.76	6.3	4.5	9.43			26.2	2.82	2.72	Pumpkin V. Sh.
GW-132	A15	187.83	3.8	3.1	11.44			66.5	2.78	2.77	Pumpkin V. Sh.
GW-134	A16	44.45	9.9	2.7	9.46*			31.9	2.73	2.69	Nolichucky Sh.
GW-134	A17	58.27	12.2	3.4	11.52*			51.2	2.78	2.70	Nolichucky Sh.
GW-134	A18	80.29	3.2	3.8	12.04*			25.4	2.79	2.71	Nolichucky Sh.
GW-134	A19	99.80	2.9	4.3	13.29			42.7	2.79	2.69	Nolichucky Sh.
GW-134	A20	109.53	4.9	4.3	15.87			56.6	2.76	2.77	Nolichucky Sh.
GW-134	A21	151.59	3.9	4.0	9.16			51.9	2.79	2.70	Nolichucky Sh.
GW-134	A22	158.27	4.7	5.1	11.60			58.2	2.70	2.68	Nolichucky Sh.
GW-134	A23	171.86	14.7	4.2	11.95			38.0	2.79	2.67	Nolichucky Sh.
GW-134	A24	181.14	4.1	3.7	11.74			23.1	2.77	2.69	Nolichucky Sh.
GW-134	A25	201.19	10.4	3.2	10.57			49.8	2.80	2.67	Nolichucky Sh.
Wol-1	B1	12.04			13.00*						Nolichucky Sh.
Wol-1	B2	12.95									Nolichucky Sh.
Wol-1	B3	26.67	4.4	4.2		3.67		96.8	2.83	2.74	Nolichucky Sh.
Wol-1	B4	38.41	5.3	4.1				41.5	2.79	2.71	Nolichucky Sh.
Wol-1	B5	57.38	6.0	5.2	10.81			49.1	2.82	2.72	Nolichucky Sh.
Wol-1	B6	81.43									Nolichucky Sh.
Wol-1	B7	99.90	10.9	3.2	11.80			30.9	2.77	2.71	Nolichucky Sh.
Wol-1	B8	243.84	15.4	3.4	7.43			54.0	2.79	2.67	Maryville Ls.
Wol-1	B9	320.09	7.8	3.5	6.84			51.1	2.79	2.74	Rutledge Ls.
Wol-1	B10	352.60	3.5	3.2	5.35	5.15		50.4	2.79	2.76	Pumpkin V. Sh.
0.5MW012A	C2	51.44	3.9	3.1	12.84			18.1	2.77	2.72	Maryville Ls.
0.5MW012A	C3	148.10	3.6	4.5	6.44			27.2	2.78	2.68	Rutledge Ls.
0.5MW012A	C4	83.10	11.8	4.2	4.58			23.3	2.81	2.73	Rogersville Sh.
0.5MW012A	C5	118.10			9.59						Rogersville Sh.
0.5MW012A	C6	38.34				5.41	7.3				Maryville Ls.
0.5MW012A	C7	135.13	3.7	4.5	7.97	5.94		33.3	2.78	2.70	Rogersville Sh.
0.5MW012A	C8	138.83					6.0				Rogersville Sh.

replaced meteoric cement during analysis. The possible influence of these two factors on the reported effective porosity values is considered to be small.

4. Comparison of effective porosity data from the same sampling intervals reveals the presence of distinct types of data triads (a data triad encompasses helium porosimetry, mercury porosimetry and immersion-saturation data from the same sampling interval). Type I data triads are the most common form and display high and congruent effective porosity values based on the immersion-saturation method and helium porosimetry with low values based on mercury porosimetry. This can be explained with the fact that the mercury porosimeter is limited to mercury intrusion-pressures which correspond to a minimum accessible pore-throat size of 3 nm. Apparently, much pore space is sheltered behind access pore-throats of sizes <3 nm. A large number of pore throats are <3 nm either through compaction or, more likely, because of diagenetic overprint with cement coating the surfaces of pore throats thereby . narrowing the connecting and access paths to pores. The data might also indicate the presence of secondary dissolution pores sheltered by pore throats <3 nm. Type II data triads display low and congruent effective porosity values based on helium and mercury porosimetry and on the immersion-saturation method. This might be seen as a final stage in the development from type I data triads with continuing cementation, or as the initial stage following cementation before development of secondary dissolution pores. Type III and type IV data triads display very low and very high values of effective porosity, respectively, based on helium porosimetry. Otherwise, these data triads are in line with type I data triads. There is reason to believe that the deviating helium-porosimetry data might be inaccurate.

5. Pore-throat-size distribution data show a range from 3 nm to 5000 nm, with a majority of sizes between 3 nm and 100 nm. The minimum value is determined by equipment limitations. The curves are mostly unimodal (some bimodal) with the mode resting consistently within the 5 nm-size class. The geometric mean of pore-throat-sizes of sampling intervals ranges from 18.1 nm to 96.8 nm (Table 9). Data on measured pore-throat sizes and their distribution may be useful for evaluating the ability and extent of contaminant species to access the interconnected pore space of the mudrock matrix through diffusion.

6. Data on specimen bulk-density and specimen grain-density (Table 9) display a mean of 2.71 $g \cdot cm^{-3}$ (standard deviation of 0.03 $g \cdot cm^{-3}$) and 2.77 $g \cdot cm^{-3}$ (standard deviation of 0.03 $g \cdot cm^{-3}$), respectively, based on 33 measurements each. These data may be useful especially for geophysical surveys on the ORR.

7. The immersion-saturation method is considered appropriate in determining the effective porosity of Conasauga Group mudrock. Mercury porosimetry underestimated effective porosity, whereas helium porosimetry provided useful effective porosity data, although for part of the data set analytical problems must be suspected. All three analysis techniques combined, however, provide a powerful set of methods to investigate and clarify the pore-space characteristics of fine-grained siliciclastic rocks. The usefulness of the radial diffusion-cell method is currently limited by the type and nature of the specimens available from the Conasauga Group.

66

REFERENCES

American Petroleum Institute (1960): Recommended practices for core-analysis procedure. API Recommended Practice 40 (RP40), first edition, American Petroleum Institute, Washington D. C., 44 p.

Baxter, P. M. (1989): *Clay Mineral Diagenesis in the Pumpkin Valley Shale, Oak Ridge, Tennessee.* Unpubl. Master's Thesis, Louisiana State University, Baton Rouge, 197 p.

Blatt, H., Middleton, G. V., and Murray, R. C. (1980): *Origin of Sedimentary Rocks.* Prentice-Hall, Englewood Cliffs, NJ, 782 p.

Bush, D. C, and Jenkyns, R. E. (1970): Proper hydration of clays for rock property determinations. Journal of Petroleum Technology, July, p. 800 - 804.

deLaguna, W. T., Tamura, T., Weeren, H. O., Struxness, E. G., McClain, W. C., and Sexton, R. C. (1968): *Engineering Development of Hydraulic Fracturing as a Method for Permanent Disposal of Radioactive Wastes.* ORNL-4259.

Diment, W. H., and Robertson, E. C. (1963): Temperature, thermal conductivity, and heat flow in a drilled hole near Oak Ridge, Tennessee. Journal of Geophysical Research, v. 68, p. 5035-5047.

Dorsch, J. (1995): *Determination of Effective Porosity of Mudrocks - A Feasibility Study.* ORNL/GWPO-019.

Dreier, R. B. and Koerber, S. M. (1990): *Fault Zone Identification in the Area surrounding the Y-12 Plant and its Waste Management Areas.* Y/TS-656.

Drost-Hansen, W. (1991): Some effects of vicinal water on the sedimentation process, compaction, and ultimate properties of sediments. In: Bennett, R. H., Bryant, W. R., and Hulbert, M. H., eds., *Microstructures of Fine-grained Sediments,* p. 259-266.

Foreman, J. L. (1991): *Petrologic and Geochemical Evidence for Water-rock Interaction in the mixed Carbonate-siliciclastic Nolichucky Shale (Upper Cambrian) in East Tennessee.* Ph. D. Dissertation, University of Tennessee, Knoxville, TN, 228 p.

Germain, D., and Frind, E. O. (1989): Modelling of contaminant migration in fracture networks: Effects of matrix diffusion. Proceedings Int. Symp. on Contaminant Transport in Groundwater, Stuttgart, Germany (April 1989).

Goldstrand, P. M., and Menefee, L. S. (in preparation): *Preliminary Porosity Data for the Maryville Limestone and Rogersville Shale from Wag 5, Melton Valley, Tennessee..*

Grim, R. E. (1962): *Applied Clay Mineralogy.* McGraw-Hill, New York, 422 p.

Hasson, K. O., and Haase, S. C. (1988): Lithofacies and paleogeography of the Conasauga Group, (Middle and Late Cambrian) in the Valley and Ridge province of east Tennessee. Bull. Geol. Soc Am., v. 100, p. 234-246.

Hatcher, R. D., Jr., Lemiszki, P. J., Dreier, R. B., Ketelle, R. H., Lee, R. R., Lietzke, D. A., McMaster, W. M., Foreman, J. L., and Lee, S. Y. (1992): *Status Report on the Geology of the Oak Ridge Reservation.* ORNL/TM-12074.

Issler, D. R., and Katsube, T. J. (1994): Effective porosity of shale samples from the Beaufort MacKenzie Basin, northern Canada. In: *Current Research, 1994-B.* Geological Survey of Canada, p. 19-26.

Katsube, T. J. (1992): Statistical analysis of pore-size distribution data of tight shales from the Scotian Shelf. In: *Current Research, Part E*. Geological Survey of Canada, Paper-1E, p. 365-372.

Katsube, T. J., and Best, M. E. (1992): Pore structure of shales from the Beaufort-Mackenzie Basin, Northwest Territories. In: *Current Research, Part D*. Geological Survey of Canada, Paper 92-1E, p. 157-162.

Katsube, T. J., and Issler, D. R. (1993): Pore-size distributions of shales from the Beaufort-Mackenzie Basin, northern Canada. In: *Current Research, Part E*. Geological Survey of Canada, Paper-1E, p. 123-132.

Katsube, T. J., and Scromeda, N. (1991): Effective porosity measuring procedure for low porosity rocks. In: *Current Research, Part E*. Geological Survey of Canada, Paper 91-1E, p. 291-297.

Katsube, T. J., and Williamson, M. A. (1994): Effect of shale diagenesis on shale nano-pore structure and implications for sealing capacity. Clay Minerals, v. 29, p. 451-461.

Katsube, T. J., and Williamson, M. A. (1995): Critical depth of burial of subsiding shales and its effect on abnormal pressure development. Proceedings of the Oil and Gas Forum '95 ("Energy from Sediments"), Geological Survey of Canada Open File 3058, p. 283-286.

Katsube, T. J., Bloch, J., and Issler, D. R. (1995): Shale pore structure evolution under variable sedimentation rates in the Beaufort-Mackenzie Basin. Proceedings of the Oil and Gas Forum '95 ("Energy from Sediments"), Geological Survey of Canada Open File 3058, p. 211-215.

Katsube, T. J., Mudford, B. S., and Best, M. E. (1991): Petrophysical characteristics of shales from the Scotian Shelf. Geophysics, v. 56, p. 1681-1689.

Katsube, T. J., Scromeda, N., and Williamson, M. (1992a): Effective porosity from tight shales from the Venture gas field, offshore Nova Scotia. In: *Current Research, Part D*. Geological Survey of Canada, Paper 92-1D, p. 111-119.

Katsube, T. J., Williamson, M., and Best, M. E. (1992b): Shale pore structure evolution and its effect on permeability. In: *Symposium Volume III of the Thirty-Third Annual Symposium of the Society of Professional Well Log Analysts (SPWLA)*. The Society of Core Analysts Preprints, Oklahoma City, Oklahoma, Paper SCA-6214, p. 1-24.

Kopaska-Merkel, D. C. (1988): New applications in the study of porous media: Determination of pore-system characteristics on small fragments (part I). Northeastern Environmental Science, v. 7, p. 127-142.

Kopaska-Merkel, D. C. (1991): *Analytical Procedure and Experimental Design for Geological Analysis of Reservoir Heterogeneity using Mercury Porosimetry*. Alabama Geological Survey Circular 153, 29 p.

Krushin, J. (1993): Entry pore-throat size of nonsmectite shales. American Association of Petroleum Geologists Abstracts with Program, Annual Meeting, Denver, Colorado.

Lee, S. Y., Hyder, L. K., and Alley, P. D. (1987). *Mineralogical Characterization of Selected Shales in Support of Nuclear Waste Repository Studies*. ORNL/TM-10567.

Lee, S. Y., Hyder, L. K., and Alley, P. D. (1991): Microstructural and mineralogical characterization of selected shales in support of nuclear waste repository studies. In: Bennett, R. H., Bryant, W. R., and Hulbert, M. H., eds., *Microstructures of Fine-grained Sediments*, Springer-Verlag, Heidelberg, p. 545-560.

Lemiszki, P. J., and Hatcher, R. D., Jr. (1992): 5. Structure of the Oak Ridge Reservation. In: R. D. Hatcher, Jr., P. J. Lemiszki, R. B. Dreier, R. H. Ketelle, R. R. Lee, D. A. Lietzke, W. M. McMaster, J. L. Foreman, and S. Y. Lee, *Status Report on the Geology of the Oak Ridge Reservation.* ORNL/TM-12074, p. 109-178.

Loman, J. M., Katsube, T. J., Correia, J. M., and Williamson, M. A. (1993): Effect of compaction on porosity and formation factor for tight shales from the Scotian Shelf, offshore Nova Scotia. In: *Current Research, Part E.* Geological Survey of Canada, Paper 93-1E, p. 331-335.

Luffel, D. L., and Howard, W. E. (1988): Reliability of laboratory measurement of porosity in tight gas sands. SPE Formation Evaluation, December, p. 705-710.

Markello, J. R., and Read, J. F. (1981): Carbonate ramp-to-deeper shale shelf transitions of an Upper Cambrian intrashelf basin, Nolichucky Formation, southwest Virginia Appalachians. Sedimentology, v. 28, p. 573-597.

Markello, J. R., and Read, J. F. (1982): Upper Cambrian intrashelf basin, Nolichucky Formation, southwest Virginia Appalachians. Bull. Am. Assoc. Petroleum Geol., v. 66, p. 860-878.

McKay, L. D., Gillham, R. W., and Cherry, J. A. (1993): Field experiments in a fractured clay till 2. Solute and colloid transport. Water Resources Research, v. 29, p. 3879-3890.

Montanez, I. P. (1994): Late diagenetic dolomitization of Lower Ordovician, Upper Knox Carbonates: A record of the hydrodynamic evolution of the Southern Appalachian basin. American Association of Petroleum Geologists Bulletin, v. 78, p. 1210-1239.

Mussman, W. J., Montanez, I. P., and Read, J. F. (1988): Ordovician Knox paleokarst unconformity, Appalachians. In: James, N. P., and Choquette, P. W., eds., *Paleokarst,* Springer-Verlag, Heidelberg, p. 211-228.

Neretnieks, I. (1980): Diffusion in the rock matrix: An important factor in radionuclide retardation? Journal of Geophysical Research, v. 85, p. 4379-4397.

Nightingale, E. R. (1959): Phenomenological theory of ion solvation. J. Phys. Chem, v. 63, p. 1381-1387.

Novakowski, K. S., and van der Kamp, G. (in press): The radial diffusion method 2. A semi-analytical model for the determination of apparent diffusivity, porosity and adsorption. Water Resources Research.

Olhoeft, G. R., and Johnson, G. R. (1989): Densities of rocks and minerals. In: Carmichael, R. S., ed., *Practical Handbook of Physical Properties of Rocks and Minerals.* CRC Press, Boca Raton, p. 141-176.

Read, J. F. (1989): Controls on evolution of Cambrian-Ordovician passive margin, U. S. Appalachians. In: Crevello, P. D., Wilson, J. L., Sarg, J. F., and Read, J. F., eds., *Controls on Carbonate Platform and Basin Development.* SEPM Special Publication 44, p. 147-165.

Rieke, H. H., III, and Chilingarian, G. V., eds. (1974): *Compaction of Argillaceous Sediments.* Developments in Sedimentology 16. Elsevier, Amsterdam, 424 p.

Rodgers, J. (1953): *Geologic map of East Tennessee with Explanatory Text, Scale 1:125000.* Bulletin Tennessee Division of Geology, v. 55.

Rootare, H. M. (1970): A review of mercury porosimetry. Perspectives of Powder Metallurgy, v. 5, p. 225-252.

Sanford, W. E., Jardine, P. M., and Solomon, D. K. (1994): Examining matrix diffusion in fractured shales with noble gases. Geological Society of America Abstracts with Programs, v. 26, p. A362.

Scromeda, N., and Katsube, T. J. (1993): Effect of vacuum-drying and temperature on effective porosity determination for tight rocks. In: *Current Research, Part E.* Geological Survey of Canada, Paper-1E, p. 313-319.

Scromeda, N., and Katsube, T. J. (1994): Effect of temperature on drying procedures used in porosity measurements of tight rocks. In: *Current Research, Part E.* Geological Survey of Canada, Paper-1E, p. 283-289.

Shevenell, L. M., Moore, G. K., and Dreier, R. B. (1994): Contaminant spread and flushing in fractured rocks near Oak Ridge, Tennessee. Ground Water Monitoring & Remediation, v. 14, p. 120-129.

Soeder, D. J. (1988): Porosity and permeability of eastern Devonian gas shales. SPE Formation Evaluation, v. 3, p. 116-138.

Solomon, D. K., Moore, G. K., Toran, L. E., Dreier, R. B., and McMaster, W. M. (1992): *A Hydrologic Framework for the Oak Ridge Reservation.* ORNL/TM-12026.

Srinivasan, K., and Walker, K. R. (1993): Sequence stratigraphy of an intrashelf basin carbonate ramp to rimmed platform transition: Maryville Limestone (Middle Cambrian), southern Appalachians. Bull. Geol. Soc. Am., v. 105, p. 883-896.

Tang, D. H., Frind, E. O., and Sudicky, E. A. (1981): Contaminant transport in fractured porous media: Analytical solution for a single fracture. Water Resources Research, v. 17, p. 555-564.

Toran, L., Sjoreen, A., and Morris, M. (1995): Sensitivity analysis of solute transport in fractured porous media. Geophysical Research Letter, v. 22, p. 1433-1436.

van der Kamp, G., Van Stempvoort, D. R., Wassenaar, L. I. (in press): The radial diffusion method 1. Using intact cores to determine isotopic composition, chemistry and effective porosities for groundwater aquitards. Water Resources Research.

Wardlaw, N. C. (1976): Pore geometry of carbonate rocks as revealed by pore casts and capillary pressure. American Association of Petroleum Geologists Bulletin, v. 60, p. 245-257.

Wardlaw, N. C., McKellar, M., and Yu, Li (1988): Pore and throat size distribution determined by mercury porosimetry and by direct observation. Carbonates and Evaporites, v. 3, p. 1-15.

Washburn, E. W. (1921): Note on a method of determining the distribution of pore sizes in a porous material. Proceedings of the National Academy of Sciences, v. 5, p. 115-116.

Walker, K. R., Foreman, J. L., and Srinivasan, K. (1990): The Cambrian Conasauga Group of eastern Tennessee: A preliminary general stratigraphic model with a more detailed test for the Nolichucky Formation. Proceedings Appalachian Basin Industrial Associates, v. 17, p. 184-189.

Weaver, C. E. (1984): *Shale-slate Metamorphism in southern Appalachians.* Developments in Petrology 10, Elsevier, Amsterdam, 239 p.

Wickliff, D. S., Solomon, D. K., and Farrow, N. D. (1991): *Preliminary Investigation of Processes that affect Source Term Identification.* ORNL/ER 59.

APPENDIX I: Notation System Of Sampling Intervals And Specimens

Sampling intervals are coded with a capital letter immediately followed by a number (e.g., A17). Several specimens are available from each sampling interval for the different petrophysical measurements. A suffix following the sample-interval code indicates for which petrophysical technique the specimen was used.

Sampling Intervals

Code **A:** samples are from coreholes GW-132, GW-133, and GW-134 from the Whiteoak Mountain thrust sheet;
Code **B:** samples are from corehole Wol-1 from the Copper Creek thrust sheet;
Code **C:** samples are from corehole Bechtel 05.MW012A from the Copper Creek thrust sheet (WAG 5).

The GW-cores and the Wol-1 core are available in the corebarn (Building 7042 at X-10), whereas the Bechtel core 05.MW012A is stored at the Bechtel field office at X-10. The number following the code letter simply indicates the numbered sample interval from the respective cores. More detail on the sampling intervals (drill depth, stratigraphic units) is provided in Appendix II.

Specimens from Sampling Intervals

Specimens with the suffix -a, -b, or -c are irregularly shaped chips, whereas specimens with the suffix -e are cylinders. Specimens generally weigh between 3 to 10 g.

Suffix -a: denotes chips used for mercury porosimetry;
Suffix -b: denotes chips used for helium porosimetry;
Suffix -c: denotes chips used for the immersion-saturation method;
Suffix -cr: denotes additional chips used for the immersion-saturation method;
Suffix -d: denotes larger core segments which were used to obtain core plugs; also material used for radial diffusion-cell method (when appropriate);
Suffix -e: denotes cylindrical core-plug segments (commonly drilled from specimen d) of known volume used for the immersion-saturation method.
Suffix -er: denotes additional cylindrical core-plug segments of known volume used for the immersion-saturation method.

The number attached to some suffixes denotes that there were more than one specimen available for analysis (usually for the immersion-saturation method).

APPENDIX II: Sampling Intervals

Summary information on sampling locations of specimens: designation of sample (intervals), cores and core-box numbers, drill depths, and stratigraphic units.

Sampling Intervals

Sample	Core	Drill Depth	Stratigraphic Unit
A1	GW-133 (Box 6)	134' 9" (41.07 m)	Maryville Ls.
A2	GW-133 (Box 17)	220' 5" (67.18 m)	Maryville Ls.
A3	GW-133 (Box 20)	264' 2" (80.52 m)	Maryville Ls.
A4	GW-133 (Box 25)	314' 6" (95.86 m)	Maryville Ls.
A5	GW-133 (Box 32)	375' 9" (114.53 m)	Maryville Ls.
A6	GW-133 (Box 40)	455' 2" (138.73 m)	Rogersville Sh.
A7	GW-133 (Box 48)	535' 2" (163.12 m)	Rogersville Sh.
A8	GW-133 (Box 49)	543' 2" (165.56 m)	Rogersville Sh.
A9	GW-132 (Box 6)	150' 9" (45.95 m)	Rutledge Ls.
A10	GW-132 (Box 13)	214' 4" (65.33 m)	Rutledge Ls.
A11	GW-132 (Box 21)	297' 8" (90.73 m)	Pumpkin Valley Sh.
A12	GW-132 (Box 26)	337' 10" (102.97 m)	Pumpkin Valley Sh.
A13	GW-132 (Box 35)	428' 10" (130.71 m)	Pumpkin Valley Sh.
A14	GW-132 (Box 35)	429' (130.76 m)	Pumpkin Valley Sh.
A15	GW-132 (Box 35)	616' 3" (187.83 m)	Pumpkin Valley Sh.
A16	GW-134 (Box 12)	145' 10" (44.45 m)	Nolichucky Sh.
A17	GW-134 (Box 17)	191' 2" (58.27 m)	Nolichucky Sh.
A18	GW-134 (Box 24)	263' 5" (80.29 m)	Nolichucky Sh.
A19	GW-134 (Box 30)	327' 5" (99.80 m)	Nolichucky Sh.
A20	GW-134 (Box 34)	359' 4" (109.53 m)	Nolichucky Sh.
A21	GW-134 (Box 47)	497' 4" (151.59 m)	Nolichucky Sh.
A22	GW-134 (Box 50)	519' 3" (158.27 m)	Nolichucky Sh.
A23	GW-134 (Box 54)	563' 10" (171.86 m)	Nolichucky Sh.
A24	GW-134 (Box 60)	617' 3" (181.14 m)	Nolichucky Sh.
A25	GW-134 (Box 64)	660' 1" (201.19 m)	Nolichucky Sh.
B1	Wol-1 (Box 3)	39' 6" (12.04 m)	Nolichucky Sh.
B2	Wol-1 (Box 3)	42' 6" (12.95 m)	Nolichucky Sh.
B3	Wol-1 (Box 8)	87' 6" (26.67 m)	Nolichucky Sh.
B4	Wol-1 (Box 12)	126' (38.41 m)	Nolichucky Sh.
B5	Wol-1 (Box 18)	188' 3" (57.38 m)	Nolichucky Sh.
B6	Wol-1 (Box 27)	267' 2" (81.43 m)	Nolichucky Sh.
B7	Wol-1 (Box 34)	327' 9" (99.90 m)	Nolichucky Sh.
		327' 2" (99.72 m)	Nolichucky Sh.
B8	Wol-1 (Box 84)	800' (243.84 m)	Maryville Ls.
B9	Wol-1 (Box 111)	1050' 2" (320.09 m)	Rutledge Ls.
B10	Wol-1 (Box 123)	1156' 10" (352.60 m)	Pumpkin Valley Sh.
C2	0.5MW012A (Betchel #6)	168' 10" (51.44 m)	Maryville Ls.
C3	0.5MW012A (Betchel #28)	485' 8" (148.1 m)	Rutledge Ls.
C4	0.5MW012A (Betchel #11)	272' 6" (83.1 m)	Rogersville Sh.
C5	0.5MW012A (Betchel #18)	387' 7" (118.1 m)	Rogersville Sh.
C6	0.5MW012A (Betchel #2)	125' 8" (38.34 m)	Maryville Ls.
C7	0.5MW012A (Betchel #22)	443' 5" (135.13 m)	Rogersville Sh.
C8	0.5MW012A (Betchel #24)	455' 6" (138.83 m)	Rogersville Sh.

APPENDIX III: Results - Immersion-Saturation Method (cylindrically shaped specimens)

Summary of effective porosity data obtained from cylindrically shaped specimens with the immersion-saturation method. ϕ_{I2} refers to effective porosity, h and d are specimen height/thickness and diameter, respectively, V refers to the calculated specimen volume. W_{SAT} and W_{DRY} refer to the measured weight of the water-saturated specimen and to the weight of the dried specimen, respectively, whereas ΔW gives the difference between the saturated and dry specimen weights. 'lost' refers to specimens which disintegrated during the experiments; '-' refers to unreported data, because the specimen was either lost, or displayed characteristics during the experiment which caused the measurements/calculations to be judged unreliable.

Immersion-Saturation Porosimetry Data (cylindrical forms)

Specimen	h [mm]	d [mm]	V [mm^3]	W_{SAT} [g]	W_{DRY} [g]	ΔW [g]	ϕ_{I2} [%]
A1-e	5.36	25.29	2691.48	7.24	7.05	0.19	7.08
A3-e	6.15	25.30	3093.29	8.46	8.17	0.29	-
A7-e	10.25	25.28	5143.53	14.01	13.56	0.45	-
A8-e	7.60	25.21	3792.09	10.49	10.17	0.32	-
A9-e	5.72	25.32	2881.66	7.80	7.50	0.29	-
A10-e	4.18	25.30	2098.89	5.67	5.50	0.17	-
A12-e	10.48	25.28	5258.40	lost	-	-	-
A15-e	10.47	25.28	5254.39	lost	-	-	-
B3-e	10.89	25.27	5463.21	14.92	14.72	0.20	3.67
B10-e	10.79	25.30	5421.26	14.89	14.61	0.28	5.15
C6-e	27.10	9.32	1848.84	4.91	4.81	0.10	5.41
C7-e	16.58	9.28	1120.20	3.04	2.97	0.07	5.94

APPENDIX IV: Results - Immersion-Saturation Method (irregularly shaped specimens)

Summary of effective porosity data obtained from irregularly shaped specimens with the immersion-saturation method; ϕ_{II} refers to effective porosity values; W_{SAT} and W_{DRY} refer to the measured weight of the water-saturated specimen and to that of the dried specimen, whereas ΔW gives the difference between the saturated and dry specimen weight; δ_{Hg} refers to the bulk density of the specimen as determined by mercury porosimetry (used in calculating effective porosity); A refers to reliable values and B to values judged reliable (values in **bold**); u refers to unreliable values, l to specimens lost during the experiment, and S designates measurements where saline (NaCl) solution was used as a saturation liquid; the asterisk denotes effective porosity values which were calculated with an assumed bulk density (δ_{Hg} in *italics*) and not with a measured bulk density value from the specimen.

Immersion-Saturation Porosimetry Data (irregularly shaped specimens)

Specimen	W_{SAT} [g]	W_{DRY} [g]	ΔW [g]	δ_{Hg} [g·cm^{-3}]	ϕ_{II} [%]	Comment
A1-c	7.3282	6.9029	0.4253	2.64	16.27	u
A1-cr1	3.6128	3.5567	0.0561	2.64	4.16	A
A1-cr2	3.0208	2.9264	0.0944	2.64	8.52	B
A1-cr3	4.2145	4.0556	0.1589	2.64	10.34	B
A2-c	7.9369	7.5631	0.3738	2.71	13.39	u
A2-cr1	3.9560	3.7827	0.1733	2.71	12.42	B
A2-cr2	4.1569	3.9841	0.1728	2.71	11.75	u
A2-cr3	2.4056	2.3132	0.0924	2.71	10.83	u
A2-cr4	1.9023	1.8306	0.0717	2.71	10.61	A
A2-cr5	2.4795	2.3796	0.0999	2.71	11.38	B
A3-c	5.8927	5.6028	0.2899	2.73	14.13	u
A3-cr1	3.5571	3.3983	0.1588	2.73	12.76	B
A3-cr2	5.7556	5.4948	0.2608	2.73	12.96	u
A3-cr3	1.6112	1.5657	0.0455	2.73	7.93	u
A3-cr4	2.6748	2.5722	0.1026	2.73	10.89	B
A4-c	4.1075	3.8973	0.2102	2.72	14.67	u
A4-cr1	lost	-	-	2.72	-	l
A4-cr2	1.8015	1.7117	0.0898	2.72	14.27	u
A5-c	8.6659	8.2389	0.4270	2.70	13.99	u
A5-cr1	lost	-	-	2.70	-	l
A5-cr2	2.5885	2.4827	0.1058	2.70	11.51	B
A6-c	7.5445	7.2579	0.2866	2.67	10.54	u
A6-cr1	3.8859	3.7609	0.1250	2.67	8.87	S
A6-cr2	4.4880	4.3051	0.1829	2.67	11.34	B
A6-cr3	5.5949	5.3803	0.2146	2.67	10.65	u
A6-cr4	3.8784	3.7322	0.1462	2.67	10.46	B
A6-cr5	4.7582	4.5873	0.1709	2.67	9.95	u
A7-c	5.3924	5.1701	0.2223	2.71	11.65	u
A7-cr1	3.0244	2.9000	0.1244	2.71	11.62	B
A7-cr2	4.6788	4.5053	0.1735	2.71	10.44	B
A7-cr4	4.2077	4.0472	0.1605	2.71	10.75	u
A7-cr5	3.0690	2.9355	0.1335	2.71	12.32	u
A8-c	8.7645	8.4497	0.3148	2.74	10.21	u
A8-cr1	4.2103	4.0656	0.1447	2.74	9.75	B
A8-cr2	6.4124	6.1558	0.2566	2.74	11.42	u
A8-cr3	5.4243	5.2304	0.1939	2.74	10.16	u
A9-c	8.5221	8.1523	0.3698	2.71	12.29	u*
A9-cr1	4.0651	3.8958	0.1693	2.71	11.78	u*
A9-cr2	3.6208	3.4849	0.1359	2.71	10.57	u*
A9-cr3	7.3583	7.1177	0.2406	2.71	9.16	B*
A10-c	6.7918	6.5348	0.2570	2.72	10.70	u
A10-cr1	4.3642	4.2024	0.1618	2.72	10.47	u
A10-cr2x	3.3188	3.1818	0.1370	2.72	11.71	u
A10-cr2xx	2.4340	2.3528	0.0812	2.72	9.39	A
A11-c	7.9845	7.6369	0.3476	2.70	12.29	u
A11-cr1	4.9834	4.8089	0.1745	2.70	9.80	u
A11-cr2	2.8445	2.7592	0.0853	2.70	8.35	B
A11-cr3	5.1314	4.9461	0.1853	2.70	10.12	B
A11-cr4	2.0754	2.0054	0.0700	2.70	9.42	u
A11-cr5	3.7192	3.5582	0.1610	2.70	12.22	u
A12-c	7.9571	7.5838	0.3733	2.72	13.39	u
A12-cr1	3.0436	2.9396	0.1040	2.72	9.62	S
A12-cr2	3.0234	2.9126	0.1108	2.72	10.35	B
A13-c	6.3970	6.0700	0.3270	2.72	14.65	u*
A13-cr1	3.5903	3.4446	0.1457	2.72	11.51	u*
A13-cr2	4.6435	4.4566	0.1869	2.72	11.41	B*
A14-c	3.8445	3.7157	0.1288	2.72	9.43	A
A14-cr1	3.8089	3.7008	0.1081	2.72	7.95	u
A15-c	4.2620	4.0930	0.1690	2.77	11.44	A
A15-cr1	3.7147	3.5799	0.1348	2.77	10.43	u
A15-cr_x	8.1667	7.8940	0.2727	2.77	9.57	u

A15-cr_xx	6.2314	6.0485	0.1829	2.77	8.38	u
A16-c	6.5145	6.2654	0.2491	2.69	10.69	u
A16-cr1	3.3040	3.1958	0.1082	2.69	9.11	B
A16-cr2	3.5575	3.4352	0.1223	2.69	9.58	B
A16-cr3	4.1371	3.9972	0.1399	2.69	9.41	B
A16-cr4	3.9512	3.8133	0.1379	2.69	9.73	B
A17-c	5.5813	5.2657	0.3156	2.70	16.18	u
A17-cr1	3.1502	3.0041	0.1461	2.70	13.13	B
A17-cr2	3.7834	3.6166	0.1668	2.70	12.45	B
A17-cr3	4.7712	4.6172	0.1540	2.70	9.01	u
A17-cr4	3.6828	3.5642	0.1186	2.70	8.98	B
A18-c	7.3423	6.9554	0.3869	2.71	15.07	u
A18-cr1	2.8409	2.7195	0.1214	2.71	12.10	B
A18-cr2	lost	-	-	2.71	-	l
A18-cr3	1.2809	1.2267	0.0542	2.71	11.97	B
A19-c	3.6370	3.3681	0.2689	2.69	21.48	u
A19-cr1	2.0708	1.9613	0.1095	2.69	15.02	u
A19-cr2	lost	-	-	2.69	-	l
A19-cr3	3.7316	3.5559	0.1757	2.69	13.29	B
A20-c	5.3531	5.0631	0.2900	2.77	15.87	B
A21-c	7.3751	7.0301	0.3450	2.70	13.25	u
A21-cr1	3.4117	3.2605	0.1512	2.70	12.52	u
A21-cr2	3.0193	2.8885	0.1308	2.70	12.23	u
A21-cr3	3.5351	3.3753	0.1598	2.70	12.78	u
A21-cr4	4.2790	4.1041	0.1749	2.70	11.51	u
A21-cr5	4.0911	3.9568	0.1343	2.70	9.16	B
A22-c	6.6814	6.4043	0.2771	2.68	11.60	B
A23-c	9.1940	8.8001	0.3939	2.67	11.95	A
A24-c	2.6330	2.5229	0.1101	2.69	11.74	A
A25-c	2.8137	2.7066	0.1071	2.67	10.57	A
B1-c	4.3691	4.1158	0.2533	2.72	16.74	u*
B1-cr1	3.0391	2.8643	0.1748	2.72	16.60	u*
B1-cr2	2.4580	2.3466	0.1114	2.72	12.91	B*
B1-cr3	2.4179	2.3068	0.1111	2.72	13.10	B*
B2-c	lost	-	-	2.72	-	l
B2-cr1	2.8991	2.7524	0.1467	2.72	14.50	S
B2-cr2	lost	-	-	2.72	-	l
B3-c	lost	-	-	2.74	-	l
B3-cr1	3.2745	3.1221	0.1524	2.74	13.37	S
B3-cr2	1.2612	1.1855	0.0757	2.74	17.50	u
B4-c	3.4265	3.2369	0.1896	2.71	15.87	u
B4-cr1	2.0937	1.9866	0.1071	2.71	14.61	u
B4-cr2	3.3616	3.1940	0.1676	2.71	14.22	u
B4-cr3	4.0157	3.8412	0.1745	2.71	12.31	S
B5-c	5.4416	5.2202	0.2214	2.72	11.54	B
B5-cr1	4.1477	3.9995	0.1482	2.72	10.08	B
B5-cr2	13.1298	11.8924	1.2374	2.72	28.30	u
B6-c	4.2000	4.0000	0.2000	2.71	13.55	u*
B6-cr1	3.7520	3.5887	0.1633	2.71	12.33	u*
B7-c	4.8307	4.6292	0.2015	2.71	11.80	A
B8-c	6.5071	6.3309	0.1762	2.67	7.43	A
B9-c	6.2522	6.0999	0.1523	2.74	6.84	A
B10-c	10.0725	9.8810	0.1915	2.76	5.35	A
C2-c	4.9687	4.7448	0.2239	2.72	12.84	A
C3-c	5.1447	5.0240	0.1207	2.68	6.44	B
C3-cr1	7.4455	7.2104	0.2351	2.68	8.74	u
C4-c	6.6881	6.5777	0.1104	2.73	4.58	A
C5-c	3.7429	3.6154	0.1275	2.72	9.59	A*
C7-c	6.4331	6.2486	0.1845	2.70	7.97	A

APPENDIX V: Results - Radial Diffusion-Cell Method

Summary of the measurement data from the experiments with the radial diffusion-cell method.

Radial Diffusion-Cell Measurement Data

date	time	elapsed time (days)	conc. (ppm)	C/C0	specimen
					C6-d
5/23/95	10:00	0	1000	1	
5/23/95	11:03	0.04	1060	1.06	
5/23/95	16:30	0.27	1000	1	
5/24/95	8:50	0.95	1060	1.06	
5/24/95	9:35	0.98	992	0.992	
5/24/95	15:32	1.23	952	0.952	
5/25/95	10:30	2.02	895	0.895	
5/25/95	15:30	2.23	886	0.886	
5/26/95	9:15	2.97	856	0.856	
5/26/95	12:35	3.11	842	0.842	
5/26/95	16:00	3.25	844	0.844	
5/30/95	8:35	6.94	797	0.797	
5/31/95	8:50	7.95	779	0.779	
6/2/95	8:25	9.93	785	0.785	
6/5/95	8:30	12.94	692	0.692	
6/7/95	8:45	14.95	337	0.337	
6/9/95	8:42	16.95	351	0.351	
6/12/95	8:37	19.94	357	0.357	
6/14/95	9:30	21.98	371	0.371	
5/23/95	9:45	0	1000	1	specimen
5/23/95	11:00	0.05	1020	1.02	C8-d
5/23/95	16:30	0.28	968	0.968	
5/24/95	8:47	0.96	988	0.988	
5/24/95	9:32	0.99	924	0.924	
5/24/95	15:29	1.24	968	0.968	
5/25/95	10:25	2.03	847	0.847	
5/25/95	15:25	2.24	855	0.855	
5/26/95	9:12	2.98	816	0.816	
5/26/95	12:33	3.12	809	0.809	
5/26/95	16:00	3.26	792	0.792	
5/30/95	8:33	6.95	778	0.778	
5/31/95	8:47	7.96	757	0.757	
6/2/95	8:23	9.94	764	0.764	
6/5/95	8:30	12.95	238	0.238	
6/7/95	8:40	14.95	137	0.137	
6/9/95	8:40	16.95	142	0.142	
6/12/95	8:35	19.95	161	0.161	
6/14/95	9:30	21.99	175	0.175	

APPENDIX VI: Results - Mercury Porosimetry

Summary of effective porosity and specimen bulk-density data obtained with mercury porosimetry. ϕ_{Hg1} refers to effective porosity of pore space accessed by pore throats less than or equal to 10 μm, ϕ_{Hg2} refers to effective porosity of pore space accessed by pore throats up to 250 μm, and δ_{Hg} refers to specimen bulk-density.

Mercury-Porosimetry Data

Specimen	δ_{Hg} [g·cm^{-3}]	ϕ_{Hg1} [%]	ϕ_{Hg2} [%]	Specimen	δ_{Hg} [g·cm^{-3}]	ϕ_{Hg1} [%]	ϕ_{Hg2} [%]
A1-a	2.64	3.8	4.2	B1-a			
A2-a	2.71	4.9	5.6	B2-a			
A3-a	2.73	3.1	3.9	B3-a	2.74	4.2	5.3
A4-a				B4-a	2.71	4.1	4.7
A5-a	2.70	3.4	3.7	B5-a	2.72	5.2	6.0
A6-a	2.67	3.0	3.4	B6-a			
A7-a	2.71	3.5	3.9	B7-a	2.71	3.2	3.7
A8-a	2.74	4.4	5.3	B8-a	2.67	3.4	4.1
A9-a				B9-a	2.74	3.5	4.2
A10-a	2.72	2.9	3.3	B10-a	2.76	3.2	3.7
A11-a	2.70	3.8	4.3				
A12-a	2.72	3.0	4.9	C2-a	2.72	3.1	4.1
A13-a				C3-a	2.68	4.5	4.8
A14-a	2.72	4.5	5.0	C4-a	2.73	4.2	4.8
A15-a	2.77	3.1	3.7	C5-a			
A16-a	2.69	2.7	3.1	C6-a			
A17-a	2.70	3.4	3.9	C7-a	2.70	4.5	5.1
A18-a	2.71	3.8	4.2	C8-a			
A19-a	2.69	4.3	5.0				
A20-a	2.77	4.3	5.2				
A21-a	2.70	4.0	4.7				
A22-a	2.68	5.1	6.1				
A23-a	2.67	4.2	4.7				
A24-a	2.69	3.7	4.1				
A25-a	2.67	3.2	3.9				

APPENDIX VII: Results - Helium Porosimetry

Summary of effective porosity and specimen grain-density data obtained with helium porosimetry. ϕ_{He} refers to effective porosity, δ_{He} refers to specimen grain-density.

Helium-Porosimetry Data

Specimen	δ_{He} [g·cm^{-3}]	ϕ_{He} [%]	Specimen	δ_{He} [g·cm^{-3}]	ϕ_{He} [%]
A1-b	2.73	11.4	B1-b		
A2-b	2.78	12.7	B2-b		
A3-b	2.74	10.2	B3-b	2.83	4.4
A4-b			B4-b	2.79	5.3
A5-b	2.74	7.6	B5-b	2.82	6.0
A6-b	2.72	11.5	B6-b		
A7-b	2.75	12.7	B7-b	2.77	10.9
A8-b	2.81	19.2	B8-b	2.79	15.4
A9-b			B9-b	2.79	7.8
A10-b	2.73	5.1	B10-b	2.79	3.5
A11-b	2.77	9.3			
A12-b	2.76	10.7	C2-b	2.77	3.9
A13-b			C3-b	2.78	3.6
A14-b	2.82	6.3	C4-b	2.81	11.8
A15-b	2.78	3.8	C5-b		
A16-b	2.73	9.9	C6-b		
A17-b	2.78	12.2	C7-b	2.78	3.7
A18-b	2.79	3.2	C8-b		
A19-b	2.79	2.9			
A20-b	2.76	4.9			
A21-b	2.79	3.9			
A22-b	2.70	4.7			
A23-b	2.79	14.7			
A24-b	2.77	4.1			
A25-b	2.80	10.4			

APPENDIX VIII: Results - Pore-Throat Sizes

Tabulation of pore-throat-size data obtained with mercury porosimetry. Abbreviations are as follows: d (nm) refers to the geometric mean pore-throat sizes of the different pore-throat-size ranges (expressed in nanometers), ϕa refers to the partial porosity (expressed in percent), ϕ_{Hg1} refers to effective porosity measured by mercury porosimetry for pore-throat sizes ≤ 10 μm (expressed in percent), ϕ_{Hg2} refers to effective porosity measured by mercury porosimetry for pore-throat sizes ≤ 250 μm (expressed in percent), and dHg refers to the geometric mean of the entire pore-throat-size distribution (expressed in nanometers) for the analyzed specimen.

Pore-Throat Size Data based on Mercury Porosimetry

d (nm)	A1 φa (%)	A2 φa (%)	A3 φa (%)	A5 φa (%)	A6 φa (%)	A7 φa (%)	A8 φa (%)	A10 φa (%)	A11 φa (%)	A12 φa (%)	A14 φa (%)	A15 φa (%)	A16 φa (%)
3.2	0.34	0.65	0.36	0.27	0.27	0.49	0.60	0.35	0.43	0.35	0.54	0.28	0.22
5	0.92	1.14	0.68	0.67	0.67	0.89	0.99	0.57	0.78	0.68	0.95	0.69	0.65
7.9	0.58	0.78	0.55	0.65	0.45	0.54	0.60	0.35	0.46	0.46	0.71	0.44	0.38
12.6	0.50	0.38	0.44	0.46	0.37	0.62	0.74	0.43	0.54	0.38	0.52	0.42	0.35
20	0.37	0.60	0.36	0.49	0.40	0.35	0.38	0.30	0.35	0.33	0.49	0.36	0.32
31.6	0.26	0.24	0.16	0.27	0.16	0.22	0.27	0.19	0.24	0.19	0.27	0.17	0.19
50.1	0.29	0.70	0.16	0.22	0.21	0.22	0.33	0.22	0.46	0.19	0.57	0.19	0.30
79.4	0.26	0.16	0.16	0.16	0.16	0.19	0.25	0.08	0.08	0.11	0.14	0.11	0.11
126	0.08	0.19	0.08	0.05	0.03	0.00	0.14	0.11	0.03	0.05	0.05	0.11	0.05
200	0.11	0.08	0.05	0.05	0.11	0.00	0.00	0.05	0.08	0.05	0.11	0.03	0.05
316	0.03	0.00	0.05	0.00	0.00	0.00	0.00	0.05	0.14	0.03	0.05	0.03	0.03
501	0.00	0.00	0.05	0.03	0.05	0.00	0.00	0.08	0.11	0.05	0.08	0.08	0.03
794	0.00	0.00	0.00	0.03	0.05	0.00	0.05	0.03	0.03	0.03	0.03	0.08	0.00
1259	0.00	0.00	0.00	0.00	0.00	0.00	0.05	0.03	0.03	0.03	0.03	0.03	0.00
1995	0.00	0.00	0.00	0.03	0.00	0.00	0.03	0.00	0.03	0.03	0.03	0.03	0.00
3162	0.00	0.00	0.03	0.00	0.03	0.00	0.03	0.03	0.03	0.00	0.00	0.03	0.00
5012	0.00	0.00	0.00	0.00	0.00	0.00	0.00	0.00	0.00	0.00	0.00	0.00	0.00
7943	0.00	0.00	0.00	0.00	0.00	0.00	0.00	0.00	0.00	0.00	0.00	0.00	0.00
φHg1	3.75	4.93	3.12	3.37	2.96	3.52	4.44	2.85	3.81	2.96	4.48	3.05	2.66
φHg2	4.17	5.60	3.88	3.72	3.39	3.92	5.32	3.29	4.27	4.90	5.00	3.70	3.10
dHg	30.5	24.5	51.3	33.9	40.7	19.2	49.3	35.9	41.1	38.7	26.2	66.5	31.9

d (nm)	A17 φa (%)	A18 φa (%)	A19 φa (%)	A20 φa (%)	A21 φa (%)	A22 φa (%)	A23 φa (%)	A24 φa (%)	A25 φa (%)	B3 φa (%)	B4 φa (%)	B5 φa (%)	B7 φa (%)
3.2	0.32	0.38	0.38	0.50	0.32	0.48	0.61	0.46	0.29	0.44	0.32	0.49	0.38
5	0.70	0.84	0.99	0.97	0.84	1.21	0.91	1.08	0.80	0.77	0.87	0.95	0.73
7.9	0.57	0.60	0.83	0.72	0.62	0.80	0.64	0.70	0.51	0.60	0.62	0.71	0.51
12.6	0.43	0.49	0.56	0.61	0.59	0.62	0.59	0.54	0.37	0.66	0.57	0.65	0.46
20	0.38	0.43	0.48	0.44	0.43	0.51	0.48	0.46	0.37	0.41	0.43	0.71	0.38
31.6	0.24	0.24	0.21	0.22	0.22	0.32	0.21	0.24	0.21	0.27	0.32	0.57	0.16
50.1	0.27	0.46	0.27	0.28	0.24	0.27	0.27	0.11	0.24	0.27	0.35	0.52	0.41
79.4	0.14	0.16	0.19	0.19	0.16	0.19	0.19	0.00	0.13	0.16	0.27	0.27	0.11
126	0.11	0.11	0.08	0.14	0.22	0.13	0.13	0.00	0.11	0.19	0.14	0.19	0.05
200	0.05	0.08	0.05	0.06	0.22	0.08	0.03	0.00	0.03	0.11	0.03	0.11	0.00
316	0.05	0.00	0.08	0.06	0.05	0.11	0.03	0.00	0.03	0.11	0.08	0.00	0.00
501	0.08	0.00	0.03	0.06	0.05	0.16	0.11	0.00	0.05	0.03	0.03	0.00	0.00
794	0.03	0.00	0.03	0.03	0.00	0.11	0.00	0.00	0.00	0.03	0.03	0.00	0.00
1259	0.05	0.00	0.05	0.00	0.03	0.08	0.00	0.00	0.03	0.00	0.03	0.00	0.00
1995	0.00	0.00	0.03	0.00	0.00	0.00	0.00	0.00	0.00	0.00	0.03	0.00	0.00
3162	0.00	0.00	0.00	0.00	0.00	0.00	0.00	0.00	0.03	0.00	0.00	0.03	0.00
5012	0.00	0.00	0.00	0.00	0.00	0.00	0.00	0.08	0.00	0.16	0.03	0.00	0.00
7943	0.00	0.00	0.00	0.00	0.00	0.00	0.00	0.00	0.00	0.00	0.00	0.00	0.00
$\phi Hg1$	3.43	3.79	4.27	4.27	3.99	5.06	4.56	3.66	3.21	4.22	4.14	5.20	3.20
$\phi Hg2$	3.90	4.20	4.94	5.20	4.66	6.03	5.36	4.09	3.77	5.27	4.68	6.07	3.63
dHg	51.2	25.4	42.7	56.6	51.9	58.2	38.0	23.1	49.8	96.8	41.5	49.1	30.9

d (nm)	B8 φa(%)	B9 φa(%)	B10 φa(%)	C2 φa(%)	C3 φa(%)	C4 φa(%)	C7 φa(%)
3.2	0.24	0.33	0.30	0.19	0.35	0.49	0.43
5	0.86	0.71	0.63	0.60	0.97	0.82	0.94
7.9	0.53	0.52	0.50	0.41	0.70	0.71	0.76
12.6	0.37	0.47	0.47	0.38	0.59	0.60	0.65
20	0.45	0.41	0.30	0.35	0.51	0.44	0.57
31.6	0.21	0.22	0.41	0.22	0.21	0.33	0.51
50.1	0.24	0.44	0.36	0.22	0.67	0.27	0.32
79.4	0.11	0.11	0.08	0.14	0.16	0.19	0.22
126	0.16	0.11	0.06	0.11	0.13	0.16	0.11
200	0.11	0.05	0.03	0.05	0.05	0.11	0.00
316	0.05	0.03	0.00	0.05	0.08	0.05	0.00
501	0.05	0.11	0.00	0.05	0.03	0.00	0.00
794	0.00	0.00	0.00	0.08	0.00	0.00	0.00
1259	0.03	0.00	0.00	0.08	0.00	0.00	0.00
1995	0.00	0.03	0.00	0.05	0.00	0.00	0.00
3162	0.00	0.00	0.00	0.05	0.00	0.00	0.00
5012	0.00	0.00	0.03	0.08	0.00	0.00	0.00
7943	0.00	0.00	0.00	0.00	0.00	0.00	0.00
φHg1	3.42	3.53	3.17	3.12	4.45	4.18	4.51
φHg2	4.06	4.13	3.72	4.18	4.83	4.8	5.13
dHg	54.0	51.1	50.4	18.1	27.2	23.3	33.3

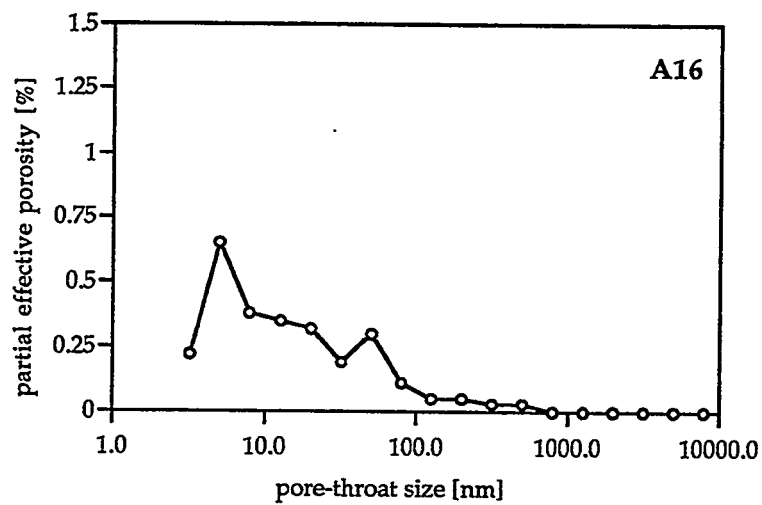# APPENDIX IX: Pore-Throat-Size Distribution Curves

Pore-throat-size distribution curves for the mudrock specimens from the Conasauga Group on the ORR analyzed with mercury porosimetry.
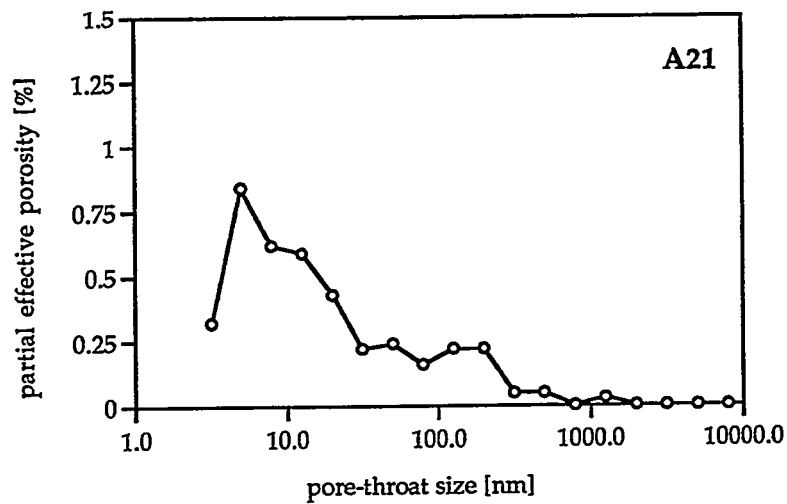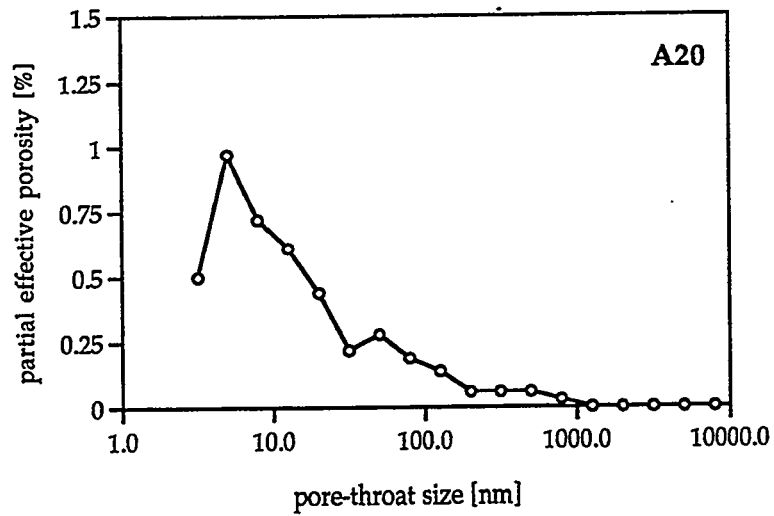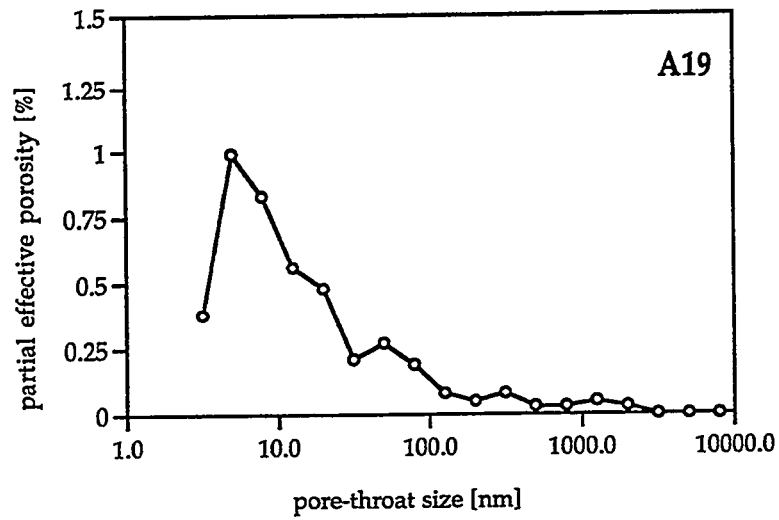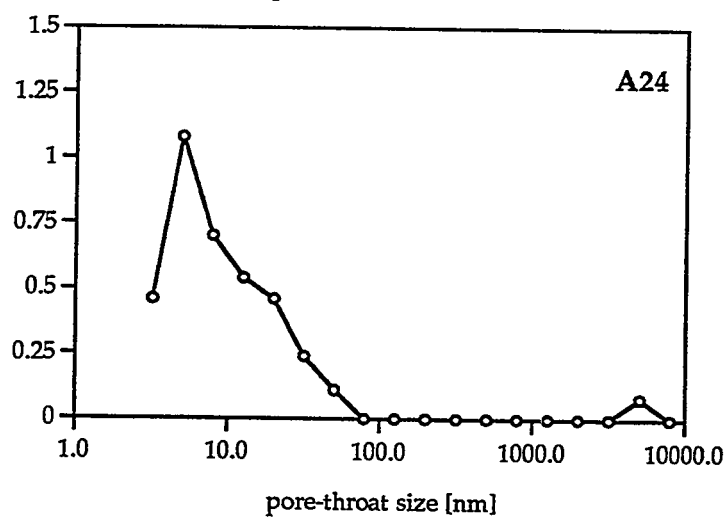
A1

partial effective porosity [%]

pore-throat size [nm]

A2

partial effective porosity [%]

pore-throat size [nm]

A3

partial effective porosity [%]

pore-throat size [nm]

A16

partial effective porosity [%]

pore-throat size [nm]

A17

partial effective porosity [%]

pore-throat size [nm]

A18

partial effective porosity [%]

pore-throat size [nm]

Figure A19: partial effective porosity [%] versus pore-throat size [nm]

Figure A20: partial effective porosity [%] versus pore-throat size [nm]

Figure A21: partial effective porosity [%] versus pore-throat size [nm]

APPENDIX X: Brief Specimen Description

For explanation of code letters, suffixes and numbers please refer to Appendix I. Weights are approximate weights at time of sampling, and not necessarily the weights at the time of analysis (e. g., further trimming of specimens prior to analysis). Specimens -e and -er were drilled from specimens -d.
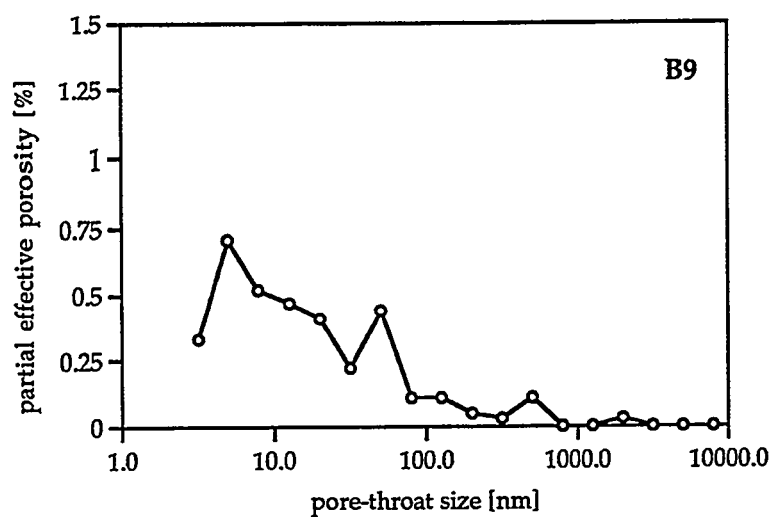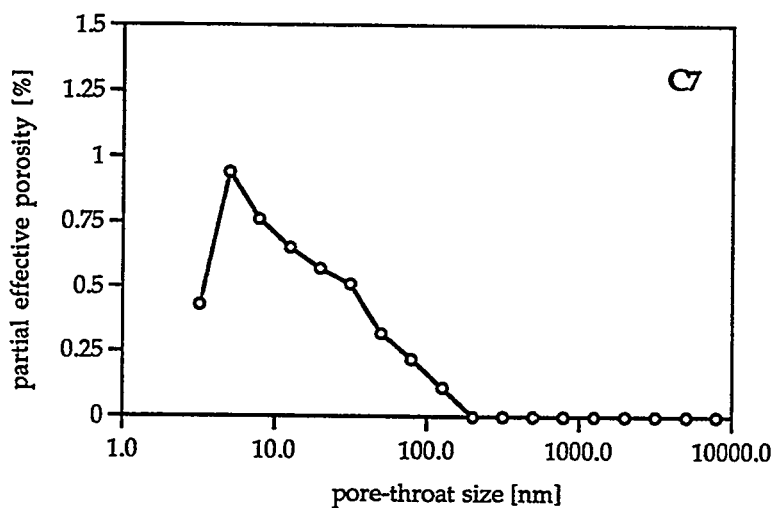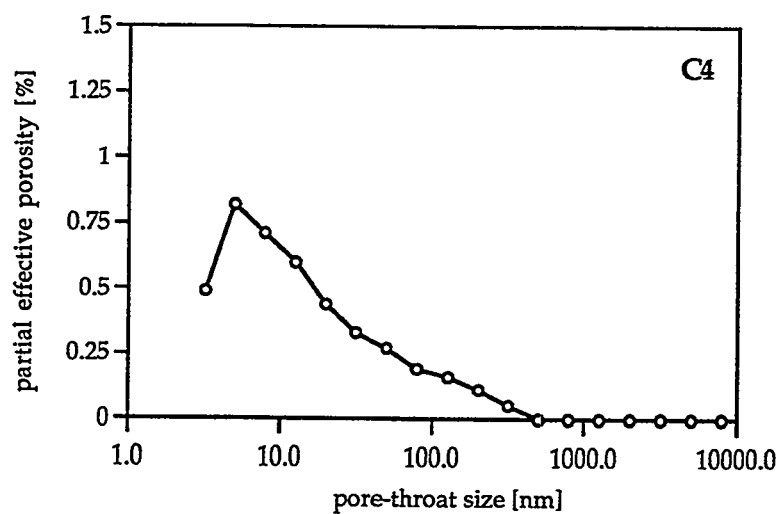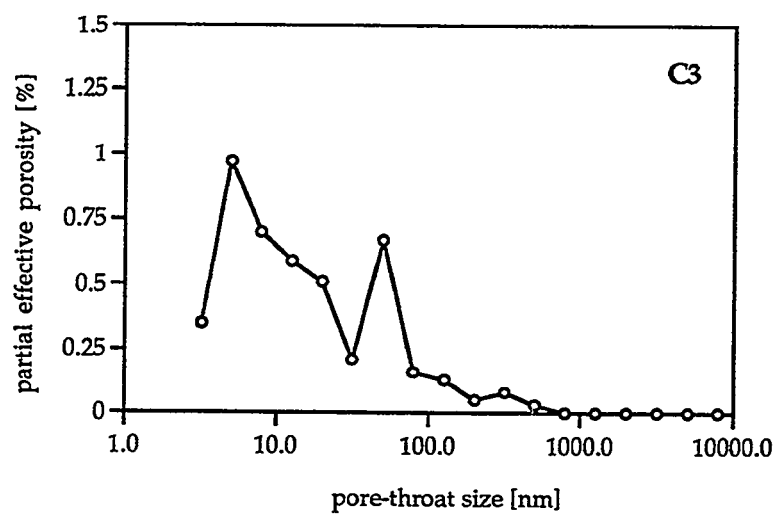
'no special observations' *means* no laminae, fractures, veins, etc. observed (would be noted specially).

SAMPLING INTERVAL	BRIEF DESCRIPTION

A1
d: gray mudstone; few laminae ($\leq$ max. 4 mm, highly laterally changing in thickness); mica; fine fracture sets lined with calcite parallel to core axis; .
a: (ca. 7.6 g); one side fracture surface (with calcite specks); small part with original core rim; specimen bottom with more shiny fracture surface;
b: (ca. 5.95 g); somewhat coarser grained than specimen d: silty mudstone; one side bound by fracture surface (with calcite specks);
c: (ca. 7.21 g); no special observations;
cr1: (ca. 3.58 g); some fracture surfaces with calcite specks visible;
cr2: (ca. 2.97 g); one side formed by fracture surfaces with calcite specks;
cr3: (ca. 5.43 g); one side, and another side partly, formed by fracture surfaces with calcite specks;
e: ; available for analysis;

A2
d: gray, silty mudstone to siltstone; trilobite fragments; bioturbation; fracture surfaces lined with calcite;
a: (ca. 6.5 g); much mica; small pockets of silt/fine sand ---> bioturbation (?);
b: (ca. 4.4 g); no special observations;
c: (ca. 7.71 g); no special observations;
cr1: (ca. 4.45 g); one side formed by fracture surface with calcite specks;
cr2: (ca. 5.41 g); one side formed by fracture surface with calcite specks;
cr3: (ca. 4.22 g); one side formed by fracture surface;
cr4: (ca. 3.52 g); with drilling rim from e-core-plug drilling; much mica;
cr5: (ca. 2.68 g); with drilling rim from e-core-plug drilling; much mica; more fragile;
e: not available for analysis;

A3
d: gray mudstone; mica; apparently some bioturbation? laminae ($\leq$ 2 mm, lateral change in thickness; fizzing = carbonate); fracture set with calcite lining parallel to core axis, shiny & polished fracture surfaces (somewhat slickensided) perpendicular to core axis;

a: (ca. 8.1 g); two sides bound by fractures (rare calcite specks); one lamina (1 mm);

b: (ca. 4.5 g); fracture surfaces at sides; one lamina ($\leq$ 1 mm);

c: (ca. 5.72 g); two sides bound by fracture surfaces; fractured internally;

cr1: (ca. 3.46 g); two sides formed by fracture surfaces; ;

cr2: (ca. 5.59 g); one side formed by fracture surface;

cr3: (ca. 3.43 g); three sides formed by fracture surfaces;

cr4: (ca. 5.70 g); with drilling rim from e-core-plug drilling; one side formed by rough fracture surface;

e: available for analysis;

A4   **d:** gray claystone; mica; distinct fracture sets parallel to core axis lined with calcite;

a: (ca. 8.05 g); one side partly bound by fracture surface (no calcite specks); specimen "bottom" mostly shiny fracture surface; much mica; somewhat coarser grained than specimen d ---> more mudstone (somewhat silty);

b: (ca. 5.8 g); claystone; mica; two sides bound by fracture surfaces (with small calcite specks); one edge with remnant of original core rim;

c: (ca. 3.99 g); bound on three sides by fracture surfaces (with small calcite specks);

cr1: (ca. 5.80 g); "top" surface is shiny; one small fossil fragment;

cr2: (ca. 4.24 g); one side formed by fracture surface with calcite specks;

e: not available for analysis;

A5   no specimen d; overall: gray (silty) mudstone;

a: (ca. 7.3 g); one side apparently bound by fracture (no calcite specks);

b: (ca. 6.5 g); one side apparently bound by fracture (no calcite specks); specimen "bottom" is a shiny fracture surface; much mica;

c: (ca. 8.44 g); exactly the same as for b;

cr1: (ca. 3.10 g); no special observations;

cr2: (ca. 5.49 g); no special observations;

A6   **d:** gray (silty) mudstone; much mica; shiny (polished) fracture surfaces;

a: (ca. 8.2 g); one side bound by fracture surface; one small edge seems to be part of original core rim;

b: (ca. 7.85 g); no special observations;

c: (ca. 9.3604 g); exactly the same as for a;

cr1: (ca. 4.7138 g); more irregular specimen, one side formed by non-rough fracture surface, no calcite specks;

cr2: (ca. 4.3944 g); three sides formed by non-rough fracture surfaces, no calcite specks;

cr3: (ca. 6.5921 g); three sides formed by non-rough fracture surfaces, no calcite specks;

cr4: (ca. 4.61 g); with drilling rim from e-core-plug drilling; thin disc; top partly sanded, base sanded;

cr5: (ca. 4.68 g); with drilling rim from e-core-plug drilling; thin disc; top and base sanded;

e: not available for analysis;

A7   **d:** gray claystone to mudstone; laminae; mica-rich in parts; fracture sets parallel to core axis: some with calcite fill, some apparently not;

a: (ca. 6.5 g); one side a "rough" fracture surface with calcite specks;

b: (ca. 4.05 g); much mica; one lamina (< 1 mm); one part (at side) "rough" fracture surface with calcite specks;

c: (ca. 5.29 g); one part (at side) "rough" fracture surface with calcite specks;

cr1: (ca. 4.45 g); one side formed by fracture surface with calcite lining;

cr2: (ca. 4.60 g); one side formed by fracture surface with calcite specks;

cr4: (ca. 4.15 g); with drilling rim from e-core-plug drilling; thin disc; top and bottom sanded;

cr5: (ca. 3.05 g); with drilling rim from e-core-plug drilling; thin disc; more fragile (small hairline fractures?);

e: available for analysis;

A8 d: gray claystone; one trilobite fragment; very fine sand/silt laminae (max. ca. 4 mm thick); fractures ?

a: (ca. 7.4 g); much mica; one lamina (1 mm);

b: (ca. 4.4 g); no special observations;

c: (ca. 8.60 g); much mica; one lamina (ca. 1.5 mm thick);

cr1: (ca. 4.14 g); one coarser grained lamina/lens (ca. 2 mm, silt, dies out laterally within specimen!);

cr2: (ca. 6.28 g); with drilling rim from e-core-plug drilling; bottom sanded, top partly sanded;

cr3: (ca. 5.34 g); with drilling rim from e-core-plug drilling; bottom sanded, top partly sanded;

e: available for analysis;

A9 d: gray mudstone to claystone; laminae (≤ 2 mm, laterally discontinuous - pinch-&-swell); fractured: fracture surfaces parallel to core axis mostly with calcite fill and non-shiny;

a: (ca. 9.7 g); some calcite specks along one side; internally calcite-lined fracture;

b: (ca. 5.0 g); two to three laminae (1 mm);

c: (ca. 8.33 g); one side formed by original core rim —> sanded off;

cr1: (ca. 7.08 g); one side formed by fracture surface with calcite specks;

cr2: (ca. 4.73 g); one side formed by fracture surface with calcite specks;

cr3: (ca. 7.74 g); with drilling rim from e-core-plug drilling; fatter disc; one carbonate lamina?

e: available for analysis;

A10 d: gray mudstone; discrete laminae (≤ 2 mm, fizzing = carbonate); fractured: non-shiny fracture surfaces parallel to core axis, shiny fracture surfaces (slickensided) perpendicular to core axis;

a: (ca. 9.5 g); bound on three sides by non-shiny fracture surfaces;

b: (ca. 5.7 g); bound on two sides by fracture surfaces (one with calcite specks);

c: (ca. 6.66 g); bound on one side by fracture surface;

cr1: (ca. 5.76 g); two side formed by fracture surface with calcite specks;

cr2: (ca. 5.63 g); two side formed by fracture surface with rare calcite specks;

e: available for analysis;

A11 d: maroon/tobacco-brown mudstone; few burrows; much mica; few laminae (≤ 1 mm); shiny fracture surface;

a: (ca. 7.55 g); no special observations;

b: (ca. 7.8 g); two laminae (1 mm);

c: (ca. 7.77 g); one burrow; one side bound by a non-shiny fracture surface;

cr1: (ca. 5.05 g); one side formed by fracture surface with calcite specks;

cr2: (ca. 2.80 g); one side formed by fracture surface with calcite specks; one corner original rim of core;

cr3: (ca. 5.29 g); with drilling rim from e-core-plug drilling; one side with rough fracture surface and minor calcite specks;

cr4: (ca. 3.75 g); with drilling rim from e-core-plug drilling; one side with rough fracture surface and minor calcite specks;

cr5: (ca. 3.66 g); with drilling rim from e-core-plug drilling; one side with rough fracture surface and minor calcite specks;

e: not available for analysis;

A12 d: maroon/tobacco-brown mudstone; few discrete 'bedding'-oblique burrows (diameter <1 cm), infilled with greenish very fine sand; much mica; silt laminae ($\leq$ 2 mm, laterally discontinuous/difference in thickness); fracture sets, some fracture sets are shiny, others are not; dispersed and patchy silt;
a: (ca. 7.3 g); no special observations;
b: (ca. 4.4 g); no special observations;
c: (ca. 9.20 g); no special observations;
cr1: (ca. 2.990g);
cr2: (ca. 3.00 g);
e: available for analysis;

A13 d: not sampled; overall: maroon/tobacco-brown claystone to mudstone; fractured (with shiny fracture surfaces);
a: (ca. 5.5 g); one side bound by straight, non-shiny fracture surface; a remnant of shiny fracture surface on specimen top;
b: (ca. 3.05 g); one side bound by core rim; one side bound by straight, non-shiny fracture surface;
c: (ca. 6.29 g); two sides bound by straight, non-shiny fracture surfaces; specimen "bottom" exhibiting shiny fracture surface(s);
cr1: (ca. 3.70 g); one side formed by fracture surface with calcite specks; "top" surface shiny; one corner remnant of original core rim;
cr2: (ca. 4.56 g); one side formed by fracture surface with calcite specks; "top" surface shiny; .
e: not available for analysis;

A14 d: maroon mudstone; silt laminae ($\leq$ 2 mm, lateral change in thickness); one fracture surface cutting through specimen (smaller rest piece of core specimen is missing);
a: (ca. 5.0 g); one oblique burrow (?!);
b: (ca. 3.6 g); core plug (from UT drilling campaign);
c: (ca. 4.18 g); long side formed by original rim of core —> cropped and sanded off; one side fracture surface;
cr1: (ca. 3.94 g); "top" surface shiny;
cr2: (ca. 3.85 g); one side formed by fracture surface with calcite specks; "top" surface shiny;
e: not available for analysis;

A15 d: maroon/tobacco-brown mudstone; laminae ($\leq$ 1 mm); shiny fracture surfaces as specimen "top" and "bottom";
a: (ca. 8.1 g); one side bound by somewhat shiny, crinkled fracture surface;
b: (ca. 6.0 g); small remnant of shiny fracture surface;
c: (ca. 4.43 g); no special observations;
cr1: (ca. 4.32 g); "top" surface in part shiny;
cr2: (ca. 6.58 g); one side formed by fracture surface;
e: available for analysis;

A16 d: gray mudstone to claystone; one lamina ($\leq$ 2 mm);
a: (ca. 7.9 g); same; no lamina;
b: (ca. 5.5 g); no special observations;
c: (ca. 6.74 g); no special observations; note: there are small overhangs: it is very important to wipe water sheen off completely and carefully before weighing following water saturation!
cr1: (ca. 3.25 g); two sides formed by fracture surfaces with rare calcite specks;
cr2: (ca. 3.59 g); one side formed by fracture surface with rare calcite specks;
cr3: (ca. 4.07 g); one side formed by fracture surface with rare calcite specks;

cr4: (ca. 3.89 g); with drilling rim from e-core-plug drilling; one side with rough fracture surface, no calcite specks;

e: not available for analysis;

A17 d: grayish-maroon mudstone; laminae (≤ 1 mm); shiny fracture surface ("bottom" of specimen);

a: (ca. 5.4 g); one side: non-mineralized, smooth fracture surface;

b: (ca. 5.7 g); one side: non-mineralized, smooth fracture surface;

c: (ca. 6.60 g); small remnant of shiny fracture surface on specimen "top";

cr1: (ca. 3.10 g); part of one side formed by fracture surface with calcite specks;

cr2: (ca. 4.24 g); two sides partly formed by fracture surfaces with some calcite specks;

cr3: (ca. 4.71 g); with drilling rim from e-core-plug drilling; trilobite imprint;

cr4: (ca. 3.63 g); with drilling rim from e-core-plug drilling; one side broken surface;

e: not available for analysis;

A18 d: maroon/tobacco-brown mudstone; laminae (≤ 1 mm); shiny fracture surfaces, 'bedding'-oblique calcite veins (≤ 3 mm, laterally changing thickness);

a: (ca. 7.8 g); no special observations;

b: (ca. 5.2 g); no special observations;

c: (ca. 6.97 g); no special observations;

cr1: (ca. 2.77 g); no special observations;

cr2: (ca. 6.29 g); one side formed by fracture surface with calcite specks; irregularly shaped piece;

cr3: (ca. 2.75 g); with drilling rim from e-core-plug drilling;

e: not available for analysis;

A19 d: maroon/tobacco-brown mudstone; shiny fracture surfaces (slickensided);

a: (ca. 7.0 g); somewhat shiny "bottom" surface;

b: (ca. 5.5 g); no special observations;

c: (ca. 8.98 g); no special observations;

cr1: (ca. 4.63 g); no special observations;

cr2: (ca. 4.46 g); one side formed by fracture surface with calcite specks;

cr3: (ca. 5.65 g); with drilling rim from e-core-plug drilling; top and base sanded;

e: not available for analysis;

A20 d: gray claystone (to mudstone);

a: (ca. 6.6 g); no special observations;

b: (ca. 5.4 g); no special observations;

c: (ca. 5.80 g); no special observations;

cr1: (ca. 4.14 g); one side formed by fracture surface with rare calcite specks;

cr2: (ca. 5.38 g); mica, appears a bit coarser grained;

e: not available for analysis;

A21 d: dark-gray claystone/shale to mudstone/shale; some silt laminae (≤ 2 mm); shiny fracture surfaces, very thin calcite-filled fractures;

a: (ca. 6.3 g); no special observations;

b: (ca. 5.45 g); no special observations;

c: (ca. 7.39 g); no special observations;

cr1: (ca. 3.57 g); no special observations;

cr2: (ca. 3.25 g); no special observations;

cr3: (ca. 3.44 g); one side partly formed by fracture surface with rare calcite specks;

cr4: (ca. 4.24 g); with drilling rim from e-core-plug drilling; one minor part of one side rough fracture, with calcite specks;

cr5: (ca. 4.03 g); with drilling rim from e-core-plug drilling; one side with rough fracture surface and calcite specks; top and base sanded;

e: not available for analysis;

A22   d: gray claystone;
a: (ca. 5.5 g); no special observations;
b: (ca. 6.3 g); no special observations;
c: (ca. 7.81 g); no special observations;
cr1: (ca. 6.49 g); "top" surface partly formed by fracture surface with rare calcite specks;
cr2: (ca. 6.91 g); one side formed by fracture surface with rare calcite specks;
e: not available for analysis;

A23   d: gray claystone; discrete fractures (no calcite filling observed, but might be there;
a: (ca. 4.85 g); no special observations;
b: (ca. 4.3 g); no special observations;
c: (ca. 8.98 g); few fracture surfaces oblique to 'bedding';
cr1: (ca. 3.88 g); one side formed by fracture surface with rare calcite specks;
cr2: (ca. 4.15 g); one side formed by fracture surface with rare calcite specks;
e: not available for analysis;

A24   d: gray claystone; some shiny fracture surfaces;
a: (ca. 6.7 g); same; one lamina (1 mm); some tiny calcite specks (left over from fracture fills ?);
b: (ca. 5.1 g); some coarser material (50% claystone, 50% mudstone); "top" is a fracture surface;
c: (ca. 7.22 g); one side bound by non-shiny fracture surface;
cr1: (ca. 3.55 g); one side formed by fracture surface with some calcite specks;
cr2: (ca. 3.75 g); one side partly formed by shiny fracture surface;
e: not available for analysis;

A25   d: gray claystone; fractures visible, incl. small, discontinuous calcite-filled fractures; lamination (≤ 2 mm);
a: (ca. 7.55 g); one lamina (1 mm);
b: (ca. 4.6 g); no laminae;
c: (ca. 5.61 g); one side is a fracture surface (non-shiny, no calcite specks);
cr1: (ca. 3.13 g); no special observations;
cr2: (ca. 3.60 g); one side formed by fracture surface with some calcite specks;
e: not available for analysis;

B1   d: maroon mudstone; fracture surfaces (partly with calcite lining;
a: (ca. 7.4 g); bound in part by fracture surfaces (including "bottom"), some calcite specks;
b: (ca. 4.4 g); one side bound by fracture (with calcite specks);
c: (ca. 9.0919g); nice broken surfaces at sides;
cr1: (ca. 3.7399 g); "top" surface formed by shiny fracture surface;
cr2: (ca. 4.14 g); with drilling rim from e-core-plug drilling; one side broken;
cr3: (ca. 5.29 g); with drilling rim from e-core-plug drilling;
e: not available for analysis;

B2   no specimen d; overall: maroon claystone-mudstone; fracture surfaces: shiny and non-shiny (with calcite specks);
a: (ca. 6.6 g); apparent fracture surfaces (shiny and non-shiny);
b: (ca. 5.8 g); maroon mudstone (somewhat grittier than specimen a);
c: (ca. 6.73 g); two to three fractures run clearly through the specimen, are of the rough & calcite-speckled type (—> interesting to analyze: continuous calcite or series of specks with gaps in-between? calcite vein, fill of discontinuous fracture, to be

counted to matrix porosity and not to interconnected fracture framework?); one side with fracture of same type;

cr1: (ca. 4.64 g); one side formed by a fracture surface with calcite specks;

cr2: (ca. 2.58 g); one side formed by a fracture surface with calcite specks;

B3   **d:** gray claystone; one marl band (1 cm thick, lateral change in thickness —> down to 5 mm; indistinct top and base); shiny fracture surfaces;

a: (ca. 8.2 g); some fracture surfaces (with calcite specks) at side, shiny specimen "top" and "bottom" surfaces;

b: (ca. 6.6 g); see a;

c: (ca. 5.54g); one side bound by rough fracture + calcite specks —> sanded off;

cr1: (ca. 4.50 g);

cr2: (ca. 2.99 g);

e: available for analysis;

B4   **d:** gray mudstone; many shiny fracture surfaces;

a: (ca. 6.9 g); specimen "top" and "base" with shiny polished fracture surfaces;

b: (ca. 6.3 g); specimen "top" with shiny polished fracture surfaces; mica; remnant of original core rim on one side;

c: (ca. 5.38 g); one side bound by rough fracture surface with calcite specks —> partly sanded off; note: some tiny "overhangs"; "top" and "base" are shiny, probably fracture surfaces; one side is fracture surface, ± smooth/not rough, no calcite specks;

cr1: (ca. 3.00 g);

cr2: (ca. 3.53 g);

cr3: (ca. 4.04 g); two sides formed by a fracture surfaces, one with calcite specks;

e: not available for analysis;

B5   **d:** gray mudstone; much mica; discontinuous limestone lamina (≤ 1 cm); fractured: shiny & polished fracture surfaces, many thin calcite veins;

a: (ca. 8.5 g); one side with fracture (with calcite specks), specimen "bottom" more shiny fracture surface;

b: (ca. 6.2 g); mica; sides are more or less fracture surfaces, specimen "top" and "bottom" are more shiny fracture surfaces;

c: (ca. 5.32 g); "bottom" is shiny fracture; one side bound by a rough fracture surface with calcite specks;

cr1: (ca. 4.06 g); "top" and "bottom" surfaces formed by shiny fracture surfaces; two sides formed by fracture surfaces with calcite specks; appears/feels more rough: silt content (?);

cr2: (ca. 13.03 g); cylinder piece; base sanded, top oblique fracture/vein with abundant calcite specks;

e: not available for analysis;

B6   no specimen d; overall: maroon mudstone;

a: (ca. 8.2 g); specimen "top" and "bottom" are shiny & polished fracture surfaces; one side fracture surface, one side part of original core rim;

b: (ca. 4.8 g); shiny fracture surfaces indicated throughout specimen;

c: (ca. 6.14 g); "top" is partly a shiny fracture surface; lots of tiny "overhangs";

cr1: (ca. 4.50 g); "top" formed by shiny fracture surface;

B7   **d:** gray mudstone; laterally discontinuous marl layers (<1 cm thick); fracture surfaces: shiny and polished perpendicular to core axis, and non-shiny and calcite-lined parallel to core axis;

a: (ca. 7.12 g); shiny fracture surfaces; one specimen side formed by calcite-coated fracture surface; another side apparently part of original core rim;

b: (ca. 5.55 g); same as for a;

c: (ca. 5.97 g); many shiny and rough fracture surfaces;

cr1: (ca. 2.65 g); bound on all sides by more or less shiny fracture surfaces;

cr2: (ca. 2.87 g); bound on almost all sides by more or less shiny fracture surfaces; more
fragile;

e: not available for analysis;

B8 d: gray mudstone; shiny and polished, and non-shiny (vein calcite) fracture surfaces;

a: (ca. 7.4 g); appears to be completely transected by shiny and polished fracture
surfaces; much sparry calcite; "a strange piece of rock"; slickensided?

b: (ca. 4.95 g); micaceous; shiny, irregular;

c: (ca. 6.44 g); some shiny smooth surfaces on parts of "bottom" and "top";

e: not available for analysis;

B9 d: gray mudstone; shiny and polished fracture surfaces; one side (base) highly
irregular; base in part calcite-lined/specks, slickensided;

a: (ca. 7.9 g); some parts are shiny; apparently some calcite;

b: (ca. 6.7 g); some parts are shiny; apparently some calcite; specimen "bottom" is flat,
shiny and polished fracture surface;

c: (ca. 6.19 g); "bottom" and "top" with ± shiny fracture surfaces;

cr1: (ca. 3.30 g); one side formed by remnant of original core rim; another (short) side
formed by somewhat shiny fracture surface;

cr2: (ca. 3.79 g); one side formed by remnant of original core rim; more irregular piece;

e: not available for analysis;

B10 d: maroon mudstone; shiny and polished fracture surfaces perpendicular to core axis;
one side rougher fracture surface (with calcite specks) parallel to core axis;

a: (ca. 7.7 g); specimen "top" and "bottom" are shiny fracture surfaces; one side is
rougher fracture surface (with calcite specks); small part of one side with
remnant of original core rim;

b: (ca. 6.4 g); one side is rougher fracture surface (with calcite specks); small part of
one side with remnant of original core rim;

c: (ca. 10.01 g); shiny fracture surface at "bottom", partly at "top"; one side rough
fracture surface with calcite specks, one side part of original rim of core ;

e: available for analysis;

C2 c: (ca. 5.54 g); gray mudstone; shiny, fragile; one side formed by rough fracture
surface with minor calcite specks); "bottom" formed by a shiny fracture surface;

a: (ca. 7.3 g); shiny fracture surfaces running through specimen;

b: (ca. 6.7 g); shiny fracture surfaces; one rough fracture surface with calcite specks;

d: available for drilling;

e: not available for analysis;
<corresponds to Bechtel-core sample #6>;

C3 a: (ca. 5.2 g); dark-gray mudstone, ±silty; one apparent calcite vein running through
specimen; one side formed by rough fracture surface with calcite specks (i. e.,
vein broken open);

b: (ca. 3.7 g); shiny "bottom" and "top";

c: (ca. 5.11 g); two sides formed by rough fracture surfaces with calcite specks;

cr1: (ca. 7.34 g); piece of cylinder; one whole side obliquely "decapitated" by rough
fracture surface with only a few calcite specks;

d: available for drilling;

e: not available for analysis;
<corresponds to Bechtel-core sample #28>;

C4   b: (ca. 5.5 g); dark-gray mudstone; shiny, fragile; one side with a small remnant of the
          original core rim;
       a: (ca. 5.7 g); shiny, fragile;
       c: (ca. 6.65 g); shiny; some silt;
       d: not available;
       e: not available;
          <corresponds to Bechtel-core sample #11>;

C5   a: (ca. 5.25 g); gray silty mudstone/siltstone; shiny, slightly brown, micaceous; some
          laminae (1 mm thick);
       b: (ca. 5.5 g); dark-gray silty mudstone; some laminae (1 mm thick); one fracture with
          calcite fill), hair-thick, running through specimen;
       c: (ca. 3.69g); dark-gray mudstone (finer grained than a, b); friable; one lamina (≤ 1
          mm); micaceous; with small irregularities due to breaking perpendicular to
          bedding;
       d: not available;
       e: not available for analysis;
          <corresponds to Bechtel-core sample #18>;

C6   e: (ca. 4.95 g); core plug of small dimensions (left from drilling for radial diffusion -cell
          method);
       d: this is used for radial diffusion-cell method;
          light-gray, finer grained mudstone; micaceous; coherent but feels more delicate
          than specimen C8; some silt laminae (≤ 1 mm), no bioturbation visible; numerous
          calcite veins (≤ 1 mm); some grooves from drilling at the sides;
       a, b, c: no specimens available;
          <corresponds to Bechtel-core sample #2>;

C7   e: (ca. 3.25 g); core plug of small dimensions (left from drilling for radial diffusion-cell
          method);
       d: this is used for radial diffusion-cell method;
       a: (ca. 6.0 g); dark-gray (silty) mudstone; "bottom" formed by a shiny fracture surface;
          some silt laminae (<1 mm thick);
       b: (ca. 3.4 g); dark-gray mudstone; some shiny fracture surfaces (including "bottom");
       c: (ca. 6.38 g); dark-gray mudstone; some shiny fracture surfaces, highly uneven
          appearance; with small irregularities due to breaking perpendicular to
          bedding;
          <corresponds to Bechtel-core sample #22>;

C8   e: (ca. 3.75 g); dark-gray mudstone; core plug of small dimensions (left from drilling for
          radial diffusion-cell method);
       d: this is used for radial diffusion-cell method;
          maroonish gray, silty mudstone; feels gritty; compact and hard; high silt and
          sand (very fine to fine) content, organized in laminae; laminae uninterrupted in
          upper part of specimen, chaotically disrupted in lower part of specimen because
          of abundant bioturbation; crossed by numerous calcite veins (≤ 1 mm), with one
          through-going vein swelling up to 2.5 mm in thickness;
       a, b, c: no specimens available;
          <corresponds to Bechtel-core sample #24>;

108

Internal Distribution

1. L. D. Bates, 1001, MS-7169
2. F. P. Baxter, 3504, MS-6317
3. D. M. Borders, 1509, MS-6400
4. H. L. Boston, 4500-N, MS-6200
5. H. M. Braunstein, 130MIT, MS-6282
6. A. J. Caldanaro, 1509, MS-6400
7. R. B. Clapp, 1509, MS-6400
8. K. W. Cook, 1330, MS-7298
9. T. L. Cothron, 1001, MS-7155
10. J. H. Cushman, 1059, MS-6422
11. N. H. Cutshall, C207, MS-7172
12. M. F. P. DeLozier, 1037, MS-7355
13. A. F. Dieffendorf, 1509, MS-6400
14. W. E. Doll, 1509, MS-6400
15-21. J. Dorsch, 1509, MS-6400
22. R. B. Dreier, 1509, MS-6400
23. T. O. Early, 1509, MS-6400
24. J. M. Forstrom, 0303-8, MS-7314
25. D. E. Fowler, 1505, MS-6035
26. C. W. Francis, 3504, MS-6317
27. D. W. Frazier, 4500-N, MS-6198
28. B. J. Frederick, 4500-N, MS-6204
29. S. B. Garland, II, 7078-B, MS-6402
30. C. W. Gehrs, 1505, 6036
31. P. L. Goddard, 1330, MS-7298
32. J.-P. Gwo, 4500-N, MS-6203
33. C. S. Haase, 1330, MS-7298
34. R. D. Hatcher, Jr., 1509, MS-6400
35. D. S. Hicks, 1509, MS-6400
36. S. G. Hildebrand, 1505, MS-6037
37. J. Hodgins, 9983-58, MS-8248
38. Lucius Holder, Jr., 3001, MS-6029
39. D. D. Huff, 1509, MS-6400
40. G. K. Jacobs, 1505, MS-6036
41. W. K. Jago, 9207, MS-8225
42. P. M. Jardine, 1505, MS-6038
43. S. B. Jones, 9207, MS-8225
44. P. Kanciruk, 0907, MS-6490
45. R. H. Ketelle, 4500N, MS-6185
46. B. L. Kimmel, 4500-S, MS-6125
47. A. J. Kuhaida, 7078-B, MS-6402
48. R. R. Lee, 4500-N, MS-6185
49. S. Y. Lee, 1505, MS-6038
50. P. J. Lemiszki, 1509, MS-6400
51. R. S. Loffman, 4500-S, MS-6102
52. R. J. Luxmoore, 1505, MS-6038
53. J. F. McCarthy, 1505, MS-6036
54. L. W. McMahon, 9116, MS-8098
55. G. R. Moline, 1509, MS-6400
56. C. M. Morrissey, 1505, MS-6035
57. P. J. Mulholland, 1505, MS-6036
58. J. B. Murphy, 4500-N, MS-6198
59. C. E. Nix, 6026-C, MS-6395
60. M. J. Norris, 9983-AH, MS-8247
61. J. E. Nyquist, 1509, MS-6400
62. F. S. Patton, Jr., 1001-B, MS-7169
63. D. Pridmore, 6556F, MS-6348
64. T. Purucker, 105MIT, MS-6452
65. D. E. Reichle, 4500-N, MS-6253
66. C. T. Rightmire, 1509, MS-6400
67. T. H. Row, 4500-N, MS-6254
68. W. E. Sanford, 1509, MS-6400

69. F. E. Sharples, 1505, MS-6036

70. L. G. Shipe, 0303-8, MS-7314

71. D. S. Shriner, 1505, MS-6038

72. R. L. Siegrist, 1505, MS-6038

73. E. D. Smith, 1505, MS-6038

74. S. H. Stow, 1505, MS-6035

75. M. F. Tardiff, 4500-N, MS-6198

76. L. E. Toran, 1509, MS-6400

77. J. R. Trabalka, 3047, MS-6020

78. J. C. Wang, 4500-N, MS-6185

79. D. R. Watkins, 3504, MS-6317

80-84. D. B. Watson, 1509, MS-6400

85. O. R. West, 1505, MS-6036

86. R. K. White, 1330, MS-7298

87. S. L. Winters, 1509, MS-6400

88. T. F. Zondlo, 1509, MS-6400

89-93. ESD Library

94. Central Research Library

95. ORNL-Y-12 Technical Library

96-97. Laboratory Records Department

98. Laboratory Records, ORNL-RC

99. ORNL Patent Office

External Distribution

100. Jerry Archer, Geraghty & Miller Inc., 97 Midway Lane, Oak Ridge, TN 37830

101. Richard Arnseth, SAIC, 301 Laboratory Rd., Oak Ridge, TN 37830

102. Ernest Beauchamp, C-260 Jackson Plaza, MS-7614, R13, Oak Ridge, TN 37830

103. Robert Benfield, TDEC/DOE Oversight, 761 Emory Valley Rd., Oak Ridge, TN 37830

104. R. H. Bennett, Seafloor Geosciences Division, Naval Ocean Research and Development Activity, Stennis Space Center, MS 39529-5004

105. G. W. Bodenstein, USDOE-OR Federal Bldg., Oak Ridge, TN 37830

106. Paul Craig, Environmental Consulting Engineers, P.O. Box 22668, Knoxville, TN 37933

107. S. N. Davis, 6540 Box Canyon Drive, Tucson, AZ 85745

108. Director, Center for Management, Utilization, and Protection of Water Resources, Tennessee Technological University, P.O. Box 5082, Cookeville, TN 38505

109. S. G. Driese, Department of Geological Sciences, University of Tennessee, Knoxville, TN 37996

110. B. E. Dugan, Department of Civil and Mineral Engineering, University of Minnesota, Minneapolis, MN 55455

111. W. M. Dunne, Department of Geological Sciences, University of Tennessee, Knoxville, TN 37996

112. J. L. Foreman, Exxon Production Research Co., P. O. Box 2189, Houston, TX 77252-2189

113. J. F. Franklin, College of Forest Resources, Anderson Hall AR-10, University of Washington, Seattle, WA 98185

114. P. M. Goldstrand, Department of Geological Sciences, MS-172, University of Nevada, Reno, NV 89557

115. Jim Harless, TDEC/DOE Oversight, 761 Emory Valley Rd., Oak Ridge, TN 37830

116. R. C. Harriss, Institute for the Study of Earth, Oceans, and Space, University of New Hampshire, Durham, NH 03824

117. P. Hofmann, Department of Energy, 3 Main St., Oak Ridge, TN 37830

118. G. M. Hornberger, Dept. of Environmental Sciences, University of Virginia, Charlottesville, VA 22903

119. D. R. Issler, Geological Survey of Canada, Institute of Sedimentary and Petroleum Geology, 3303-33rd Street N.W., Calgary, Alberta, CANADA T2L 2A7

120. G. Y. Jordy, Office of Program Analysis, Office of Energy Research, ER-30, G-226, USDOE, Washington, D.C. 20545

121-122. H. E. Julian, TVA Engineering Laboratory, PO Drawer E, Norris,TN 37828

123-127. T. J. Katsube, Geological Survey of Canada, Mineral Resources Division, 601 Booth Street, Ottawa, Ontario, CANADA K1A 0E8

128. D. C. Kopaska-Merkel, Geological Survey of Alabama, 420 Hackberry Lane, Tuscaloosa, AL 35486

129. O. C. Kopp, Department of Geological Sciences, University of Tennessee, Knoxville, TN 37996

130. J. Krushin, Amoco Production Co., 501 Westlake Park Boulevard, PO Box 3092, Houston, TX 77253-3092

131. P. E. Lamoreaux & Assoc. Inc., P.O. Box 2310, Tuscaloosa, AL 35403

132. D. A. Lietzke, Lietzke Soil Services, Route 3, Box 607, Rutledge, TN 37861

133. Changsheng Lu, Jacobs ER Team, 125 Broadway Ave. Oak Ridge, TN 37830

134. L. D. McKay, Department of Geological Sciences, University of Tennessee, Knoxville, TN 37996

135. W. M. McMaster, 1400 West Racoon Valley Rd.

136. Manager, CH2M Hill, 599 Oak Ridge Turnpike, Oak Ridge, TN 37830

137. Manager, HSW Environmental Consultants, 687 Emory Valley Rd., Oak Ridge, TN 37830

138. Manager, Radian/Lee Wan Assoc., 120 South Jefferson Circle, Oak Ridge, TN 37830

139. Manager, Systematic Management Services, 673 Emory Valley Rd., Oak Ridge, TN 37830

140. G. K. Moore, Route 4, Box 927, Waynesboro, TN 38485

141. Ronit Nativ, Dept. of Soil and Water Sci., Faculty of Agriculture, Hebrew University of Jerusalem, P.O. Box 12, Rehovot 76100, ISRAEL

142. M. J. Neton, Geologic & Environmental Services, 701 Cherokee Blvd., Suite G, Chattanooga, TN 37405

143. C. E. Neuzil, U. S. Geological Survey, 431 National Center, MS 431, Reston, VA 22092

144. K. S. Novakowski, National Water Research Institute, 867 Lakeshore Rd., Burlington, Ontario L7R 4A6, CANADA

145. Chudi Nwangwa, TDEC/DOE Oversight, 761 Emory Valley Rd., Oak Ridge, TN 37830

146. R. H. Olsen, Microbiology & Immunology Dept., University of Michigan, Medical Sciences II, #5605, 1301 East Catherine St., Ann Arbor, MI 48109-0620

147. A. Patrinos, Environmental Sciences Division, Office of Health & Environmental Research, ER-74, USDOE, Washington, D.C. 20585

148. J. Pattchett, Amoco Research, PO Box 3385, Tulsa, OK 74102

149. R. Pawlowicz, Bechtel, 151 Lafayette Dr. Oak Ridge, TN 37830

150. W. K. Puff, Dames and Moore, 575 Oak Ridge Turnpike, Oak Ridge, TN 37830

151. F. Quinones, Chief, Tennessee District, WRD, U.S. Geological Survey, 810 Broadway, Suite 500, Nashville, TN 37203

152. G. D. Reed, Dept. of Civil Engineering, University of Tennessee, 62 Perkins Hall, Knoxville, TN 37996-2010

153. J. Schieber, Dept. of Geology, University of Texas, Arlington, Box 19049, 500 Yates St., Arlington, TX 76019

154. N. Scromeda, Geological Survey of Canada, Mineral Resources Division, 601 Booth Street, Ottawa, Ontario, CANADA K1A 0E8

155. D. Shults, Tennessee Dept. of Environment and Conservation, Div. of Radiological Health, TERRA Bldg., 150 Ninth Ave. North, Nashville, TN 37243-1532

156. W. C. Sidle, Environmental Protection Division, USDOE-OR, P.O. Box 2001, Oak Ridge, TN 37831-8739

157. J. Smoot, Dept. of Civil Engineering, University of Tennessee, 62 Perkins Hall, Knoxville, TN 37996-2010

158. D. K. Solomon, 2381 Beacon Drive, Salt Lake City, Utah 84108

159. D. A. Stephenson, South Pass Resources, Inc., 8669 East San Alberto Drive, Suite 101, Scottsdale, AZ 85258

160. L. Tourkow, 2116-D Shade Valley Road, Charlotte, NC 28205

161. B. A. Tschantz, Dept. of Civil Engineering, University of Tennessee, 62 Perkins Hall, Knoxville, TN 37996-2010

162. G. van der Kamp, Environment Canada, 11 Innovation Blvd., Saskatoon, Saskatchewan S7N 3H5, CANADA

163. K. R. Walker, Department of Geological Sciences, University of Tennessee, Knoxville, TN 37996

164. W. White, 542 Glenn Road, State College, PA 16803

165. F. J. Wobber, Environmental Sciences Division, Office of Health & Environmental Research, Office of Energy Research, ER-74, USDOE, Washington, D.C. 20585

166. J. Young, Camp Dresser & McGee, Suite 500, 800 Oak Ridge Turnpike, Oak Ridge, TN 37830

167-168. S. C. Young, Environmental Consulting Engineers, P. O. Box 22668, Knoxville, TN 37933

169. Office of Assistant Manager for Energy Research & Development, USDOE-OR, P.O. Box 2001, Oak Ridge, TN 37831-8600

170-172. Office of Scientific & Technical Information, P.O. Box 62, Oak Ridge, TN 37831